

**MULTI-OBJECTIVE OPTIMIZATION OF ORGANIC
RANKINE CYCLE BASED WASTE HEAT RECOVERY
SYSTEMS USING ARTIFICIAL INTELLIGENCE**



**A thesis submitted to
Department of Mechanical Engineering
Bangladesh University of Engineering & Technology
Dhaka**

**by
Rafe Md. Abu Zayed**


**IN PARTIAL FULFILLMENT OF THE REQUIREMENTS
FOR
THE DEGREE OF MASTERS IN SCIENCE
IN
MECHANICAL ENGINEERING**


June, 2022


Certificate of Approval


The thesis titled, "MULTI-OBJECTIVE OPTIMIZATION OF ORGANIC RANKINE CYCLE BASED WASTE HEAT RECOVERY SYSTEMS USING ARTIFICIAL INTELLIGENCE", submitted by Rafe Md. Abu Zayed, Roll No: 1018102076, Session: October/2018, has been accepted as satisfactory in partial fulfillment of the requirements for the degree of MASTER OF SCIENCE IN MECHANICAL ENGINEERING on 25 June, 2022.


BOARD OF EXAMINERS

1. 

Dr. Md. Zahurul Haq
Professor
Department of ME, BUET, Dhaka
(Supervisor) Chairman
2. 

Dr. Muhammad Ashiqur Rahman
Professor & Head
Department of ME, BUET, Dhaka
(Ex-Officio) Member
3. 

Dr. Mohammad Mamun
Professor
Department of ME, BUET, Dhaka
Member
4. 

Dr. Kazi Arafat Rahman
Assistant Professor
Department of ME, BUET, Dhaka
Member
5. 

Dr. Md. Ziaur Rahman Khan
Professor
Department of EEE, BUET, Dhaka
Member (External)

Candidate's Declaration

I, hereby, declare that this thesis or any part of it has not been submitted elsewhere for the award of any degree or diploma. And also declare that all information in this document has been obtained and presented in accordance with academic rules and ethical conduct. I also declare that, as required by these rules and conduct, I have fully cited and referenced all material and results that are not original to this work.

Rafe Md. Abu Zayed

Rafe Md. Abu Zayed

Acknowledgements

I would like to express my sincere appreciation to my supervisor, Professor Dr. Md. ZahurulHaq whose expertise, understanding, generous guidance and support made it possible for me to work on a topic that was of great interest to me. For his unwavering support, I am truly grateful. He always knew where to look for the answers to obstacles while leading me to the right source, theory and perspective.

A debt of gratitude is owed to my parents and sisters, without their love and support, I would not have come this far.

I would also like to thank Ashfak Yeafi for helping me with the programming of the neural network part of my work. I am thankful to Rafiul Reaz Omi for helping me with the illustrations of this work.

Abstract

Waste heat recovery (WHR) technology is gaining popularity in recent years to address global energy crisis and provide an environment friendly robust alternative for utilizing medium and low grade heat. Among the available technologies for WHR purpose, Organic Rankine Cycle (ORC) is a reliable method in respect of the working fluid property, cycle configuration and efficiency, economy, and robustness. Therefore, optimization of the ORC for WHR purpose is becoming a promising research topic in the energy sector. However, most of the work on ORC optimization have focused on the traditional approach of acquiring the cycle state points from the direct thermodynamic modelling, which can be complex and time consuming. In this study, an efficient method of ORC optimization for WHR is presented based on artificial intelligence (AI) technique. Based on four ORC configurations namely Basic ORC, Reheating ORC, Internal Regenerative ORC, and Combined Reheating Internal Regenerative ORC, a database is constructed with nine pre-selected organic working fluid for training an AI framework. The prediction performances of four machine learning (ML) algorithms, namely Linear Regression (LR), Support Vector Regression (SVR), Decision Tree Regression (DTR), and Random Forest Regression (RFR), are compared and RFR is observed to produce the best prediction results. After that, a Back Propagation Neural Network (BPNN) is trained with the formulated dataset and the prediction results are compared with that of RFR. It is found that, BPNN is faster but more data sensitive whereas RFR can produce fairly accurate prediction result with less amount of data than BPNN. From the sensitivity analysis, two parameters namely heat source temperature and reheating pressure ratio are found to be the most influential in ORC performance. Based on this analysis, an optimization framework is constructed keeping the trained AI algorithms as proxy model to generate the objective function data. The optimized thermal and exergy efficiency are found to be close to one another for traditional thermodynamic modelling, RFR, and BPNN which indicates that the proposed ANN scheme can effectively be used as a proxy model for thermodynamic analysis during the optimization process. Furthermore, the RFR and BPNN work nearly 7 times and 20 times faster than the traditional approach, indicating that they can successfully be used as a less complex and less time consuming alternative for ORC modelling.

List of Symbols

\dot{m}	Mass flow rate of the fluid stream
\dot{Q}	Rate of heat transfer
\dot{W}	Rate of work
T	Temperature
h	Specific enthalpy
s	Specific exergy
Ex	Exergy
i	Exergy destruction
Φ	Exergy of heat transfer
ψ	Flow exergy
λ	Reheating pressure ratio
η_r	Regenerator efficiency
η_{th}	Thermal efficiency
η_{ex}	Exergy efficiency
T_{sc}	Degree of supercooling
T_{ppe}	Pinch point temperature difference in the evaporator
η_p	Pump isentropic efficiency
η_t	Turbine isentropic efficiency
<i>Abbreviations</i>	
ORC	Organic Rankine Cycle

BORC	Basic Organic Rankine Cycle
RORC	Reheating Organic Rankine Cycle
IORC	Internal Regenerative Organic Rankine Cycle
CRIORC	Combined Reheating Internal Regenerative ORC
AI	Artificial intelligence
ML	Machine learning
ANN	Artificial neural network
GA	Genetic algorithm
LR	Linear regression
SVR	Support vector regression
DTR	Decision tree regression
RFR	Random forest regression
BPNN	Back propagation neural network
MAE	Mean absolute error
MSE	Mean squared error
MRE	Mean relative error

Subscript

i	inlet
o	outlet
cv	Control volume
0	Atmospheric state
HS, h	Heat source

f	fluid
EVAP	Evaporator
TBN	Turbine
PUMP	Pump
CND, Con	Condenser
REH	Reheater
REG	Regenerator

Table of Contents

CERTIFICATE OF APPROVAL	II
CANDIDATE’S DECLARATION	III
ACKNOWLEDGEMENTS	IV
ABSTRACT	V
LIST OF SYMBOLS	VI
LIST OF FIGURES	XI
1 INTRODUCTION	1
1.1 WASTE HEAT RECOVERY & ORGANIC RANKINE CYCLE (ORC).....	1
1.2 ARTIFICIAL INTELLIGENCE & MACHINE LEARNING ALGORITHM	2
1.3 OPTIMIZATION OF ORC.....	4
1.4 OBJECTIVE OF THIS THESIS	4
1.5 OUTLINE OF THIS THESIS.....	5
2 LITERATURE REVIEW	7
2.1 ORC BASED WASTE HEAT RECOVERY SYSTEMS	7
2.2 SELECTION OF WORKING FLUID.....	8
2.3 OPTIMIZATION OF ORC PARAMETERS	10
2.4 USE OF AI FOR OPTIMIZATION PURPOSE.....	12
3 ARTIFICIAL INTELLIGENCE AND OPTIMIZATION ALGORITHM	15
3.1 ARTIFICIAL INTELLIGENCE ALGORITHM	15
3.1.1 <i>Machine Learning Algorithm</i>	15
3.1.1.1 Linear Regression (LR).....	16
3.1.1.2 Support Vector Regression (SVR)	18
3.1.1.3 Decision Tree Regression (DTR).....	20
3.1.1.4 Random Forrest Regression (RFR)	22
3.1.2 <i>Deep Learning: Back Propagation Neural Network (BPNN)</i>	25
3.1.3 <i>Evaluation Metrics</i>	28
3.1.3.1 Mean Absolute Error (MAE)	28
3.1.3.2 Mean Squared Error (MSE)	29
3.1.3.3 Mean Relative Error (MRE).....	29
3.1.3.4 R² value	29
3.2 OPTIMIZATION ALGORITHM: GENETIC ALGORITHM	30
4 THERMODYNAMIC MODELLING	33
4.1 FUNDAMENTAL THERMODYNAMIC EQUATIONS	33

4.1.1	<i>Mass Balance Equation</i>	33
4.1.2	<i>Energy Balance Equation</i>	34
4.1.3	<i>Exergy Balance Equation</i>	35
4.2	PROPOSED CYCLE CONFIGURATIONS	36
4.2.1	<i>Basic organic Rankine cycle (BORC)</i>	36
4.2.2	<i>Reheating Organic Rankine Cycle (RORC)</i>	37
4.2.3	<i>Internal Regenerative Organic Rankine Cycle (IORC)</i>	38
4.2.4	<i>Combined Reheating Internal Regenerative Cycle (CRIORC)</i>	39
4.3	COMPONENT WISE ENERGY AND EXERGY BALANCE EQUATIONS	39
4.3.1	<i>Evaporator</i>	39
4.3.2	<i>Turbine</i>	40
4.3.3	<i>Pump</i>	41
4.3.4	<i>Condenser</i>	41
4.3.5	<i>Reheater</i>	42
4.3.6	<i>Regenerator</i>	42
4.4	OVERALL SYSTEM ANALYSIS & PERFORMANCE INDICATOR.....	43
4.5	ESTIMATION OF EVAPORATOR OPERATING CONDITIONS WITH ‘TARGET-TEMPERATURE LINE’ METHOD	43
5	RESULTS AND DISCUSSION	47
5.1	THERMODYNAMIC MODELLING ASSUMPTION	47
5.2	SELECTION OF POTENTIAL WORKING FLUID FOR ORC	49
5.3	HYPER PARAMETER SELECTION FOR THE ML ALGORITHMS.....	50
5.3.1	<i>Linear Regression (Lasso)</i>	51
5.3.2	<i>Support Vector Regressor</i>	52
5.3.3	<i>Decision tree regression</i>	54
5.3.4	<i>Random forest regression</i>	56
5.4	SELECTION OF ML ALGORITHM & DETERMINATION OF MODEL PERFORMANCE METRICS FOR INDIVIDUAL WORKING FLUID.....	58
5.5	HYPER PARAMETERS & PERFORMANCE METRICS FOR INDIVIDUAL WORKING FLUIDS FOR BPNN	68
5.6	COMBINED MODEL PERFORMANCE PREDICTION.....	71
5.7	SENSITIVITY ANALYSIS AND MULTI PARAMETER OPTIMIZATION	72
5.7.1	<i>Sensitivity analysis for cycle parameters</i>	73
5.7.2	<i>Multi parameter optimization of the ORC configurations</i>	81
6	CONCLUSION	89
	REFERENCE	91

List of Figures

Figure 3.1	Schematic diagram of linear regression.....	18
Figure 3.2	Schematic diagram of SVR algorithm.....	19
Figure 3.3	Schematic diagram of decision tree regressor	21
Figure 3.4	Schematic diagram of Random forest algorithm	23
Figure 3.5	Schematic diagram of BPNN of this study.....	26
Figure 3.6	Flowchart of genetic algorithm.....	31
Figure 4.1	Schematic diagram of BORC	36
Figure 4.2	Schematic diagram of RORC	37
Figure 4.3	Schematic diagram of IORC.....	38
Figure 4.4	Schematic diagram of CRIORC	39
Figure 4.5	Graphical demonstration of the target temperature line construction [95].....	45
Figure 5.1	Effect of regularization parameter on the performance of Lasso regression for (a) thermal efficiency (b) exergy efficiency	52
Figure 5.2	Effect of epsilon on the performance of support vector regression for (a) energy efficiency (b) exergy efficiency	53
Figure 5.3	Effect of maximum tree depth on the performance of decision tree for (a) thermal efficiency (b) exergy efficiency	55
Figure 5.4	Effect of the number of trees on the performance of Random forest regressor for (a) thermal efficiency (b) exergy efficiency.....	56
Figure 5.5	Comparison of predicted efficiency by ML with simulated result of BORC, (a) thermal efficiency, (b) exergy efficiency.....	59
Figure 5.6	Comparison of predicted efficiency by ML with simulated result of RORC, (a) thermal efficiency, (b) exergy efficiency.....	59
Figure 5.7	Comparison of predicted efficiency by ML with simulated result of IORC, (a) thermal efficiency, (b) exergy efficiency.....	59
Figure 5.8	Comparison of predicted efficiency by ML with simulated result of CRIORC, (a) thermal efficiency, (b) exergy efficiency.....	60

Figure 5.9	Performance metrics of ML algorithms for BORG with R227ea as working fluid	60
Figure 5.10	Performance metrics of ML algorithms for BORG with RC318 as working fluid	61
Figure 5.11	Performance metrics of ML algorithms for BORG with R236fa as working fluid	61
Figure 5.12	Performance metrics of ML algorithms for BORG with R236ea as working fluid	62
Figure 5.13	Performance metrics of ML algorithms for BORG with R245fa as working fluid	62
Figure 5.14	Performance metrics of ML algorithms for BORG with R123 as working fluid	63
Figure 5.15	Performance metrics of ML algorithms for BORG with R113 as working fluid	63
Figure 5.16	Performance metrics of ML algorithms for BORG with Cyclopentane as working fluid	64
Figure 5.17	Performance metrics of ML algorithms for BORG with Cyclohexane as working fluid	64
Figure 5.18	Box plot of thermal efficiency and heat source temperature for four cycle configurations	74
Figure 5.19	Box plot of exergy efficiency and heat source temperature for four cycle configuration	74
Figure 5.20	Effect of pinch point temperature difference on thermal efficiency for four cycle configuration	75
Figure 5.21	Effect of pinch point temperature difference on exergy efficiency for four cycle configuration	75
Figure 5.22	Effect of degree of supercooling on thermal efficiency for four cycle configuration	76
Figure 5.23	Effect of degree of supercooling on exergy efficiency for four cycle configuration	76
Figure 5.24	Effect of condensing temperature on thermal efficiency for four cycle configurations	77
Figure 5.25	Effect of condensing temperature on exergy efficiency for four cycle configurations	77

Figure 5.26	Effect of reheating ratio on thermal efficiency for two cycle configuration	78
Figure 5.27	Effect of reheating ratio on exergy efficiency for two cycle configuration.....	78
Figure 5.28	Effect of regenerator efficiency on thermal efficiency for two cycle configuration	78
Figure 5.29	Effect of regenerator efficiency on exergy efficiency for two cycle configuration	78

List of Tables

Table 5-1	System Simulation Parameters of ORC.....	48
Table 5-2	Thermo-physical Properties of working fluids	49
Table 5-3	Optimal parameters for Lasso regressor with performance indicator.....	52
Table 5-4	Performance of SVR for different kernel functions.....	53
Table 5-5	Optimal parameters for support vector regressor with performance indicator	54
Table 5-6	Default values of hyper parameters for decision tree regression.....	54
Table 5-7	Performance of Decision tree for different split criterion.....	55
Table 5-8	Optimal value of maximum tree depth for decision tree along with performance indicator	56
Table 5-9	Optimal value of number of trees for decision tree along with performance indicator	57
Table 5-10	Selected hyper parameters for the studied algorithms	57
Table 5-11	Performance metrics of RFR for RORC configuration	65
Table 5-12	Performance metrics of RFR for IORC configuration.....	66
Table 5-13	Performance metrics of RFR for CRIORC configuration	67
Table 5-14	Model parameters for the studied BPNN.....	67
Table 5-15	Performance metrics of BPNN for BORC configuration	68
Table 5-16	Performance metrics of BPNN for RORC configuration	69
Table 5-17	Performance metrics of BPNN for IORC configuration.....	70
Table 5-18	Performance metrics of BPNN for CRIORC configuration	71
Table 5-19	Performance metrics of ANN models for thermal efficiency prediction.....	72
Table 5-20	Performance metrics of ANN models for thermal efficiency prediction.....	72
Table 5-21	Optimization limit for heat source temperature and reheating ratio	81
Table 5-22	Genetic algorithm parameters.....	82
Table 5-23	Optimized parameters for R227ea CRIORC	84
Table 5-24	Optimized parameters for RC318 CRIORC	84

Table 5-25	Optimized parameters for R236fa CRIORC.....	85
Table 5-26	Optimized parameters for R236ea CRIORC	85
Table 5-27	Optimized parameters for R245fa CRIORC.....	86
Table 5-28	Optimized parameters for R123 CRIORC.....	86
Table 5-29	Optimized parameters for R113 CRIORC.....	87
Table 5-30	Optimized parameters for Cyclopentane CRIORC	87
Table 5-31	Optimized parameters for Cyclohexane CRIORC.....	88

1 Introduction

1.1 Waste Heat Recovery & Organic Rankine Cycle (ORC)

Waste heat recovery is an efficient and reliable technology of utilizing waste heat generated in various industrial processes. This process is popular worldwide nowadays not only because of its ability of optimizing energy consumption but also for its effectiveness to reduce carbon footprints of traditional fossil fuel based industrial system. Like any typical heat exchanging process, two distinct waste heat recovery technologies are generally implemented in any industrial process-direct recovery and indirect recovery. The former process utilizes the waste heat directly while a heat recovery evaporator or heat exchanger is commonly used in the later process. In industrial approach, generally a suitable thermodynamic cycle is adopted to implement the mentioned heat exchanging process. Several thermodynamic cycles like Rankine cycle, Brayton cycle, Kalina cycle, Stirling cycle, refrigeration cycle, etc. are the most common techniques for utilization of the waste heat. Among them Rankine cycle is the most common technology because of its simple structure, reliability, and higher thermal and exergy efficiency.

In traditional Rankine cycle, water is widely used as the working fluid for its easily availability and relatively cheap economy. This conventional arrangement is known as Steam Rankine cycle (SRC) and is a well-established technology in the traditional medium or large scale power plant. However, the thermodynamic performance of an Rankine cycle is heat source temperature dependent and SRC is suitable for heat source temperature of over 500 °C. Moreover, at present low and medium grade heat sources like solar energy, geothermal energy, biomass energy, wind energy, waste heat recovery from running power plants, etc. are gaining attention because of the ongoing energy crisis throughout the world. The working temperature of these sources can vary from 90 °C to roughly 500°C. For these type of low and medium grade heat source, the performance of SRC falls significantly and complexity is introduced to the system because of the fluid machineries associated [1]. Therefore, selection of suitable working fluid is crucial to the efficient operation of low and medium grade power plant infrastructures and is a popular research topic nowadays.

In organic Rankine cycle (ORC), tradition SRC is modified by replacing the working fluid with suitable organic fluids. The working principle of it is necessarily similar to SRC. In its basic configuration, there are four steps involved. The working organic fluid is pumped to the evaporator, where it gains energy by being heated from the heat source. After that, some portion of this energy is extracted by expanding the fluid into the turbine, and the rest of it is rejected in

the condenser to complete the cycle. Sometimes necessary adjustments are made to increase the efficiency of the cycle or to operate it under optimal condition like reheaters, regenerators, etc.

For low grade heat utilization, ORC shows better performance than SRC in various aspects. Because of the high saturation and superheating temperature of water, superheating at higher temperature is necessary to avoid two phase expansion phenomena in turbine, which can introduce corrosion at the existing fluid machineries' blade otherwise. Organic fluids, on the other hand, is dry in nature, and can work in single phase in relatively low temperature because of their low boiling point temperature. Thus, the thermal efficiency of the ORC is relatively high than SRC for same working temperature because of the reduction of superheating process. Further, better temperature matching is achieved in the evaporator for lower temperature difference between the hot and cold fluid, which leads to less exergy destruction in turn [2].

ORC configuration is also a feasible option to design simple fluid machinery structures mainly because of the thermodynamic properties of typical organic fluids. The latent heat of vaporization of the working fluids play a key role in determining the mass flow rate of it as the flow rate is decreased with the increase of the latent heat for same operating conditions (heat source temperature and pinch point temperature difference). However, because of the comparatively smaller latent heat of organic fluids, the mass flow rate is usually larger. Therefore, traditional technologies can be applied in designing the fluid machineries without any complexities which in turn makes the arrangement economically viable. Further, the size of the fluid machineries (turbines) depends on the expansion ratio of the working fluids and smaller machineries are achievable for fluids with lower expansion ratio. Organic fluids match this criteria as the saturation pressure of them is comparatively low which results in low expansion ratio across the evaporator. Because of this, fewer expansion stage in turbine work is required which results in compact machineries. Moreover, ORC can also eliminate the requirement of superheating the fluid before turbine expansion and can only introduce regeneration work between the expander and the pump. Thus, it is more efficient than the traditional SRC.

Organic fluids can condense under positive pressure compared to steam which usually requires negative condensing pressure for same environmental condition. Thus arrangements for vacuum pressure is eliminated which in turns results in compact pump, and connecting pipe fittings.

1.2 Artificial Intelligence & Machine learning Algorithm

Artificial intelligence (AI) is the driving force of today's smart machines intended to perform various decision dependent process by mimicking the concept of human intelligence formulation. This intelligence structure is formulated by learning from related real life generated

data. Data analysis is vital to AI as it helps analyze data and find existing or suitable correlations among them. AI is built targeting the cognitive learning process of human, from learning to analyzing data and finally making necessary adjustment based on the application. In the learning process various algorithms are available for analyzing the big data in a systematic manner. After selecting the suitable algorithm, necessary adjustment and tuning is made to get best prediction performance from the AI. At present, the use of AI is increasing in every sectors of engineering as it can provide detail information for a comparatively complex task and replace the manual human labor with precision and accuracy. Fields like robotics, computer vision, machine learning, automation, etc. are completely built on the concept of AI.

Machine learning (ML) is a specialized branch of AI that is used to predict the outcome of any modelling scheme based on statistical analysis. Based on the analysis from a given dataset, ML predicts the outcome of a newly imposed input condition eliminating the recreation of the dataset as well as the previous operations again. ML can broadly be classified into two categories, supervised and unsupervised machine learning. The supervised version of ML is a guided training as the dataset is labelled here unlike the unsupervised one, where the algorithm first tries to find any existing correlations between the data. In thermodynamic analysis, supervised learning is preferred mostly as the training parameters are known here. Supervised learning can further be classified into classification and regression problem. The former is applicable for discrete output type while the later can produce output of any continuous value. For thermodynamic application, the output data type is continuous mostly, so regression scheme is mostly preferred. Several ML algorithms are in practice. Among them the most common ML algorithms are linear regression, support vector machine, decision tree, random forest etc.

Recently deep learning is gaining popularity over conventional ML scheme. Deep learning is a specialized version of ML where algorithms mimicking the human brain structure are used. The inherent characteristics of deep learning can significantly improve the performance of a machine learning scheme. The prime example of deep learning is artificial neural network, which is widely used in engineering related problems nowadays.

In recent years, AI algorithms are integrated with traditional physics driven analysis to predict the outcome of the analysis in a simpler and less-time consuming way. Owing to the improvement in data science and computer architecture to handle big data, AI is gaining popularity to replace the traditional analytic approach. In ORC analysis in the similar fashion, AI algorithms are playing crucial parts in predicting various thermodynamic aspects such as the prediction of thermo-chemical properties of the fluids, prediction of various state properties, prediction of cycle efficiencies like thermal and exergy efficiency etc. As a result, AI is being considered as a viable replacement of traditional thermodynamics based analysis and used to

optimize various ORC cycle aspects. The flexibility of AI approaches are making the ORC optimization process easier and less time consuming.

1.3 Optimization of ORC

The thermodynamic performance of ORC greatly depends on the operating parameters, cycle configurations, and the working fluid selection. Because of the flexibility of choosing these parameters and configurations, optimization of the cycle is crucial to the proper execution of the cycle. For optimization purpose, an objective function is required based on which the scheme is built and this process is known as single objective optimization. However, for complex thermodynamic problems, multi objective optimization can be required. Conventionally, more attention is given to the energy and exergy output from the cycle. Therefore, energy and exergy efficiency are chosen as the objective function for the optimization algorithm in multi objective manner or in a single manner combining the two functions. This optimization is performed against some deciding cycle parameters like evaporator pressure or temperature, turbine and pump efficiency, pinch point temperature difference, regenerator efficiency, reheating ratio, etc. Again, usually the working fluids are pre-screened before optimization but sometimes they can be the deciding factors for optimization purpose. Further, choosing a cycle configuration can be an approach for optimization scheme, though few practice is available in literature.

For optimization purpose, various algorithms are in practice, but the most popular are the heuristic ones like genetic algorithm, particle swarm optimization, etc. These algorithms initially starts from a random solution and improve it in every step to reach the optimized solution. Heuristic methods can quickly reach the local optimization solution but sometimes fail to address the global solution. However, with proper tuning of the operation parameters, these algorithms can be a viable option to address ORC problems.

For its operation, optimization algorithms calculate the objective function in each steps. However, these objective functions are formulated using the thermodynamic concept of the cycle. Therefore, in each step, the algorithm has to undergo complex calculation process which is time consuming and demands rigorous computer architecture. The use of AI can be a feasible option in this respect. The intended AI scheme can be used as a surrogate model for calculating the objective function, bypassing the requirements of traditional rigorous calculation. Thus, the optimization process can be smooth and run in a smooth manner. So, combining the AI and the existing optimization scheme, a newer approach of optimization can be a unique option to address ORC analysis.

1.4 Objective of this Thesis

The primary goal of this study is to present an efficient and less time consuming optimization framework that incorporates an ANN scheme to predict efficiency values for 4 ORC configurations and nine working fluids and utilize the predicted result to optimize the parametric value against the energy and exergy efficiency.

The objectives of this study can be summarized as below:

- a) To develop four distinct thermodynamic models namely BORC, RORC, IORC, and CRIORC with nine of the pre-selected working fluids for waste heat recovery purpose.
- b) To construct a dataset containing parametric data and their corresponding efficiency values from the abovementioned developed model in order to train the ANN framework.
- c) To select a suitable ML scheme out of four common frameworks with the highest prediction performance based on the constructed dataset.
- d) To formulate an ANN scheme with the previously selected ML algorithm and a pre-selected BPNN scheme
- e) To perform multi-objective optimization (considering thermal efficiency and exergy efficiency) of the ORC using the formulated ANN scheme as the proxy model to predict objective function values in an efficient and less time consuming manner.

1.5 Outline of this Thesis

The aim of this work is to provide an efficient alternative to traditional thermodynamic modelling and optimization of ORC. To fulfill this aim, this thesis is structured in a way that it can clearly discuss the importance of this particular topic and demonstrate the proper methodologies to explain the modelling procedure.

Chapter 2 begins with the literature review of the most recent WHR technologies used in ORC modelling. The traditional and AI approaches to select suitable working fluids are discussed then. The recent works regarding optimization in ORC are discussed afterwards. Finally, the literature review regarding AI integration in ORC are discussed to demonstrate the current progress in this field and scopes of improvement.

In chapter 3, both the AI algorithms and optimization algorithm used in this study are described. Four distinct ML algorithm along with a deep learning BPNN algorithm are discussed under AI algorithm section. In optimization algorithm section, the genetic algorithm is explained to give a overview of the optimization process of this study.

The thermodynamic modelling of the proposed four ORC configurations are discussed in chapter 4. Starting with the thermodynamic formulation of the cycle process, the component-wise and overall energy and exergy analysis are discussed. The adoption of a novel target temperature line method is also explained in the chapter.

In chapter 5, the results from the modelling and optimization of the ORC are discussed. Starting with the hyperparameter tuning of the four ML algorithms, the most suitable ML algorithm is screened in this chapter. After that, a comparative analysis of the ML algorithm with BPNN is demonstrated for single fluid and combined fluid arrangement. Finally, with the established AI scheme, a framework of multi parameter optimization is discussed and a comparative analysis between the methods are shown.

The key findings of this study are discussed in chapter 6.

2 LITERATURE REVIEW

2.1 ORC Based Waste Heat Recovery Systems

In recent years, more attention is being paid to both energy saving and pollutant emission control due to the growing demand for energy consumption worldwide. Owing to the increasing trend in energy price and associated environmental challenges, focus is concentrated on effectively utilizing existing low and medium grade thermal energy sources such as industrial waste heat energy, ocean thermal energy, solar energy, biomass energy, etc. Among them waste heat is the most common form of industrial low or medium grade heat. Waste heat can mainly be classified into three categories, high grade heat (Over 650 °C), medium grade heat (230 °C – 650 °C), and low grade heat (<230 °C)[3]. Currently available technologies for the utilization and recycle of waste heat include organic Rankine cycle(ORC)[4], Brayton cycle[5], supercritical Carbon Di-oxide cycle[6], Kalina cycle[7], absorption refrigeration cycle[8], Stirling cycle[9] etc. Among the available technologies, ORC shows potential in recovering low and medium grade heat because of its reliability, flexibility in configuration, and thermo-economic advantages.

Therefore, searching for optimized configurations of ORC is becoming an international hot research topic in recent years. Several aspects are available for determining optimal design criteria for ORC including the proper selection of the working fluid, proper selection of the cycle configuration, optimization of the existing cycle parameters, optimization of working parameters and sizing of a particular cycle component, etc.[10].

At present, most of the works on ORC are based on either mathematical thermodynamic modeling[11–14] or experimental observation[15–18]. Li et al. [19]considered temperature fluctuations and inherent random behavior of heat source and proposed a novel 1-stage 5-level whole-system to meet this challenge. Zahedi et al. [20] adopted a four metric evaluation of an ORC system combined with solar, steam Rankine cycle and biogas. Apart from the core thermodynamic efficiencies like energy and exergy, their work also concentrated on economic and environmental aspect of ORC. Similar approach of exergoeconomic assessment was investigated by Nondy et al. [21] for four different ORC configurations. Mieloszyk et al. [22] experimented with a FBG sensor to improve the micro turbine performance of the ORC. Goma et al. [23] worked with the hybridization of a solar collector with ORC to investigate the economic and energy efficiency of the system with R245f as the working fluid. Similar approach of integration of ORC with solar collector was adopted by Bellos et al. [24] for low grade waste heat recovery. From their investigation, the system energy efficiency is found to be

maximum around 20% when toluene is used as the working fluid. A novel transient response control strategy of ORC was proposed by Marchionni et al. [25]. They adopted four proportional integration control schemes to analyse the behavior of an ORC equipped with radial turbine.

The mentioned theoretical and experimental methods lack viability when the design process becomes complex with more design variables and constraints. Besides, these methods are highly knowledge-intensive as proper selection of working fluids and cycle components depend on the professional knowledge of related engineers. Moreover, owing to high dependency on heat source temperature, mass flow rate, sink temperature, etc., these methods are case sensitive and needed to be redesigned with the change of application.

Due to the growing adaptability and development of artificial intelligence (AI) in data-driven problems, a trend to integrate energy system modelling with AI is gaining popularity, especially in modelling process where sufficient training data is available. Following this trend, researchers are focusing on the construction of suitable AI model with the help of machine learning and other available algorithm which can optimize the performance of ORC system. Currently, AI is used in several aspects of the design development of an ORC system such as selection of proper working fluids[26], selection of optimal cycle configuration[27,28], and multi parametric optimization of the cycle[29,30]. In some cases, to attain more accuracy as well as reduce computational time, hybrid models are used combining traditional approaches and AI techniques.

2.2 Selection of working fluid

Selection of working fluid is crucial for the design of an ORC system. The thermo-physical properties of the working fluid attribute to the determination of system parameters such as range of operating temperature, size of the heat exchanging area in heat exchanger, condenser, or regenerator, size of the turbo machinery like pump and turbine, green house gas emission control criteria etc. The important physical and chemical properties in selection of a optimal working fluid thus include critical temperature and pressure, boiling temperature and pressure, thermal conductivity, ozone depletion potential (ODP), global warming potential (GWP) etc.[31].

Traditionally the selection of working fluid are performed manually by experts or engineers with standard heuristic methods based on practical experience and knowledge. In most of the cases, potential working fluids are sorted based on their performance on a pre-designed ORC system. In some cases, component sizing and selection are performed against the list of potential working fluids to obtain optimum thermo-economic efficiency. Along with maintaining the

standard GWP and ODP protocol, different heuristic methods are in practice such as near critical region triangle method[32], Jacob number method[33] etc. The manual selection procedure of these methods make the job tedious for researchers because of the wide range of availability of the working fluids. Besides, these models require frequent redesigning owing to the emergent of new potential working fluids.

Selection of suitable working fluid largely depends on the physical and chemical properties of the fluid and their effects on the cycle which can be calculated via different mathematical equations or experiment. Because of the availability of wide range of working fluid dataset, a new trend of AI based data-driven fluid property prediction method is in practice which can be implemented as a surrogate method to reduce the calculation procedure and time in traditional heuristic approaches.

Some of the AI research work on potential working fluid selection is based on predicting thermodynamic properties from other related thermodynamic properties. Huster et al.[34] trained an artificial neural network (ANN) model with 37 working fluid out of 122 preselected fluids from the thermodynamic property library CoolProp to perform deterministic global optimization in a reduced-space formulation of a simple ORC cycle using waste heat from a diesel truck. The goal of this model was to predict the temperature, thermal conductivity, enthalpy, density, viscosity, and Prandtl number from input parameters (pressure and entropy). This work was further extended to investigate the thermo-economic behavior of a transcritical ORC cycle[35]. Recently, Peng et al. [36] developed a machine learning model to predict the performance of a BORC and a RORC using data of 106 working fluids. Four basic processes occurring in these cycles were modelled separately with an ANN model based on which other cycle performance parameters could be calculated.

Many of the working fluids can be classified into several functional group based on their similarity in molecular structure. Standard grouping methods such as group contribution method (GCM) [37], molecular-based equations of state method [38], etc. can be applied to generate property of old and new working fluid of the same group. Recently with the advent of computer aided molecular design (CAMD), these methods are integrated with AI to quickly and accurately predict the thermodynamic properties of the working fluids based on their grouping structure, equations of state and associated data generated by them. CAMD can be used to even predict the feasibility of currently non-existent working fluid application in ORC system.

The concept of CAMD in ORC application was first introduced by Papadopoulos et al. [39], where they used CAMD to screen suitable working fluid for an ORC system. This work was further extended to investigate the viability of CAMD in fluid mixture application. Similar work can be found in the work of Su et al. [40,41].

Recently, Y.Chen et al. [42] adopted a CAMD model for the proper screening of the working fluid to improve ORC cycle performance. For ANN training purpose, this ANN-GCM based model used conventional GCM generated thermo-physical properties as output corresponding to input molecular group indexing number and gained more flexibility in calculation timing and determining properties of new working fluids. An improved work of this study was conducted by Peng et al. [43] where instead of one ANN-GCM model, three different ANN-GCM models were used to evaluate and predict the performance of a subcritical ORC configuration.

2.3 Optimization of ORC Parameters

The most common practice of optimization of an existing ORC system is to select suitable operating parameters to gain optimal efficiencies from the cycle. Operating parameters refer to that parameters of a cycle which can be moderated according to the requirement. Basic operating parameters include pinch point temperature difference in heat exchangers (evaporator and condenser)[44,45], mass flow rate of the working fluid [46], degree of superheat [47], degree of subcooling[48], evaporating and condensing temperature and pressure[49–51] etc. For a fixed cycle configuration with definite heat source temperature and mass flow rate, optimization of operating parameters is the only way of improvement and proper adjustment of parameters can result in better cycle performance.

The general steps of any optimization scheme follow some sequential procedure including determining the objective function, deciding the decision variables to be optimized along with the constraints, finding out suitable mathematical or heuristic optimization model, constructing this model according to the decision variable and objective function and finally running this model to find out optimized parameters. In choosing objective function, single aspect (single-objective optimization) or multiple aspects (multi-objective optimization) are considered according to the scope of the problem. Some common aspects include product indicator like net power output [52], efficiency indicator like thermal efficiency and exergy efficiency, economic indicator like installation and investment cost [53], net annual profit [54], levelized energy cost[55], environmental impact indicator like emission characteristics of waste gas [56] etc.

Out of existing operating parameters, choosing the most impactful parameters is crucial to the reduction of calculation time of the optimization process. A common practice is to select the parameters based on previous and practical knowledge. Some researchers focus on investigating the viability of pre-selected operating parameters and screening out the most impactful parameters via sensitive analysis [57–60].

The viability of any optimization scheme depends on the mathematical model of optimization used in it. Traditional mathematical model can't address the non-linear nature of the ORC

system properly, so researchers adopt suitable heuristic optimization algorithm to deal with the complexity of the problem. The genetic algorithm (GA) is the most widely used heuristic algorithm in this respect. The other heuristic algorithm in practice are particle swarm optimization (PSO), artificial bee colony (ABC) etc.

Earlier work on GA focused on single parameter or multiple parameter and single objective optimization. Wang et al. [61] used GA on a R123 ORC system to optimize exergy efficiency against turbine inlet pressure. Andreasen et al. [62] adopted a multi-parameter GA approach to optimize the net power output from five decision parameters. Similar approach of multi parameter single objective optimization are also available in the literature [63–66]

The recent work on GA optimization of ORC focuses on multi parameters and multi objective optimization. Aliahmadi et al. [67] performed a multi-objective optimization to determine optimal superheater temperature difference and figure of merit of a regenerative ORC integrated with thermoelectric generator. A multi objective optimization scheme keeping the net revenue and thermal efficiency as objective function for a heat pump waste heat recovery ORC system was modelled by Shen et al. [68]. Jankowski et al. [69] adopted a Non-dominated Sorted Genetic Algorithm (NSGA) method to optimize performance parameters net power output, exergy efficiency, and thermal efficiency of a low grade waste heat recovery ORC system. A thermodynamic and economic optimization approach to determine optimal working fluid pair was proposed by Xia et al. [70] where NSGA was used on a duel loop ORC system. Similar approach of optimization is found in the work of Li et al. [71]. Sadeghi et al. [72] performed a multi objective GA optimization scheme on a combined gas turbine and ORC to find out the effect of thermo-physical and thermochemical recuperation on the combined cycle performance.

Compared to GA, there has been less work on the optimization of ORC using PSO and ABC. Ochoa et al. [73] performed a thermo-economic analysis on a natural gas engine for waste heat recovery using PSO. A flash-binary geothermal cycle was proposed by Zao et al. [74], where the duel pressure ORC binary cycle performance was optimized by PSO to obtain optimal net power output. An economic model to optimize the exergetic performance of a molten carbonated fuel cell integrated ORC system using PSO was proposed by Won et al. [75]. Recently, Sadeghi et al. [76] performed a multi objective optimization to derive maximum thermal and exergy efficiency of an ORC using binary zeotropic mixture.

The calculation of objective or fitness function is the most crucial part of the above mentioned intelligence algorithms. In all of the heuristic methods, the intermediate solutions are tested against the pre-defined objective functions and modified accordingly. In most of the cases, the calculation procedure of the objective function involves calculation of a lot of thermodynamic state properties and related equations. The traditional complex nature of the equation of states to find thermodynamic properties and the nature of the cycle equations make the total calculation

procedure sophisticated and time-consuming. Moreover, to gain more accuracy and address all the decision parameters, a wide range of search space is to be covered, which is time demanding and dependent on computer architecture. So, oftentimes researchers have to compromise the accuracy of the process or the range of decision variables to tackle these disadvantages.

2.4 Use of AI for Optimization Purpose

Recently with the advent of data science and artificial intelligence, researchers are trying to address physical system modelling with data-driven approach. These data-driven models bypass the time consuming calculation of physical variables and equations and find the inherent relationship between input design variables and output objective functions based on the available data derived from mathematical calculation or experiment. Data-driven approaches can be largely classified into machine learning (ML) and deep learning (DL) approaches. In machine learning approaches, various classification and regression learning algorithms are used. The most common classification algorithms are support vector machine (SVM), Decision tree, K-nearest neighbours, Naïve Bayes etc. and common regression algorithms are linear regression, support vector regression (SVR), Random forest regression etc. Deep learning works on artificial neural network (ANN) principle which mimics the function of a human brain neurons. Common deep learning algorithms include back propagation neural network (BPNN), Convolutional neural network (CNN), feed forward neural network, etc.

At present, ANN and SVM are widely used to model an ORC system via data-driven approach because of their higher accuracy and adaptability. Among ANN approach, application of BPNN is common for its easy implementation characteristics, and in dealing with regression problem, SVR is used which is the regression version of SVM.

Most of the literary work on data-driven ORC system modelling approach include the application of ANN. An early study of Arslan et al. [77] discussed the use of ANN in an ORC binary system to predict the value of objective function (power output and pump power)during optimization from five input parameters. Similar approach is found in the work of Rashidi et al. [78] where ANN was used to predict the objective function value for the use in ABC algorithm for a regenerative ORC system.

A multilayer perception (MLP) artificial neural network (ANN) model was used by Massimiani et al. [79] for the global optimization of a small scale regenerated ORC using R1234f as the working fluid. With the training dataset from a thermodynamic model calculated via MATLAB, this ANN model was used to maximize the power output keeping the size of the heat exchanger minimum.

G.Zhao et al. [80] used a BPNN model to predict the optimal high pressure to maximize efficiencies of a transcritical ORC using R1234ze as the working fluid keeping heat source temperature, turbine and pump efficiency as the input parameters. The prediction of the effect of different parameters on thermal and exergy efficiency of the cycle using ANN was also discussed in their work.

Apart from training the ANN with mathematical equation derived training dataset, some works focused on predicting objective function value from experimental data. Among them, Yang et al. [81] used a commercial diesel engine exhaust data to predict the performance of an ORC using a BPNN model. The experimental data were used to predict the effect of different cycle parameters on the power output and the evaporator outlet temperature. Based on this BPNN model, a multi objective optimization was performed to maximize the power output and minimize the evaporator outlet temperature.

Z.-X. He et al. [82] trained a BPNN with 950 experimental dataset from a 3KW ORC experiment platform to predict the effect of six cycle operating parameters on the thermal efficiency and net work output of the cycle. The trained BPNN was then used to optimize the operation parameters for the improvement of performance of the experimental cycle

A regression based predictive model in a BPNN to predict the power output of a cement plant based waste heat recovery system was modelled by Ali et al. [83]. Four input parameters were used to train the predictive model which showed significant agreement with actual cycle data.

To predict efficiently from experimental datasets, some research work focus on the integration of regression algorithm with ANN. For example, Mert et al. [84] investigated the viability of a deep learning(DL) model developed with stepwise multi linear regression algorithm(SMLR) to predict the power output of an ORC system. Trained by the data of a 10KW experimental ORC setup, the DL-SMLR combined model gained acceptable accuracy to predict the power output of the ORC configuration.

There have also been efforts to compare and integrate conventional fuzzy model with ANN. For example, Bayram and Emre[85] developed a prediction model to analyze the effect of four cycle parameters on the efficiency ratio of an ORC with ANN and adaptive neuro-fuzzy (ANFIS) model. The results from both model were compared to assess the viability of these model with the data of five different working fluids.

Contrary to ANN application, there has been fewer works on the application of SVM to ORC modelling system alone. An earlier work of Zhang et al. [86] discussed a predictive model using SVM for set point optimization of a controlled ORC system. A predictive model to estimate the behavior of heat source during the operation of a vehicle engine waste heat recovery system using SVM was developed by Zhang et al. [87].

Besides the conventional data-driven application, a new trend is ongoing to efficiently select the suitable method by comparative analysis and adjusting the deciding parameters accordingly. The efficiency of ML method depends on its inherent characteristics and kernel function, and for ANN application, it greatly depends on the number of hidden layers and selection of activation function. Besides, the procedure of dividing the dataset into test set and training set can effect the performance of these methods. Dong et al. [88] analyzed the feasibility of using SVM and BPNN in predicting the performance of an ORC-LTPG system. Two division method, namely random division method and blocked division method, were used in two kernel functions namely Gauss Radial Based Kernel (RBF) and Linerfunction(LF) in SVM algorithm. Though the SVM model with RBF kernel showed the highest accuracy, in BPNN both the kernels showed promising results for both of the division methods.

A recent study of L.Zhao et al. [89] presented a comparative analysis of AI approaches for the performance analysis and multi objective optimization of four ORC configurations using seven working fluids. Pre-screening of three ML algorithm - decision tree, random forest, and SVR were performed based on their performance and SVR showed the best performance of all. Along with SVR, a BPNN was also used and performance of both of the algorithm were compared. Finally a hybrid method was formed for optimization purpose in GA algorithm.

Very recently principle component analysis (PCA) showed potential in predicting ORC performance. Yan et al. [90] performed a principle component analysis (PCA) on statistically identified key parameters subset dataset of a 10kW scale ORC experimental setup. Two machine learning regression models- Multi-linear regression (MLR) and Support Vector Regression(SVR) along with an ANN model were developed and compared for sorting out four key parameters out of six parameters of the existing setup.

3 ARTIFICIAL INTELLIGENCE AND OPTIMIZATION ALGORITHM

3.1 Artificial Intelligence Algorithm

Artificial intelligence (AI) mimics the working principle of human intelligence. There are multiple branches of AI which work on numerous suitable algorithm to process and analyze data for real life applications. The most crucial of them are machine learning algorithms which are a set of algorithms intended to train computing machines from real life dataset for a particular application. Among machine learning, deep learning is a specialized branch whose primary purpose is to perform AI task mimicking the structure of human brain. Both machine learning and deep learning algorithms can be feasible option for thermodynamic prediction purpose.

3.1.1 Machine Learning Algorithm

Machine learning (ML) is one of the important branches of artificial intelligence that uses statistical method to predict the values of the desired output of any modelling scheme. This algorithm can broadly be divided into supervised and unsupervised machine learning. In the supervised learning process, labeled data are utilized to construct the learning model taking direct feedback from the output during the model training process. In unsupervised learning process on the other hand, no labeled data is used. Instead, this algorithm aims to find hidden correlation and pattern in the given unlabeled data. Usually in thermodynamic process prediction supervised learning method is adopted as the dataset is generally labeled here. Similarly in this study the supervised learning scheme is used as the label of data like heat source temperature, pinch point temperature difference, condensing temperatures, exergy and thermal efficiency etc. are known and utilized as either feature variable or the target variable.

Supervised learning can further be classified into regression and classification analysis. In regression analysis, the output values are continuous, that is any real number can be predicted as the output value. In classification related problems on the other hand, discrete values are obtained in the output. This study deals with continuous value of the output data, as the value of the energy and exergy efficiency can be of any real number. So, to fulfil the prediction purpose satisfactorily and more accurately, regression scheme under the supervised learning technique is adopted in this study.

A good number of regression algorithm is available in literature but all of them are application driven and can yield different evaluation metrics value according to the nature and complexity

of the given data. Moreover, some algorithms can be vulnerable under fitting or over fitting criteria. So, careful selection of the algorithms is crucial for the successful modelling and prediction of the proposed study.

This study first explores the nature of the thermodynamic analysis obtained data under two most common linear regression algorithms which are linear regression algorithm and support vector regression algorithm. Both of the algorithms have their similarities in operations with support vector regression usually giving better accuracy owing to its inherent nature of combining the classification capacity with regression scheme. Therefore, most of the previous works on ORC modelling via machine learning focused on support vector regression owing to its general trend of higher accuracy generation. Additionally, this study also seeks to assess the viability of some common hierarchical ML algorithms for prediction purpose as they are less time consuming in nature and can produce better results if a few hyper parameters are chosen properly. This study first adopts decision tree algorithm which is a simple classical regression and classification scheme. But owing to the data dependent nature of the decision tree scheme, this study further considers an ensemble learning algorithm :the random forest algorithm, which uses the methods of decision tree sorting but usually produces better results as the inherent data dependency of the classical decision tree scheme is eliminated by generating numerous smaller decision tree model and combining them randomly to get better performance.

So, to fully avail the advantages of the traditional machine learning scheme, this study adopts four schemes and they are:

1. Linear Regression algorithm (LR)
2. Support vector regression algorithm (SVR)
3. Decision tree regression algorithm (DTR)
4. Random forest algorithm (RFR)

3.1.1.1 Linear Regression (LR)

Linear regression is the most popular and widely used machine learning algorithm in regression applications because of its simplicity and potential application. Depending on the variables or features, linear regression can be of single variable linear regression or multivariable linear regression. The linear regression starts with the construction of a hypothesis function and updating it continuously during the training procedure with the input data. For updating purpose, intermediate function like the cost function and optimization technique like the least squared function, the gradient descend algorithm etc. are implemented.

The primary objective of linear regression is to construct a function (known as the hypothesis function) which can address all of the data points with minimal error. *Figure 3.1* demonstrates

the construction of the hypothesis line of a LR algorithm. If the features vector and the weight vector are described by X and W respectively, where $X = \{X_1, X_2, X_3, \dots, X_n\}$ and $W = \{W_1, W_2, W_3, \dots, W_n\}$, then the hypothesis function for linear regression can be written as,

$$h(x) = W^T X \quad (3.1)$$

During the training phase of linear regression algorithm, the weight values are adjusted iteratively in order to produce the minimum prediction error. For this purpose, a cost function is constructed which calculates the deviation of the predicted hypothesis function data with the labeled training data.

For n number of input parameters, if the labeled training data vector is Y , then the cost function can be described as,

$$J(W) = \frac{1}{2n} \sum_{i=1}^n \{h(X_i) - Y_i\}^2 + \lambda \sum_{i=1}^n |W_i| \quad (3.2)$$

In the cost function described by equation (3.2), the first term on the right hand side indicates the mean squared error for the given dataset. Here, the deviation from the original data is squared in order to avoid negative value during calculation. Furthermore, the average of the summed squares are calculated to include the effects of all the data points in prediction performance. The second term is called the regularization term where λ is known as the regularization parameter. Without the presence of this regularization term, the linear regression possesses a natural tendency of overfitting the given data which can result in poor prediction accuracy for unknown input dataset. The regularization term checks this phenomena and provide a moderate solution between overfitting and underfitting criteria by its inherent characteristics. Linear regression where this type of regularization criteria is implemented is also known as the Lasso regression. Lasso regression can be of either L1 type or L2 type. This study adopts the L1 type Lasso regression as described by (3.2)

So, the objective of this algorithm is to minimize the value of the cost function $J(W)$ and consequently updating the weight vectors. This objective falls under the optimization operation and any standard optimization scheme can be used here. However, for this purpose, the gradient descend algorithm is the most simple and widely in practice. In this scheme, randomized initial values of the weight vector is assumed first. After that, these values are continuously updated using the following equation,

$$W_j = W_j - \alpha \frac{\partial}{\partial W_j} J(W) \quad (3.3)$$

The function of equation (3.3) is to adjust the gradient in order to reach a local minima. Here, α indicates the learning rate of the model, the value of which should be chosen carefully to prevent overshooting or undershooting. Usually, the value is kept at 0.01.

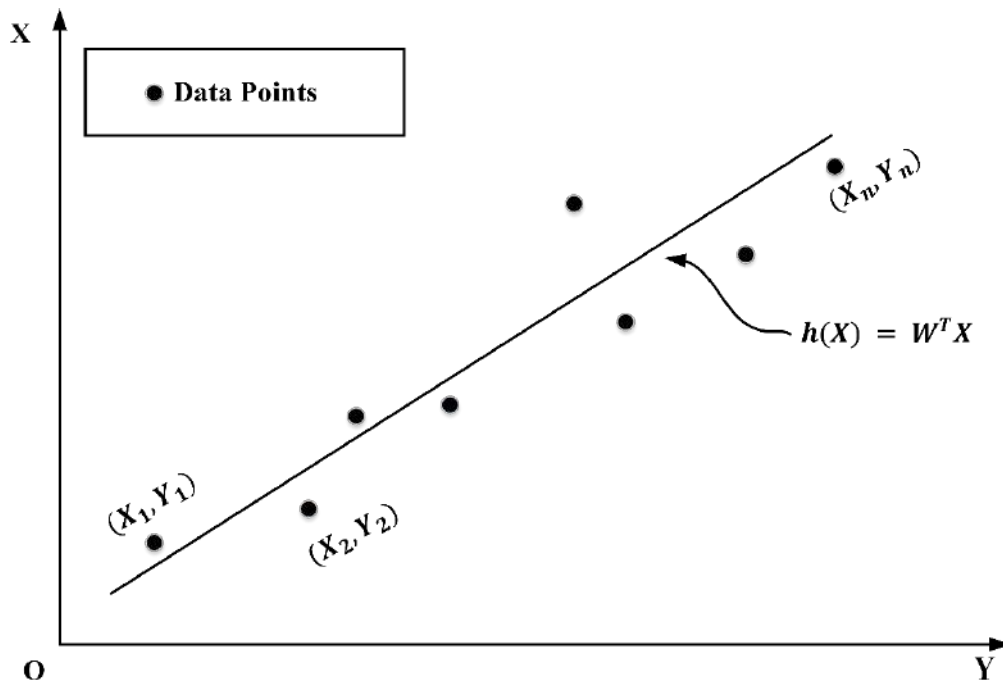


Figure 3.1 Schematic diagram of linear regression

To pacify the calculation process of the gradient descend algorithm for minimizing cost function value, standard optimization techniques can be used, Several schemes are in practice for this purpose like Adagrad, Adam, Adamax, RMSProp etc.

3.1.1.2 Support Vector Regression (SVR)

Support vector regression (SVR) is a specialized version of the support vector machine (SVM) algorithm applied to regression related applications. In SVM classification algorithm, the training dataset is subdivided into several groups according to the class or label of the dataset with the help of support vectors across several hyper planes. But in its linear application, a merge of SVM classification process and linear regression process is applied. Instead of calculating the loss function with respect to the tentative linear hypothesis function as followed by typical linear regression method described in 3.1.1.1, this method tries to minimize an interval band distance on both side of the linear function line and calculates the loss function on or outside of the interval gap line.

Figure 3.2 illustrates the process of SVR. Here, W is the weight vector set, b is the bias set, and X is the input parameters set. At first, a hypothesis line like in the LR algorithm is formulated which maintains the following equation,

$$f(x) = W^T X + b \quad (3.4)$$

In SVR, several sub-regions are formed around this line with the help of boundary lines. In Figure 3.2, the black dots are considered to be included within the decision boundary while the white dots are left outside of the boundary. Now, to form this decision boundary region at a distance of ϵ from $f(x)$, the boundary lines should follow the following equations,

$$\text{Boundary line} = \begin{cases} W^T x + b = -\epsilon \text{ (negative boundary line)} \\ W^T x + b = \epsilon \text{ (positive boundary line)} \end{cases} \quad (3.5)$$

So, the decision boundary region can be defined as,

$$-\epsilon < Y - W^T x + b < \epsilon \quad (3.6)$$

The value of ϵ is the error value which determines the number of support vectors as well as the tolerance limit for SVR. So, the objective of this algorithm is to find best fit lines that construct the boundary of the ϵ error or decision boundary region, and the data points outside of the region is considered in the cost function analysis.

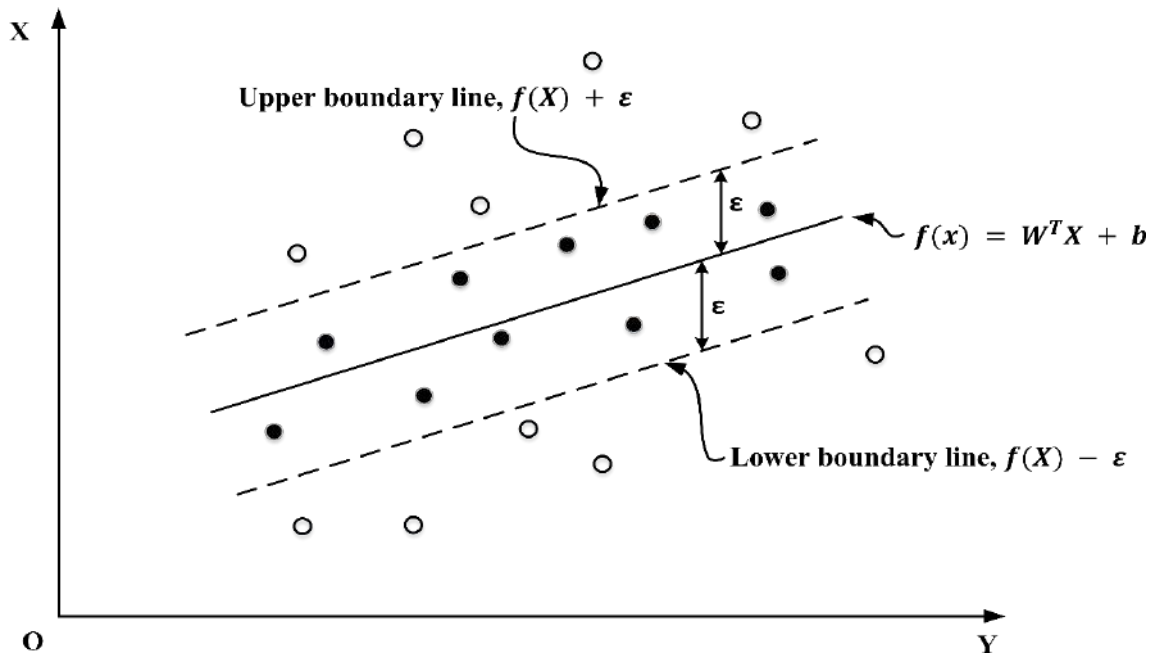


Figure 3.2 Schematic diagram of SVR algorithm [89]

If Y_i is the actual value of each data point, then the loss function for a SVR model can be derived by combining the linear regression loss function with a ϵ -insensitive loss function I_z as,

$$I_z = \frac{1}{2} \|W\|^2 + C \sum_{i=1}^n I_z(f(X_i, Y_i)) \quad (3.7)$$

Where, C is the SVR regularization parameter, which controls the margins between the SVR hyperplane and input dataset. A larger value of C usually obtains a better classification characteristics, by minimizing the value of $|W|$ and therefore obtaining a better prediction capability.

I_z controls the interval gap of the SVR model. For data points within the decision region (shown by black dots) the value of it is 0. Again, for data points on the edge or beyond the interval gap, the loss function is calculated.

The goal of this model is to minimize the loss function and obtain an optimum value of W and b . From these equations, it is evident that value of C and ϵ play major role in determining the loss functions and can be used for hyper parameter tuning.

Additionally, kernel function plays a vital role in the optimization process of the optimizer. For mapping the data points at higher level and the ease of linear separation, several kernel functions are in practice like radial basis function (RBF), polynomial kernel, Laplace RBF kernel, linear kernel etc. Therefore, the viability of these kernel function should be tested by hyper parameter tuning. The value of ϵ defines the support vector regions and a lower value of it tends to improve the model performance. However, it also increases the computational time and complexity. Therefore, an optimal value should be chosen in hyper parameter tuning process.

3.1.1.3 Decision Tree Regression (DTR)

Decision tree regression algorithm is an ML algorithm used for both regression and classification problem and often is labeled as Classification and Regression Tree (CART). In this statistical scheme, a decision tree which is a hierarchical tree like structure is constructed with decision\split nodes and leaf\terminal nodes from a root node containing all data or feature points. The tree continues to grow during the algorithm's learning process and can be expanded upon the complexity of the given data. The fed data is flown from the decision nodes to the leaf nodes in a top-to-down fashion based on some deterministic test function applied in each decision branch. Usually the data are split at each branch based on a binary decision function.

Figure 3.3 demonstrates the schematic of a DTR process. Let, X_i be the input parameter vector with m features defined as,

$$X_i = \{X_{i,1}, X_{i,2}, X_{i,3}, \dots, X_{i,m}\}. \quad (3.8)$$

For total n number of observation or data points, let the predictor be Y described as

$$Y = \{Y_1, Y_2, Y_3, \dots, Y_n\} \quad (3.9)$$

In order to initiate a decision tree, the input parameters are split first into two parts according to a threshold value of splitting. After that, each branch is split like this similar fashion until a terminal value is reached at the node.

Let vf be a feature variable and th be the threshold value for a branch. A decision node is denoted by t , and γ presents a candidate split which is feature variable and threshold value dependent and is denoted by $\gamma = (vf, th)$

The left side of this γ candidate split, Q_l , follows the given condition,

$$Q_l(\gamma) = (x, y) | x_{vf} \leq th_t \quad (3.10)$$

Similarly, the right side of the γ candidate split, Q_r , follows the complementary condition which is,

$$Q_r(\gamma) = (x, y) | x_{vf} > th_t \quad (3.11)$$

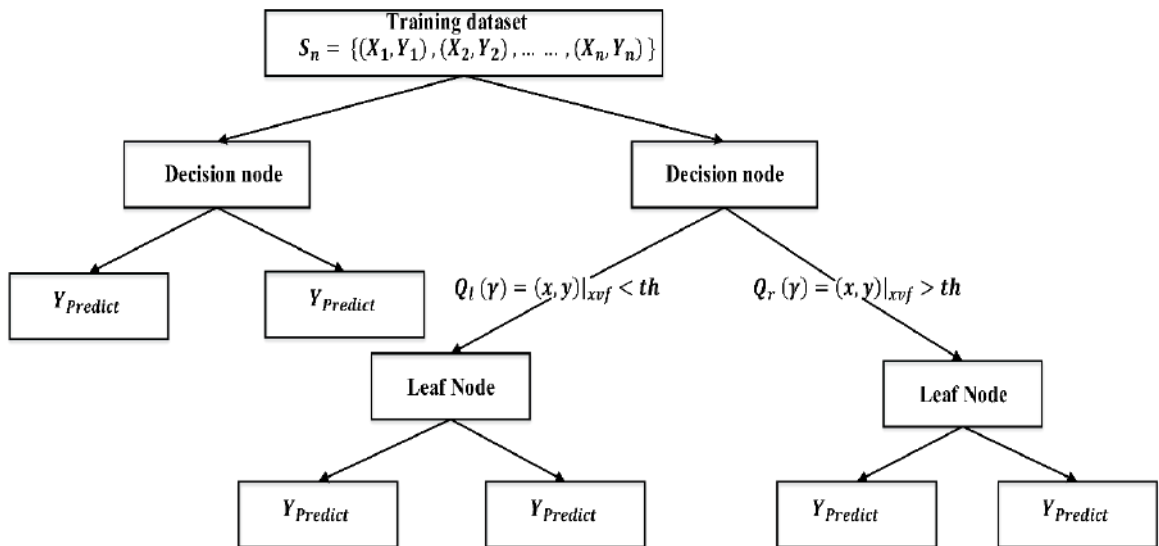


Figure 3.3 Schematic diagram of decision tree regressor

In each terminal node, single or multiple values of the predictor can be reached. As this scheme deals with regression related data, the mean value of all the predictor at the terminal is taken as

the model output from this node. So, if total n number of data/sample is present at any node t , the predicted terminal node value will be,

$$Y_t = \frac{1}{n} \sum_{i=1}^n Y_i \quad (3.12)$$

The choice of the threshold value th and feature variable vf for each split is crucial for the performance of this algorithm. For the selection of these value and variable, a fitness function is utilized. As this is a regression scheme, any regression performance metric can be used like MSE, MSE, R^2 , etc. Let the fitness function is described as S . Based on this fitness function, an impurity function at the node t is described as,

$$I(Q, \gamma) = \frac{n_l}{n} S(Q, (\gamma)) + \frac{n_r}{n} S(Q(\gamma)) \quad (3.13)$$

Where, n_l and n_r are the number of data points at the left and the right split respectively.

This impurity function is the deterministic criteria for a node split. During the training process, the objective of this algorithm is to find the best split at each node so that the impurity function is minimized. This process is continued at each split node until a terminal criteria is reached. Usually for a terminal criteria, minimum number of variables at each node is set.

Although decision tree regressor is a robust algorithm, it poses some disadvantages also. The main problem of this regressor is its data dependency as a small variation of the input data can drastically change the shape of the tree. This data dependency can also lead to over fitting tendency of this model. To avoid this problem, the parameters of this scheme should be tuned carefully.

3.1.1.4 Random Forrest Regression (RFR)

Random forest regression (RFR) is an ensemble approach to reduce the intrinsic data dependent prediction of the traditional Classifier and Regression trees (CART) method by combining a large set of non-related randomized decision trees for better prediction ability. Proposed by Breiman et al. [91] in 1984, this ensemble method adopts a bagging or bootstrap aggregation algorithm for data randomization purpose. In random forest regression, each tree is built using a deterministic algorithm by selecting a random set of variables and a random sample from the training dataset. The final output of the RF regression is the average of the outputs of all decision. Fig 3.4 demonstrates the process of a RFR algorithm.

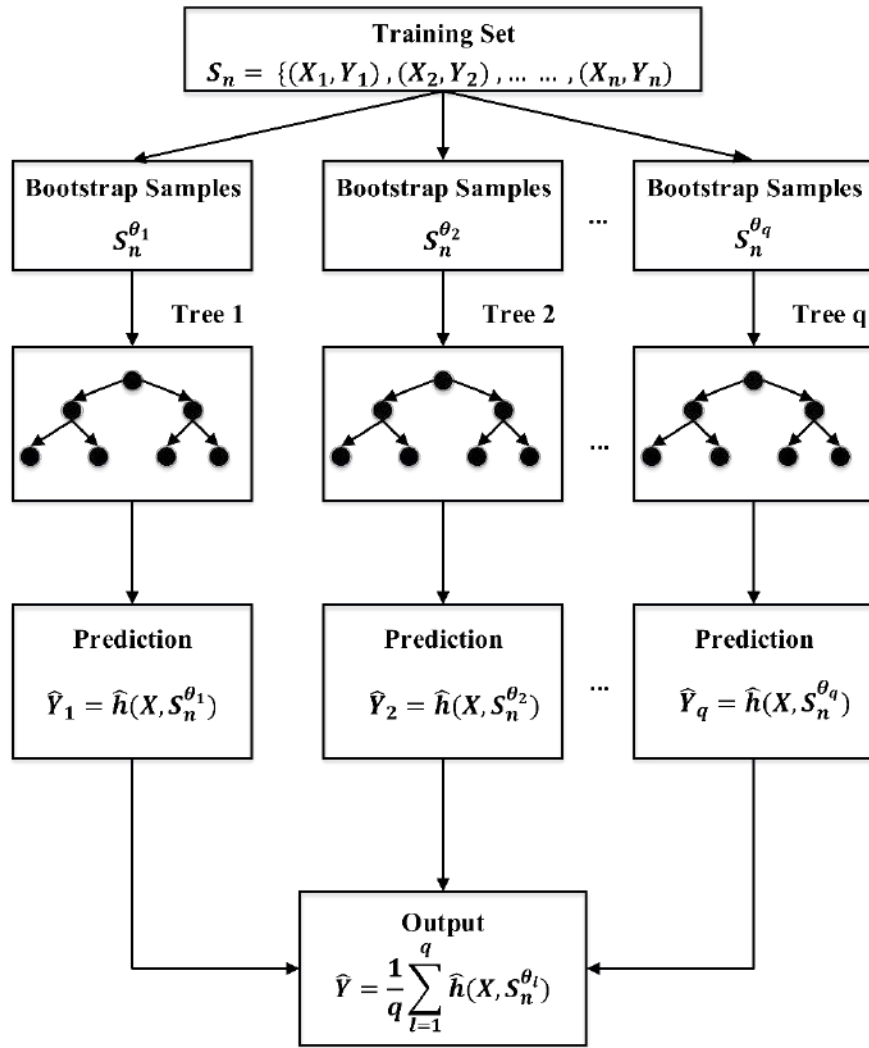


Figure 3.4 Schematic diagram of Random forest algorithm [92]

Let X_i be the input parameter vector and Y is the output parameter vector as previously stated in (3.8) and (3.9). So, a training set S_n consisting of m features can be constructed as,

$$S_n = \{(X_1, Y_1), (X_2, Y_2), (X_3, Y_3), \dots (X_n, Y_n)\} \quad (3.14)$$

The initial step of the RFR learning process is to construct several independent randomized sets of input parameters and thus constructing bootstrap sample sets. In bootstrapping process, each input parameter has an equal probability to be selected as the set is constructed picking one value after another without replacement. This ensures the stability and data diversity of the RFR process as the bootstrap samples obtained are independent from each other because of the

randomization and equiprobability of the data. For a total number of q bootstrap samples, they are denoted here as, $S_n^{\theta_1}, S_n^{\theta_2}, S_n^{\theta_3}, \dots, S_n^{\theta_q}$ respectively.

The next step is to formulate a decision tree from each sample. For this process, randomized subset of feature is selected where all the features may not be covered. After that, traditional decision tree algorithm is followed to get a predicted value of \hat{Y} from the algorithms constructed mapping function, $\hat{Y}_p = h(X, S_n^{\theta_p})$.

Followed by the bootstrapping process (randomized sample and feature selection process), the final step of this RF method aggregates all the predicted results from the algorithm formed trees by bootstrap aggregation process, which is simply taking the average value of the all decision tree predicted values [92] ,

$$\hat{Y} = \frac{1}{q} \sum_{i=1}^q h(X, S_n^{\theta_i}) \quad (3.15)$$

For hyper tuning of the RF scheme, three parameters are considered: the number of regression trees (n_{tree}), the number of features considered at each node (m_{try}), and the number of minimal size of the terminal nodes of the tree (n_{size})[93]. It is evident that with the increase of n_{tree} , the accuracy of the model also increases as the algorithm becomes more robust with the increased amount of trees. However, it is a natural tendency of this bootstrapping scheme to reach a certain accuracy value and beyond it further increase of n_{tree} has negligible effect. Furthermore, this also increases the computational time and memory, spoiling the main objective of this algorithm. It is found that the default value of $n_{tree} = 500$ can reach to a significant optimal convergent accuracy value for any kind of application.

On the other hand, m_{try} is a sensitive hyper tuning parameter requiring an optimal value to increase the model performance. With the increase of m_{try} , the prediction accuracy of each tree also increases which is expected to improve the performance of the model. However, increasing m_{try} also strengthens correlations between the trees as more common feature is established between the trees [58]. It is reported that m_{try} value equal to one third of the total features can produce a better solution [93]. Furthermore, the default value of $n_{size} = 1$ can produce significantly better solution, so the default value can be kept for the prediction purpose.

The performance of the RF algorithm further increases because of the unique inherent cross validation feature of this scheme. For a tree generation process in the training procedure, the related bootstrap sample is constructed first where the value of the parameters can be repeated. Generally, two thirds data of the original dataset is covered in each bootstrap sample leaving the rest one third of the data untouched. This untouched data is stored in another subset known as

the out-of-bag (OAB) sample. After the construction of a decision tree regressor, the associated data from the OAB is utilized to determine the performance of the tree. This built in cross validation feature greatly improves the performance of the RF model by eliminating the chance of over fitting.

The data independent characteristics of the RF model with easy hyper tuning option and intrinsic cross validation facilities make this algorithm a standard one for handling big data operations.

3.1.2 Deep Learning: Back Propagation Neural Network (BPNN)

The ML algorithms discussed in 3.1.1 are mostly linear by nature. Therefore, they may not always be effective for prediction when the dataset is considerably large in respect of calculation time and complexity. To eliminate this disadvantage, deep learning model is introduced in AI. Unlike traditional ML algorithms, deep learning algorithm is a hierarchical technique designed in a stacked fashion to address the complexity of the application. In this method, the algorithm recognizes the characteristics of the dataset in multiple layer of transfer functions which are non-linear in nature. Therefore, it is efficient in addressing comparatively large dataset as it divides it in multiple learning layers with effective transfer function and produces output in a quick manner.

Artificial neural network (ANN) is the most used form of deep learning which utilizes the core concept of deep learning. ANN adopts the learning technique of human brain neurons in data analysis perspective. Several ANNs are in practice like convolutional neural network (CNN), Radial based function neural network, feed forward neural network, back propagation neural network (BPNN) etc.

Back propagation neural network (BPNN) is one of the most widely used algorithms which is a deep learning method for more accurate prediction purpose over traditional machine learning scheme. It is used for training multi-layer artificial neural network. Among the multi-layers, the first layer is called the input layer, the last one is called the output layer, and the rest of the layers are known as hidden layers. Depending on the complexity of the problem, there can be more than one hidden layers. The inclusion of multiple layers generally improves the model accuracy but increases the computational time at the same time, so proper selection of the number of hidden layers is crucial for the efficient operation of the algorithm. In the training process of BPNN algorithm, the results from the output layer are compared with the actual ones. After that, error is calculated and it is propagated backwards to adjust the layer parameters (weights) for obtaining optimized minimum error condition.

The training process starts with feeding the training data in the input layers initially. The input layer is actually a collection of nodes which takes data from the training set directly without any prior calculation. After that, the feed data is passed to the first hidden layer. Like any linear regression process, the data is feed to a hypothesis function, $h(x)$ or Z first for each node of the hidden layer,

$$z = h(X) = W^T X + b \quad (3.16)$$

Where W denotes the weigh vector between the two layers with b as the bias.

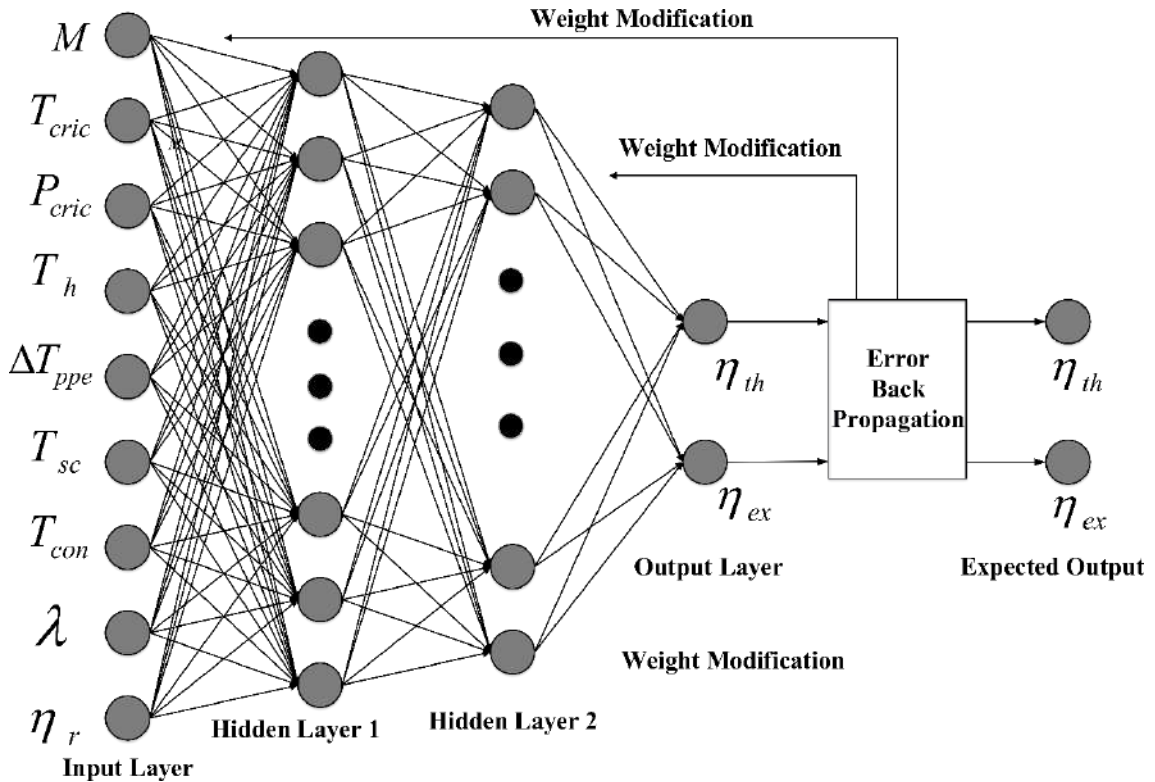


Figure 3.5 Schematic diagram of BPNN of this study

The main difference of neural network with traditional linear regression is the inclusion of an activation function after the data is feed to the hypothesis function z . The activation function basically decides whether to activate a neuron or connection of the neural network and thus flowing the data forward. It works on a non-linear scheme to produce output from the applied layer. Several activation function are in practice depending on the nature of the data and the desired output from the model. Among them the most common activation functions are:

Linear function:

It maps the output with input z as linear fashion like

$$f(z) = az + c \quad (3.17)$$

It is simple in nature and doesn't actually introduce non-linearity in the network, so it isn't useful for improving the model. Therefore, it has a limited usage and is applied between the final hidden layer and output layer usually if necessary.

Sigmoid function:

The function is commonly used in binary classification, but can also be used in regression problem in the intermediate hidden layers. The sigmoid function mainly transforms the hypothesis function value z between the intervals 0-1 from the following equation,

$$f(z) = \frac{1}{1 + e^{-z}} \quad (3.18)$$

The nature of the sigmoid function is useful to handle the larger variation of data by scaling them to a lower value.

ReLU function:

ReLU function is gaining popularity in neural network application because of its simple nature and wide adaptability. ReLU stands for Rectified Linear Unit, which is a function that doesn't activate all the neurons simultaneously. Rather, it deactivates the neuron if the hypothesis function value is less than 0 and activates it in a linear fashion otherwise. Keeping this simplistic concept, the ReLU function is defined as,

$$f(z) = \max(0, x) \quad (3.19)$$

The use of ReLU function is efficient while there are computational limitations and time constraints and it can respond to the wider range of data.

Softmax function:

The softmax function is usually used for multiclass classification problem which is a combination of multiple sigmoid function. It actually returns the value of a hypothesis function output as the probability of belonging to the studied class. For k number of classes, the softmax function can be denoted as,

$$f(z)_j = \frac{e^{z_j}}{\sum_0^k e^{z_k}} \quad (3.20)$$

This study uses ReLU function at all the hidden layers except the last layer, where softmax function is used.

After the implementation of hypothesis function and activation function , a model predicted value is obtained. Then using the concept of loss function like linear regression or support vector regression as described above, the goal of this algorithm is to obtain the optimum value of the weight vector to minimize the value of the loss function. Using the similar fashion of the linear regression, an initial value of the weight vector is assumed first (usually 1 or 0), and then they are updated according to the optimization scheme. As the error found at the output is feed backward to fine tune the weight vector, this scheme is known as BPNN.

Several optimization scheme is in practice like gradient descend, Adam, batch gradient descend etc. This study adopts the Adam optimizer as it is commonly used and handle regression problem efficiently.

3.1.3 Evaluation Metrics

It is necessary to evaluate the performance of the described ML and BPNN algorithms for efficient operation and fine tuning of the models if required. In order to evaluate the model performance, several evaluation metrics are available which vary for classification and regression analysis respectively. In regression analysis, the data set are continuous rather than discrete, so the performance or accuracy can't be measured based on the accurate prediction. Therefore, statistical approach of average, mean squared value, R^2 , etc. are considered. The aforementioned evaluation metrics suitable for this analysis is described below. For all cases the actual output is denoted by Y while the predicted data is Y' for n number of data points:

3.1.3.1 Mean Absolute Error (MAE)

Mean Absolute Error (MAE) is a straightforward robust technique of evaluation metric that takes into account the average of the actual and predicted data. The mathematical formulation for this metric is,

$$MAE = \frac{1}{n} \sum_{i=1}^n |Y_i - Y'_i| \quad (3.21)$$

If the value of MAE is smaller, better performance is indicated.

MAE may be vulnerable to larger variation between data. Moreover, if there is negative value involved, MAE may fail to accurately measure the performance of the model. Further, as MAE

is not differentiable, all optimizer may not be suitable except for gradient descend algorithm if MAE is considered in the loss function.

3.1.3.2 Mean Squared Error (MSE)

To eliminate the disadvantages of MAE, a differentiable metric is used which takes into account the squared value of the errors. Here for each data point, the error value is squared and then summed together. By taking the total average value, mean squared error (MSE) is obtained from the following equation,

$$MSE = \frac{1}{n} \sum_{i=1}^n (Y_i - Y_i')^2 \quad (3.22)$$

As the metric is differentiable, various optimization scheme can be used. Further, it eliminates the vulnerability of the calculated performance towards negative values of data. However, it is not as robust outlier as MAE.

MAE and MSE both may not be compared and understandable in case of readability as they both are input value dependent. So, for input values which have a wider variation and bigger value, MAE and MSE can be bigger even if the model is performing well. So, setting limit for better performance criteria can be troublesome.

To eliminate the readability problem of MAE and MSE, another two evaluation metrics are considered which are described below.

3.1.3.3 Mean Relative Error (MRE)

Mean relative error (MRE) scales the error value for each data point as the following fashion,

$$MRE = \frac{1}{n} \sum_{i=1}^n \frac{|Y_i - Y_i'|}{Y_i} \times 100\% \quad (3.23)$$

As can be seen in equation, MRE produces a percentage value between 0 to 100%. A smaller value of MRE indicates better prediction accuracy.

3.1.3.4 R^2 value

R^2 describes the proportion of the variance of the dataset a model can describe accurately. It is a widely accepted evaluation metric for regression analysis as it doesn't depend on the nature of

the data, rather produces a score between 0 and 1. The higher the R^2 score of the model, the better its prediction accuracy. The following equation is adopted to obtain this score,

$$R^2 = 1 - \frac{\sum_i (Y_i - Y_i')^2}{\sum_i (\bar{Y}_i - Y_i')^2} \quad (3.24)$$

It is sometimes labeled as coefficient of determination.

3.2 Optimization Algorithm: Genetic Algorithm

Usually for thermodynamic optimization purpose, heuristic optimization algorithms are adopted as they can efficiently address the complexity of large dataset and provide solution in a faster way. Several heuristic algorithms are in practice like ant colony optimization, particle swarm optimization, genetic algorithm, etc. This study adopts genetic algorithm as it can efficiently be synchronized with both traditional thermodynamic analysis and ANN approach. Introduced by professor Holland[94], Genetic algorithm (GA) is a widely used stochastic global search method which mimics the natural selection process based on Darwin's survival of the fittest principle. Unlike classical gradient based algorithms which focus on a single point solution, GA initially starts with a population consisting of possible solution sets, which in each iteration is evolved towards the optimized solution. This solution sets, which are known as individuals or chromosomes, is comprised of the parameters or the variables to be optimized against an objective function. The size of the population depends on the nature and complexity of the optimization problem. Initially consisting of individuals from random values within the search space, in each iteration (which is known as generation in GA terminology) a population is updated based on the fitness of the chromosome against a fitness function or objective function. In this study, a fitness function is constructed giving equal weightage to both thermal efficiency and exergy efficiency.

The GA depends on three important bio-inspired operations for the quality improvement of individuals in each generation which are selection, crossover, and mutation. Selection process determines the chromosomes that will undergo the crossover phase. It is crucial for the success of the subsequent GA operation. Several popular method for this selection process are in practice like the fitness proportionate selection method, the linear fitness scaling method, the Boltzman fitness scaling method, the ranked selection method, the tournament select method etc. All of the methods work on the common principle of choosing the fittest chromosome for reproduction. Some important criteria like the parents proportion, elite chromosome ratio etc. are also maintained strictly in the selection process in order to get the best possible individuals for crossover.

After selection process, the selected chromosomes undergo crossover operation which is the driving force in GA for creating variation in the population. In this operation, child chromosomes are produced by aligning two parent chromosomes picking up a random positions along their length and then swiping their tails with a probability known as the crossover probability. Based on these random positions, crossover can be of uniform crossover, single point crossover or multiple point crossover. The crossover probability are usually kept higher in order to insure the convergence towards the optimized result.

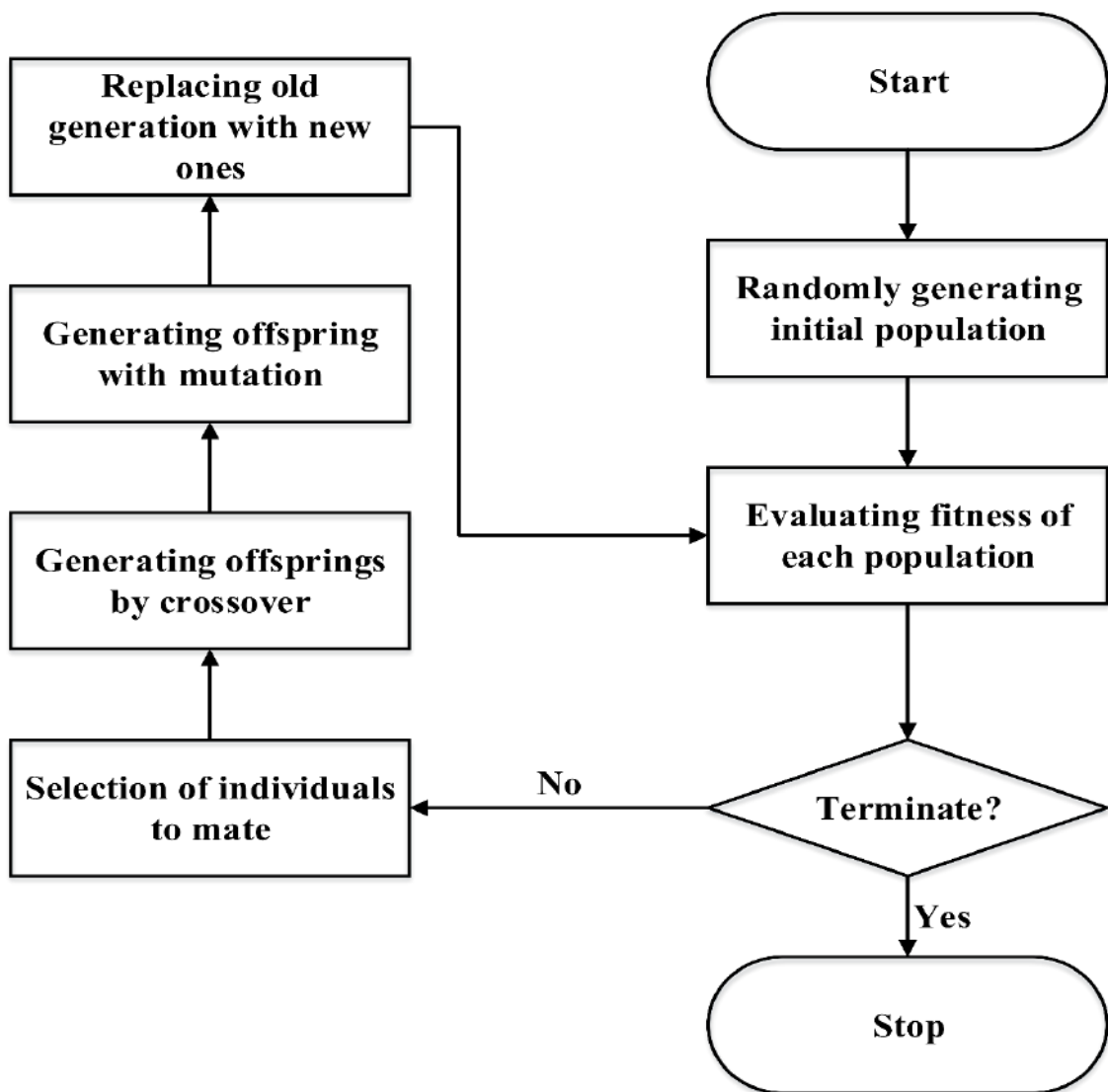


Figure 3.6 Flowchart of genetic algorithm

The GA may fail to reach global optimum solution or encounter premature convergence regardless of the proper selection of selection and crossover method for the inherent weakness involved in these operations. To encounter this problem, some values of the parameters within

an individual are altered taken from the search space against a certain probability. This process is known as the mutation operation and the mentioned probability is termed as mutation probability. Generally for GA operation, a smaller mutation probability is applied in order to encounter the premature convergence criteria after the crossover operation. The main advantage of mutation is that it puts variety into the gene pool, enabling the algorithm to explore potentially beneficial regions of the search space that might otherwise be missed.

By the successive operation of selection, crossover, and mutation, a new population is created, which is taken as the initial population for next generation. The process is terminated after a definite criteria is fulfilled or after a certain generation is reached.

4 THERMODYNAMIC MODELLING

In this chapter, the thermodynamic modelling of the proposed cycles will be discussed. This study explores four different configurations of the ORC to generate data for training the discussed machine learning schemes and establish the optimization parameter domain. To perform component wise and overall energy and exergy analysis, the knowledge of the fundamental thermodynamic relations among mass, energy and exergy is crucial, which will be discussed first. The proposed cycle configurations and working principle will be discussed afterwards. Following this, the thermodynamic balance equations will be applied for component wise and overall energy and exergy analysis.

The choice of proper evaporating temperature as well as evaporator working pressure is crucial for the efficient operation of the evaporator as it not only can reduce the exergy destruction but also indicates fluid quality for the turbine. This study adopts a simple “Target temperature line” method which is a feasible technique for deriving evaporator conditions specially for sufficient data generation purpose for machine learning. The detailed demonstration of this method will be discussed at the last part of this chapter.

4.1 Fundamental Thermodynamic Equations

For systematic thermodynamic modelling purpose, three major properties of the system are considered namely the mass, energy, and exergy of the system. The first two properties (mass and energy) are considered conserved for a system (described by the mass conservation law, and the energy conservation law/ the first law of thermodynamics). However, the exergy of a thermodynamic system isn't conserved, rather a portion of it is destroyed during the operation of the system due to the inherent irreversibilities of the system. This phenomenon is dependent on the entropy of the system and is described with the second law of thermodynamics. The following sections describe the aforementioned processes with mathematical model.

4.1.1 Mass Balance Equation

At any given time, the rate of change of mass of the control volume system can be derived by,

$$\frac{dm_{cv}}{dt} = \sum_i \dot{m}_i - \sum_e \dot{m}_e \quad (4.1)$$

where,

- cv Control volume
- i inlet
- e outlet
- \dot{m} Mass flow rate of the working fluid

For a steady state control volume system, $\frac{dm_{cv}}{dt} = 0$. So, the equation (4.1) becomes,

$$\sum_i \dot{m}_i - \sum_e \dot{m}_e = 0 \quad (4.2)$$

4.1.2 Energy Balance Equation

For a control volume system, the rate of the change of energy is derived considering the heat and the work input or output of the system as well as the internal, kinetic and potential energy of the working fluid from the below stated equation as,

$$\frac{dE_{cv}}{dt} = \dot{Q} - \dot{W} + \sum_i \dot{m}_i \left(h_i + \frac{v_i^2}{2} + gz_i \right) - \sum_e \dot{m}_e \left(h_e + \frac{v_e^2}{2} + gz_e \right) \quad (4.3)$$

Where,

- E energy of the control volume
- \dot{Q}_{cv} heat input rate to the control volume
- \dot{W}_{cv} work output from the control volume
- h enthalpy of the fluid
- v velocity of the fluid
- z Elevation from the sea level

For a steady state steady flow (SSSF) control system, the rate of the change of energy of the system, $\frac{dE_{cv}}{dt} = 0$. Besides for ORC modelling purpose, usually kinetic and potential energy of the working fluid is neglected. Considering all this, equation (4.3) can be written in general for SSSF system as,

$$\dot{Q} = \dot{W} + \sum_e \dot{m}_e h_e - \sum_i \dot{m}_i h_i \quad (4.4)$$

For energy analysis of any single component of the system, equation (4.4) will be used in this study.

4.1.3 Exergy Balance Equation

For several inlets and exits, the exergy balance equation of a control volume system can be written as,

$$\frac{dEx_{cv}}{dt} = \dot{\Phi}_Q - \left(\dot{W}_{cv} - P_0 \frac{dV_{cv}}{dt} \right) + \sum_i \dot{m}_i \psi_i - \sum_e \dot{m}_e \psi_e - \dot{I} \quad (4.5)$$

where, Ex is the exergy of the system, \dot{I} denotes the exergy destruction, and $\dot{\Phi}_Q$ describes the exergy transfer due to heat transfer \dot{Q}_j to the system at the boundary and is defined as,

$$\dot{\Phi}_Q = \sum_j \left(1 - \frac{T_0}{T_j} \right) \dot{Q}_j \quad (4.6)$$

The flow exergy ψ is the maximum amount of work that can be extracted from the system given that it is in thermal equilibrium with the environment (for temperature T_0 , pressure P_0 , and entropy s_0). Considering the entropy s , the flow exergy of any given state can be written as,

$$\psi = (h - h_0) - T_0(s - s_0) + \frac{v^2}{2} + gz \quad (4.7)$$

As in this study the kinetic and potential exergy are considered negligible, equation (4.7) can be simplified as,

$$\psi = (h - h_0) - T_0(s - s_0) \quad (4.8)$$

Finally, considering a SSSF condition, equation (4.5) can be reduced to,

$$\dot{\Phi}_Q = \dot{W}_{cv} + \sum_e \dot{m}_e \psi_e - \sum_{in} \dot{m}_i \psi_i + \dot{I} \quad (4.9)$$

For exergy analysis of any single component of the system, this study will adopt equation (4.9).

4.2 Proposed Cycle configurations

In this study, four thermodynamic cycle configurations are considered namely basic organic Rankine cycle (BORC), reheating organic Rankine cycle (RORC), internal regenerative Rankine cycle (IORC), and combined reheating- internal regenerative organic Rankine cycle (CRIORC). The thermodynamic principles of the mentioned configurations are discussed below:

4.2.1 Basic organic Rankine cycle (BORC)

Fig 4.1 demonstrates the layout of a BORC along with the process involved. In its basic configuration an ORC consists of four major components naming an evaporator, a turbine, a condenser, and a pump.

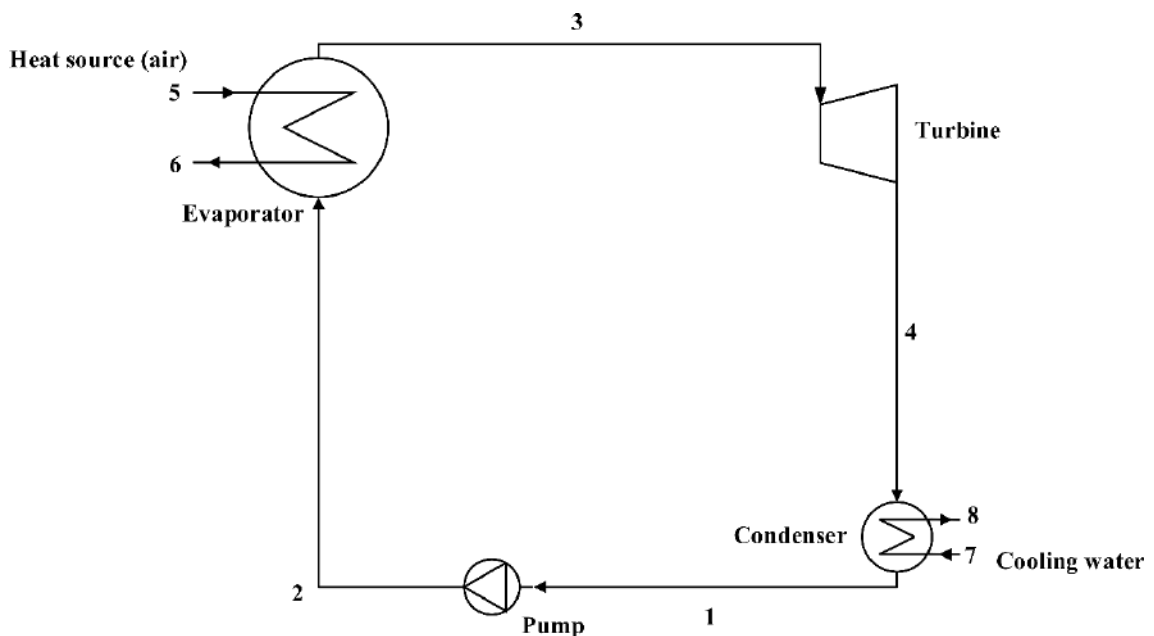


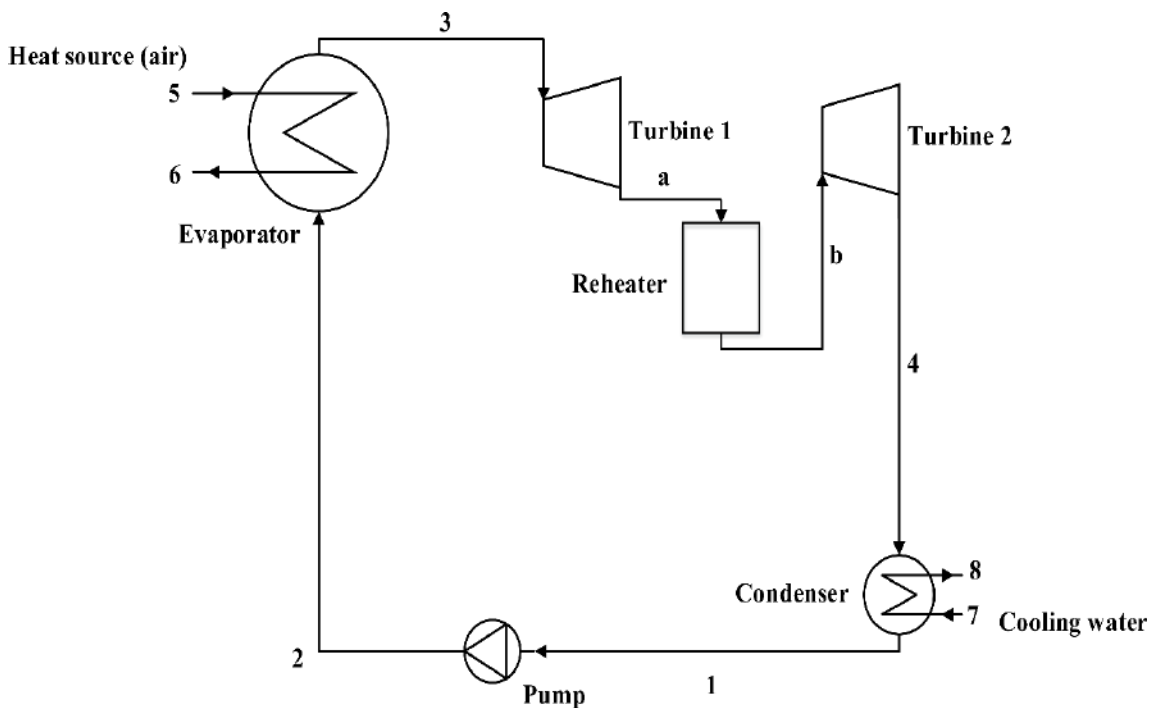
Figure 4.1 Schematic diagram of BORC

The working fluid is first pumped to a high pressure via the pump to the evaporator described by the process 1-2. This process is theoretically adiabatic though in real practice negligible amount of heat is generated. In the evaporator, the working fluid undergoes an isobaric heating process (denoted by process 2-3) which raise the temperature of it to a desired point. The degree of superheating depends on the temperature of the heating source as well as the working evaporator pressure. Afterwards, the working fluid is transported to the turbine to extract work from the energy of the working fluid (described by process 3-4). Finally, to complete the cycle, the working fluid is brought to state 1 via an isobaric heat rejection process in the condenser.

The efficiency of ORC greatly depends on the evaporating pressure and evaporator outlet temperature. If the output state of the turbine is constant, with the increase of the evaporator pressure the evaporating temperature also increases. This leads to higher cycle efficiency reducing the exergy losses within the heat exchanger and increasing turbine output. However, this can also have a dramatic reduction effect on the quality of the fluid vapor in the turbine, so care should be taken in turbine operation for higher evaporating pressure condition.

4.2.2 Reheating Organic Rankine Cycle (RORC)

Reheating of the working fluid can be a viable solution to the adverse effect of increased evaporating pressure. In a reheating cycle, work is extracted from multiple turbine instead of a single one keeping the evaporating pressure within a desirable limit. For RORC modelling purpose, this study adopts a single stage reheating incorporating two turbines as illustrated in figure 4.2. The basic process is the same as discussed in BORC operation. However unlike BORC system, the working fluid enters a reheater after turbine operation (described in process 4-a). Afterwards, via a constant pressure re heating process, the temperature of the working fluid reaches point b (which is essentially equal to the temperature of point 3) and enters the second turbine. The fluid then performs the rest of the operation in a similar fashion of the



BORC process.

Figure 4.2 Schematic diagram of RORC

It is to be noted that the basic objective of reheating is to improve steam quality of turbine, which greatly depends on the reheating pressure ratio. Increasing this ratio will theoretically increase the exergy efficiency but can introduce the dryness problem similar to BORC. So, an optimum choice of the reheating pressure ratio is vital for the realistic application of the cycle.

4.2.3 Internal Regenerative Organic Rankine Cycle (IORC)

The working fluid which finishes the turbine operation can contain significant amount of energy which is destroyed in the condensing process if remain unutilized. To capture this energy, an internal regenerator can be a viable option for ORC. Figure 4.3 illustrates the work flow of an IORC which will be utilized in this study.

As illustrated in the figure, the working fluid before entering the evaporator at stage 2 undergoes an isobaric heating operation first in the internal regenerator at reaches state 2' which enters the evaporator afterwards. To achieve this condition, it utilizes heat from the fluid coming out of the turbine at stage 4. After this heat transfer process, the fluid achieve state 4' and undergoes goes in the condensing operation like the BORC procedure. Likewise, the working fluid exists the evaporator at point 3 and undergoes the turbine operation as described before.

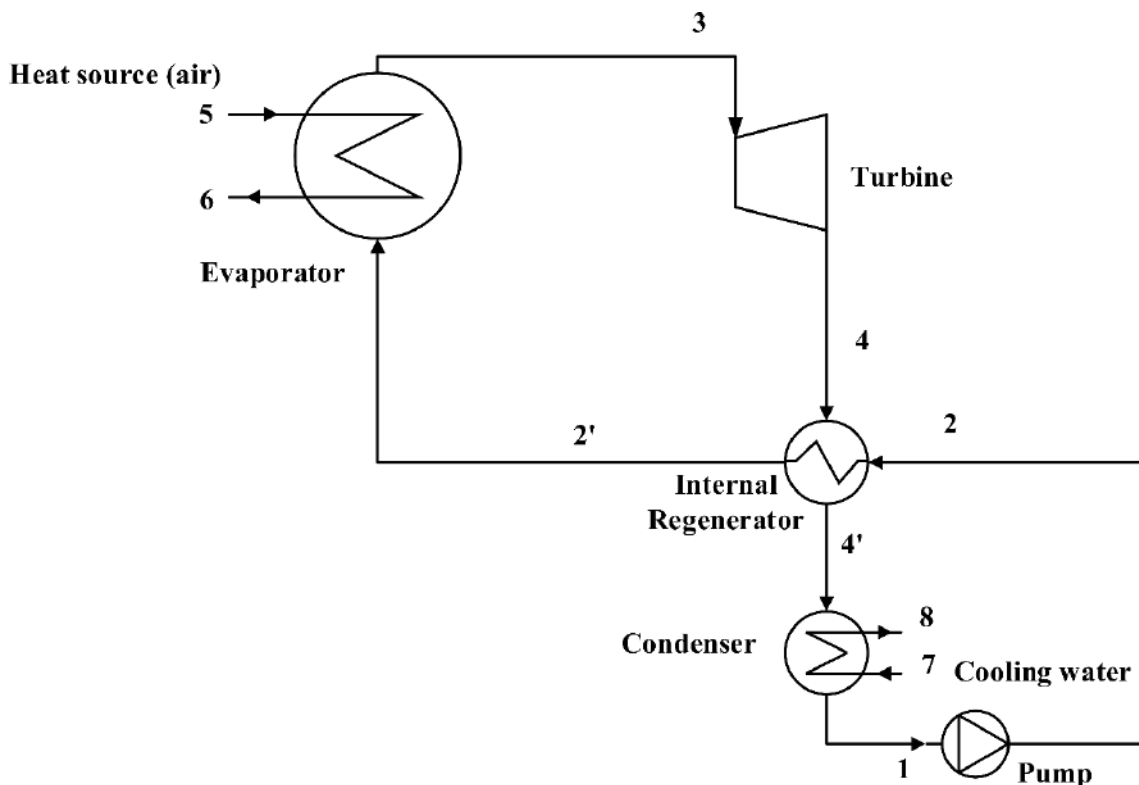


Figure 4.3 Schematic diagram of IORC

Regeneration process has a positive impact on the cycle exergy efficiency as it lessens the working temperature difference for the evaporation and condensation process. But a proper assessment is required for its viability as it also introduces complexity in the system management.

4.2.4 Combined Reheating Internal Regenerative Cycle (CRIORC)

In order to avail the advantages of reheating and regenerating, these two processes can be combined in a single cycle. Fig 4.4 illustrates the CRIORC configuration studied in this cycle with the state points previously discussed. With the proper selection of reheating pressure ratio and regenerator efficiency, this cycle can exhibit better performance over BORC, RORC, or the IORC.

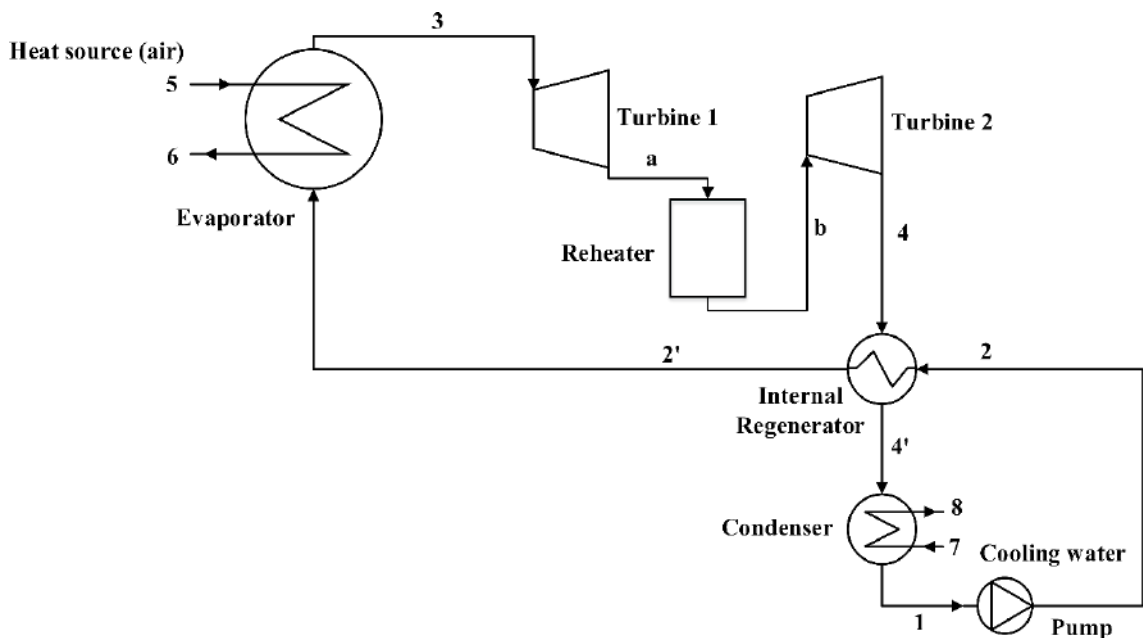


Figure 4.4 Schematic diagram of CRIORC

4.3 Component wise energy and exergy balance equations

4.3.1 Evaporator

Heat rejected by the heat source in the evaporator,

$$\dot{Q}_{HS} = \dot{m}_{HS} (h_5 - h_6) \quad (4.10)$$

Which is absorbed by the working fluid. Therefore,

$$\dot{Q}_{EV} = \dot{Q}_{HS} \quad (4.11)$$

For the evaporator, boundary work W is considered. So, from equation (4.4), the energy balance equation for the evaporator in case of BORC and RORC is,

$$\dot{Q}_{EVAP} = \dot{m}_f(h_3 - h_2) \quad (4.12)$$

Likewise, in case of IORC and CRIORC, this equation is presented as,

$$\dot{Q}_{EVAP} = \dot{m}_f(h_3 - h'_2) \quad (4.13)$$

For a single heat source with temperature T_h , exergy supplied by the heat source from equation (4.6,

$$\dot{\phi}_{EVAP} = \left(1 - \frac{T_0}{T_h}\right) \dot{Q}_{EVAP} \quad (4.14)$$

Again, for the heat transfer process in the evaporator, exergy balance from equation (4.9) can be written for BORC and RORC as,

$$\dot{m}_f(\psi_3 - \psi_2) - \dot{m}_{HS}(\psi_6 - \psi_5) + \dot{I}_{EV} = 0 \quad (4.15)$$

Which in turns leads to the exergy destruction as,

$$\dot{I}_{EVAP} = \dot{m}_f(\psi_2 - \psi_3) - \dot{m}_{HS}(\psi_5 - \psi_6) \quad (4.16)$$

Similarly, for IORC and CRIORC, this destruction is,

$$\dot{I}_{EVAP} = \dot{m}_f(\psi'_2 - \psi_3) - \dot{m}_{HS}(\psi_5 - \psi_6) \quad (4.17)$$

4.3.2 Turbine

Using equation (4.4) and considering adiabatic process, the energy balance equation of turbine for BORC and IORC is,

$$\dot{W}_{TBN} = \dot{m}_f(h_3 - h_4) \quad (4.18)$$

To get the exit state point, isentropic efficiency of the turbine is required which is described as,

$$\eta_{TBN} = \frac{h_3 - h_{4s}}{h_3 - h_4} \quad (4.19)$$

For RORC and CRIORC, the energy balance equation is,

$$\dot{W}_{\text{TBN}} = W_{\text{TBN}1} + \dot{W}_{\text{TBN}2} = \dot{m}_f(h_3 - h_a) + \dot{m}_f(h_b - h_4) \quad (4.20)$$

Again, using equation (4.9), the exergy destruction associated with turbine for BORC and IORC can be stated as,

$$\dot{I}_{\text{TBN}} = \dot{m}_f(\psi_3 - \psi_4) - W_{\text{TBN}} \quad (4.21)$$

Similarly for IORC and CRIORC, it can be written as,

$$\dot{I}_{\text{TBN}1} + \dot{I}_{\text{TBN}2} = \dot{m}_f(\psi_3 - \psi_a) + \dot{m}_f(\psi_b - \psi_4) - (W_{\text{TBN}1} + W_{\text{TBN}2}) \quad (4.22)$$

4.3.3 Pump

Using equation (4.4) and considering adiabatic process, the energy balance equation of pump is,

$$\dot{W}_{\text{PUMP}} = \dot{m}_f(h_2 - h_1) \quad (4.23)$$

Where the exit state point of the pump can be derived using the isentropic pump efficiency as,

$$\eta_{\text{PUMP}} = \frac{h_2 - h_1}{h_{2s} - h_1} \quad (4.24)$$

Again, using equation (4.9), the exergy destruction associated with the pumping process can be derived as,

$$\dot{I}_{\text{PUMP}} = \dot{m}_f(\psi_1 - \psi_2) - W_{\text{PUMP}} \quad (4.25)$$

4.3.4 Condenser

By neglecting the heat loss to the environment with no boundary work involved, the heat rejected in the condenser for BORC and RORC can be modelled as,

$$\dot{Q}_{\text{CND}} = \dot{m}_f(h_4 - h_1) \quad (4.26)$$

Which for IORC and CRIORC can be stated as,

$$\dot{Q}_{\text{CND}} = \dot{m}_f(h_{4'} - h_1) \quad (4.27)$$

Again, according to the equation (4.9), the exergy destruction in the condenser for BORC and RORC is,

$$\dot{I}_{\text{CND}} = \dot{m}_f(\psi_4 - \psi_1) + \dot{m}_w(\psi_7 - \psi_8) \quad (4.28)$$

Which for IORC and CRIORC can be stated as,

$$\dot{I}_{\text{CND}} = \dot{m}_f(\psi_{4'} - \psi_1) + \dot{m}_w(\psi_7 - \psi_8) \quad (4.29)$$

4.3.5 Reheater

Using equation (4.4), the heat required for the reheating purpose for RORC and CRIORC can be derived as,

$$\dot{Q}_{\text{REH}} = \dot{m}_f(h_b - h_a) \quad (4.30)$$

Similar to the equation (4.14), the associated exergy supplied during the reheating process is

$$\dot{\phi}_{\text{REH}} = \left(1 - \frac{T_0}{T_h}\right) \dot{Q}_{\text{REH}} \quad (4.31)$$

It is to be mentioned that during the reheating process, the inlet temperature of both of the turbine remains essentially same. So, the state points can be derived using

$$T_3 = T_b \quad (4.32)$$

Where the concept of reheating pressure ratio is utilized which can be defined by,

$$\lambda = \frac{P_a}{P_3} = \frac{P_4}{P_b} \quad (4.33)$$

4.3.6 Regenerator

Based on the equation (4.4), the heat transfer process in the regenerator can be modelled as,

$$\dot{m}_f(h_2' - h_2) = \dot{m}_f(h_4 - h_4') \quad (4.34)$$

Similar to the equation (4.9), the associated exergy supplied during the reheating process is,

$$\dot{I}_{\text{REG}} = \dot{m}_f(\psi_2 - \psi_{2'}) + \dot{m}_f(\psi_4 - \psi_{4'}) \quad (4.35)$$

In the regenerator, two thermodynamic conditions are necessarily maintained,

$$\begin{aligned} T_{4''} &= T_2 \\ T_{2''} &= T_4 \end{aligned} \quad (4.36)$$

Considering them, the regeneration efficiency is defined as,

$$\eta_r = \frac{h_2 - h_{2'}}{h_2 - h_{2''}} = \frac{h_4 - h_{4'}}{h_4 - h_{4''}} \quad (4.37)$$

4.4 Overall System Analysis & Performance Indicator

The overall work done by the system can be derived from equation (4.18), (4.20), and (4.23) as,

$$\dot{W}_{\text{net}} = \dot{W}_{\text{TBN}} - \dot{W}_{\text{PUMP}} \quad (4.38)$$

From the heat source and the reheating process described in equations (4.12), (4.13), and (4.30), the heat supplied to the system,

$$\dot{Q}_{\text{in}} = \dot{Q}_{\text{EVAP}} + \dot{Q}_{\text{REH}} \quad (4.39)$$

Where the reheat portion is only applicable for reheating cycles.

Considering these, the energy efficiency or the first law efficiency of the system can be stated as,

$$\eta_1 = \frac{\dot{W}_{\text{net}}}{\dot{Q}_{\text{in}}} \quad (4.40)$$

Again, from the exergy transfer process of equations (4.14), and (4.31), the exergy supplied to the system is,

$$\dot{\Phi}_{\text{in}} = \dot{\Phi}_{\text{EVAP}} + \dot{\Phi}_{\text{REH}} \quad (4.41)$$

So, the exergy efficiency or the second law efficiency of the system is,

$$\eta_2 = \frac{\dot{W}_{\text{net}}}{\dot{\Phi}_{\text{in}}} \quad (4.42)$$

The first law efficiency fails to address the distinction between heat and work. Moreover, the cycle power isn't always maximized for maximum thermal efficiency. The second law efficiency or the exergy efficiency, on the other hand, is vital to understand the potential useful work gain from the cycle and crucial for cycle financial and feasibility analysis. However, in this study while forming the Pareto frontier for optimization purpose, both of the efficiencies are addressed to investigate the effect of the cycle parameters on them.

4.5 Estimation of Evaporator Operating Conditions with 'Target-Temperature Line' Method

As discussed in section 5.1, evaporating pressure and evaporating temperature play a pivotal role in the exergy gain associated with the heat exchanging process within the evaporator as well as in the exergy efficiency of the cycle. Therefore, the choice of suitable evaporator

parameters is vital to minimize exergy destruction. To select suitable operating conditions, generation of sufficient parametric data along with their assessment are crucial. So, the calculation method should be simple and less time consuming to address the aforementioned conditions in a smooth manner for data prediction and optimization purpose.

This study adopts a simple ‘Target-temperature line’ method proposed by Haq[95] to obtain evaporator state condition. In this method, a line known as the ‘target temperature line’ is formed which essentially satisfies the intended pinch point condition. The aim is to find feasible operating temperatures that basically forms the stated target line by assuming pinch occurrence at certain points of the heat exchanger related to the target temperatures. This simple method is less time consuming compared to available studies and can address pure fluid or fluid mixtures.

Figure 4.5 shows the graphical demonstration of the adopted target temperature line method. The heat rejected by the heat source to the working fluid in the evaporator discussed in equation (4.10) is also known as the duty D of the heat exchanger. So,

$$D = \dot{m}_h(h_5 - h_6) = \dot{m}_f(h_3 - h_2) \quad (4.43)$$

D is divided into equal number of parts to find the pinch point along the length of the heat exchanger and construct the target line. In this study, a total 1000 parts are considered to find the pinch point effectively. The associated intermediate duty D_j can be defined as,

$$D_j = \frac{j}{1000} D = \dot{m}_h(h_{hj} - h_6) \quad (4.44)$$

Where pinch is assumed to occur at point j of the evaporator.

From equation (4.44), h_{hj} can be derived for a given j . So, associated heat source temperature at this point T_{hj} is also known from this conditions. From the pinch point temperature difference in the evaporator, ΔT_{pp} , corresponding working fluid temperature $T_{r,j}$ can be derived as,

$$T_{r,j} = T_{hj} - \Delta T_{pp} \quad (4.45)$$

Which is also known as the target temperature.

At this target temperature, the working fluid is essentially assumed to be at saturated liquid state. So, the evaporating temperature is derived as,

$$T_{EVAP, sat, j} = T_{r, j} \quad (4.46)$$

From equation (4.46), the corresponding evaporating pressure $P_{EVAP,sat,j}$ and enthalpy of the saturated liquid, h_j , are also known. In short, D_j amount of heat is required by the fluid to obtain the saturated liquid state.

As the evaporator input state is fixed by the condition of equation (4.46), the mass flow rate of the fluid can be derived as,

$$\dot{m}_f = \frac{D_j}{(h_j - h_2)} \quad (4.47)$$

Therefore, the state of the working fluid leaving the evaporator can be derived from equation (4.43) as,

$$h_{3,j} = h_2 + \frac{D}{\dot{m}_f} \quad (4.48)$$

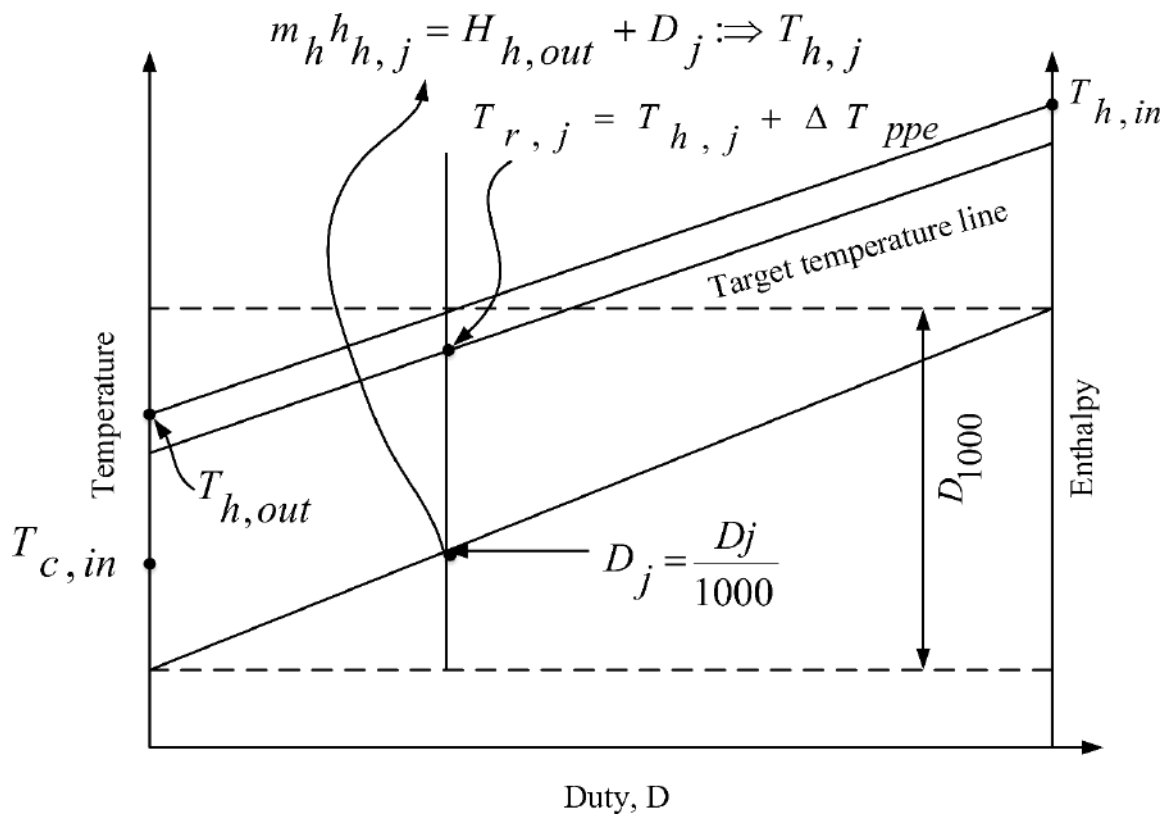


Figure 4.5 Graphical demonstration of the target temperature line construction [95]

For feasible operation of the cycle, certain conditions should be maintained. Owing to satisfy the energy balance criteria posed by the governing equations, some non-feasible scenario of evaporator should be avoided. Firstly, the evaporator exit temperature T_3 is essentially required to be under the target temperature. However the following may occur which is discarded,

$$T_3 > T_5 - \Delta T_{pp} \quad (4.49)$$

Secondly, the solution is also discarded when the target temperature is very close to the critical temperature described by the following criteria,

$$T_{\text{EVAP, sat, j}} > 0.95T_{\text{cr}} \quad (4.50)$$

Finally, the turbine input and output vapor quality (X_3, X_4) of the fluid should be greater than 0.9 to maintain dry fluid condition.

5 RESULTS AND DISCUSSION

The thermodynamic modelling schemes discussed in chapter 4 are utilized to acquire the data needed for training the proposed machine learning and deep learning algorithms. To obtain the performance data of the ORC for four distinct configurations, some assumptions are considered regarding the cycle operating conditions as well as various cycle parameters. In the beginning of this chapter, the selection criteria of initial cycle operating conditions will be discussed first. To construct reliable ANN framework, generating sufficient amount of data is crucial. Therefore, the next section will explore the framework of producing data from the previously stated ORC configuration, and dataset of 9 working fluids for 4 ORC configurations will be constructed. For any ANN scheme, tuning of the related hyper parameters is crucial for the prediction accuracy. So, the next objective of this chapter is to discuss the determination of the hyper parameters for both ML and BPNN algorithms against the given dataset. Based on the selected ANN scheme incorporating established hyper parameters, individual and combined prediction accuracy of the AI models will be discussed for the 9 preselected working fluids. After that, the effect of the cycle parameters on the cycle efficiencies will be explored based on the prediction of the previously discussed machine learning scheme. Then, the key parameters will be selected and a multi-parameter optimization of the cycles will be performed based on the formed machine learning algorithms. All the thermodynamic simulations are performed in python programming language.

5.1 Thermodynamic Modelling Assumption

Some initial system parameters are considered for thermodynamic modelling purpose. They are listed in *Table 5-1*.

In this study, dry air is taken as the heat source which is considered to be under atmospheric pressure condition. The mass flow rate of the working fluid is changed based on the evaporating pressure which is calculated by the target temperature line approach discussed in chapter 4. The condenser water inlet temperature is fixed at atmospheric temperature and mass flow rate of the condensing water is determined considering the super cooling criteria. As can be seen from *Table 5-1*, some values of the cycle parameters are fixed, while some varies within a fixed range. Parameters like heat source outlet temperature, air mass flow rate, turbine and pump isentropic ratio, etc. are fixed. However, six pivotal cycle parameters namely heat source inlet temperature, condensing temperature, degree of super cooling, pinch point temperature

difference in the evaporator, reheating pressure ratio, and regenerator efficiency are varied at a regular interval of 5 mainly to produce data for AI algorithms training purpose.

Table 5-1 System Simulation Parameters of ORC

Parameters	Value
Heat source inlet temperature (T_5)/K	373-573
Heat source outlet temperature (T_6)/K	333
Mass flow rate of air (\dot{m}_h)/kg/s	15
Condensing temperature (T_{CND})/K	308.15-311.15
Degree of supercooling(T_{sc})/K	0-11
Pinch point temperature in the evaporator (T_{pp})/K	5-20
Reheating pressure ratio (λ)	0.1-0.7
Regenerator efficiency (η_r)	0.00-1.00
Pump isentropic efficiency(η_p)	0.70
Turbine isentropic efficiency(η_t)	0.85
Atmospheric temperature (T_0)/K	293.15
Atmospheric pressure (P_0)/kPa	101.325

Besides the system parameters, some assumptions related to system operation are made in this study for simplification of the system. The major assumptions are stated below:

- The systems are in steady state and steady flow condition.
- The primary heat source in the evaporator is pure dry air under atmospheric pressure condition.
- The thermodynamic processes in the components are adiabatic.
- All the heat exchanging process in the evaporator, condenser, and regenerator happen in counterflow manner.
- Heat loss and energy loss due to friction in the piping system are negligible.

- Kinetic and potential energy and exergy change of the working fluid are negligible. So, they are ignored in calculating the change of flow energy and exergy.
- No heat is lost in the evaporator and condenser heat exchanging process.

5.2 Selection of Potential Working fluid for ORC

Selection of working fluid is crucial to three major aspects of the cycle: thermodynamic aspect, environmental aspect, and economic aspect. Thermodynamic aspect includes sustainable and viable cycle operating condition, system efficiency, component sizing, etc. Environmental aspect mainly deals with the environmental impact such as GWP, ODP, etc. of the working fluid. Economic aspect, on the other hand, is assessed against the working fluid's potential for cost minimization of the cycle operation. Considering the three aspects, fluids with optimal conditions are chosen.

Table 5-2 Thermo-physical Properties of working fluids

Working Fluid	Heat source maximum temperature (T_5)/°C	Critical temperature (T_{cr})/°C	Critical pressure (P_{cr})/MPa	Normal boiling point/°C	Molecular mass /g/mole
R227ea	110	101.74	2.93	-15.61	170.03
RC318	125	115.23	2.78	-5.97	200.031
R236fa	132	124.92	3.2	-1.44	152.04
R236ea	148	139.29	3.50	6.19	152.04
R245fa	164	154.01	3.651	15.14	134.04
R123	193	183.68	3.66	27.82	152.931
R113	224	214.06	3.39	47.59	187.38
Cyclopentane	248	238.57	4.58	49.2	126.24
Cyclohexane	290	280.45	4.08	80.75	84.16

In this study, the thermodynamic aspects are prioritized. Haervig et al. [96] proposed a general guideline of choosing the optimal fluid based on the relationship between critical temperature and heat source temperature. Based on a systematic approach on 26 working fluid, the study reported that fluids with critical temperature within 30-50 K below the heat source temperature are optimal to maximize the power output from the cycle. Rad et al. [97] investigated the performance of typical ORC for a wide range of heat source temperature condition with working fluid critical temperature below or above of 40 K of heat source. Haq[95] investigated the performance of 38 working fluid with critical temperature below or above 50 k of the heat source temperature with target temperature line method. In this work, the aforementioned method along with 9 working fluids from that study are considered which are listed in *Table 5-2*

It is to be mentioned that, the performance of ORC for this method varies within the heat source temperature range for the same working fluid. Moreover, some fluids do not yield feasible solutions within a certain subset of heat source temperature. As the objective of this study is to explore the scope of machine learning in ORC related modelling, flexibility regarding heat source temperature selection is crucial to address realistic applications. Therefore, one fluid from each temperature group is selected. Moreover, the feasible temperature range for target temperature line method is also investigated. The selected working fluids, their properties, and working temperature range are listed in *Table 5-2*

5.3 Hyper Parameter Selection for the ML algorithms.

Selection of hyper parameters of a machine learning model is user dependent but has a significant impact on the accuracy of the model. The internal parameters of a machine learning model are adjusted according to the types and characteristics of the given data. Hyper parameters, on the other hand, are data independent but the proper selection of them is vital for the selection of best model conditions. However, there is no general guideline for selecting optimal hyper parameters that can satisfy all the existing machine learning models. Hyper parameters are greatly data dependent and the optimal choice should be made based on the inherent characteristics of the data for a specific problem. Several methods are in practice for the proper selection of hyper parameters such as: Grid-search CV, Randomized search CV, Hill climbing, Bayesian optimization etc.

In this study, Randomized search CV method is chosen as it perfectly aligns with the complexity of the discussed machine learning schemes. Unlike Grid-search CV where all the possible values of hyper parameters are tested against the accuracy of the model, this method focuses on generating random values of the discussed parameters first and then evaluates the best solutions to the problem. As a result, this method is tremendously helpful to save time and

computational powers when it comes to selecting multiple hyper parameters for a specific model like Random forest, decision tree etc.

Usually in Randomized search CV, k-fold cross validation is used. In this technique, the training data is split into k number of folds or groups among which one is selected as the test dataset in every case and the remaining folds are considered as training data set. In this way each of the folds are considered as test samples once and the average performance score of all the possible cases are taken to be the score of the model. As a result, biasing of a model incorporating over-fitting or under-fitting is eliminated. Randomized search CV uses this cross validation technique to assess the accuracy of a model and finds the best hyper parameters of an algorithm upon a certain given number of iteration. In this study, k=5 is used for randomized search CV and the number of iteration is fixated at 11.

The success of Randomized search CV depends on the range of the hyper parameters given, so proper selection of this range is crucial. The following subsections describe the selection of hyper parameters values for each of the selected machine learning algorithms considering the range and using Randomized search CV as the key tool. In every case, the dataset derived from the BORC modelling is utilized to determine the characteristics of the hyper parameters as well as choosing the optimal value of it.

5.3.1 Linear Regression (Lasso)

The inherent characteristics of linear regression doesn't support any hyper parameters, so it suffers from over-fitting or under-fitting issue. To overcome this drawback, a specialist parameter is introduced in the algorithm which is known as the regularization parameter. Linear regression, incorporating this parameter, is known as the lasso regression and it can operate in a biased free manner.

Figure 5.1 demonstrates the effect of regularization parameter on the performance of Lasso regressor based on energy and exergy prediction respectively. From the figures, it is evident that the inherent characteristics of the dataset of the thermodynamic modeling allows less room for regularization as with the increase of the parameter the score of the model drops significantly.

For thermal efficiency prediction, the model doesn't experience any significant change after the regularization parameter crosses the value 0.2. However, for exergy efficiency prediction, the performance of the model drops almost linearly with the increase of the regularization parameter. So, for ORC applications, linear regression without or with smaller regularization can be a feasible option for machine learning purpose. However, a smaller range of

regularization is considered in this study in order to show the effect of hyper parameter tuning in case of the linear regression application.

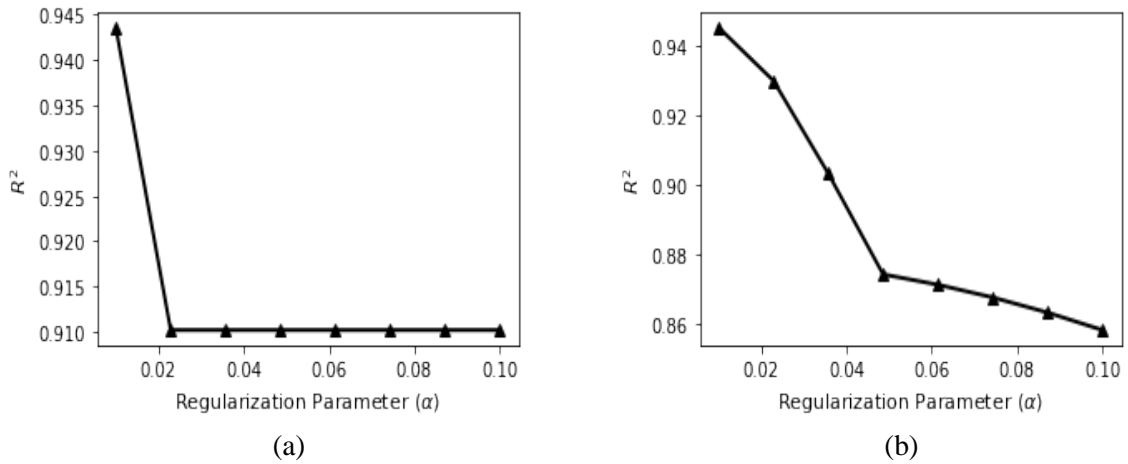


Figure 5.1 Effect of regularization parameter on the performance of Lasso regression for (a) thermal efficiency (b) exergy efficiency

Table 5-3 demonstrates the optimal parameter along with the value of the performance indicators based on the Randomized search CV method for Lasso regressor. As observed above, the model with lower regularization parameter exhibits the optimal performance.

Table 5-3 Optimal parameters for Lasso regressor with performance indicator

Efficiency prediction criteria	Optimal regularization parameter	MAE	MSE	MRE	R^2
Thermal	0.01364	0.00473	0.00003	4.56679	0.92828
Exergy	0.02273	0.01001	0.00015	3.88458	0.93036

5.3.2 Support Vector Regressor

In this study, two hyper parameters of the SVR model are optimized, namely the kernel function and the epsilon. At first, the viability of four kernel functions namely rbf, sigmoid, linear, and poly are tested setting the epsilon value to 0.001. It is found that except for the rbf and sigmoid kernel, the model performs poorly for the rest of the kernels in respect to the performance score as well as the performance time. Therefore, the rbf and the sigmoid kernels are considered for

comparison purpose and the performance of the SVR model under these kernel criteria are listed in *Table 5-4*

Table 5-4 Performance of SVR for different kernel functions

Efficiency prediction criteria	Kernel function	MAE	MSE	MRE	R^2
Thermal	RBF	0.01434	0.00032	13.68892	0.2947
	sigmoid	0.01814	0.00046	16.98408	-0.01200
Exergy	RBF	0.03049	0.00155	11.77038	0.29410
	sigmoid	0.03926	0.00223	14.74260	-0.01470

From *Table 5-4*, it is evident that rbf kernel function performs better for the SVR model for the studied dataset. Therefore, rbf is selected as the key kernel function

Further, the value of R^2 scores are very poor for both of the kernel function for the epsilon value of 0.001 which can be improved by lowering the epsilon value further as demonstrated in

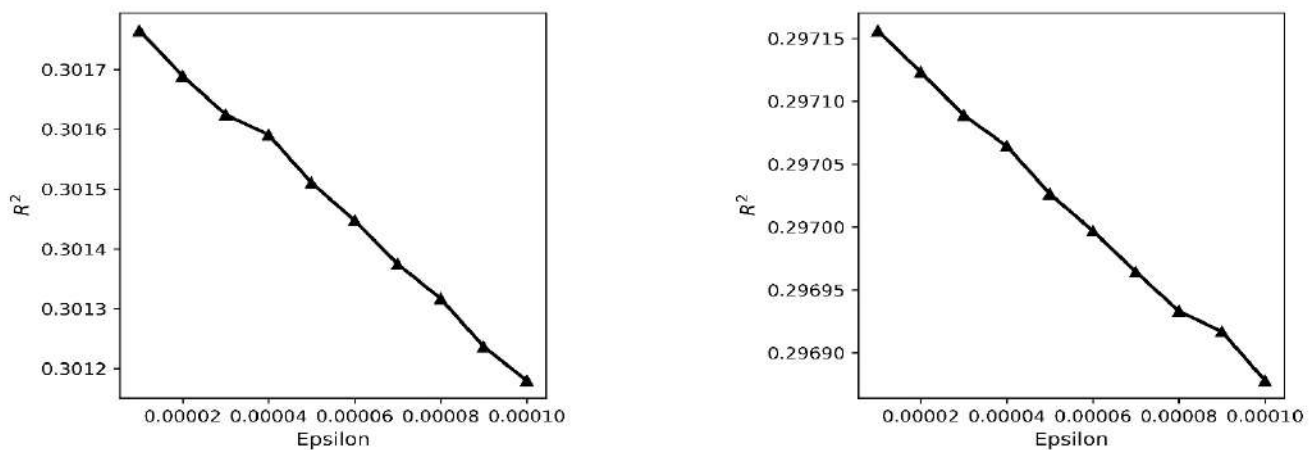


Figure 5.2.

(a)

(b)

Figure 5.2 Effect of epsilon on the performance of support vector regression for (a) energy efficiency (b) exergy efficiency

Table 5-5 demonstrates the optimal epsilon value along with the value of the performance indicators based on the Randomized search CV method for SVR algorithm. As observed above, the model with lower epsilon value exhibits the optimal performance. However, with the decrease of the epsilon value, the performance improvement of the SVR algorithm is negligible, so a lower limiting value of 0.00001 is chosen to save computational time.

Table 5-5 Optimal parameters for support vector regressor with performance indicator

Efficiency prediction criteria	epsilon	MAE	MSE	MRE	R²
Thermal	0.00001	0.01414	0.00032	13.49787	0.30177
Exergy	0.00006	0.03061	0.00155	11.69952	0.29716

5.3.3 Decision tree regression

Decision tree regressor has multiple number of hyper parameters like criterion, splitter, maximum depth, minimum sample split etc. In this study, two pivotal hyper parameters are chosen for tuning purpose namely the criterion and the maximum depth. The rest of the parameters are set as default according to the scikit learn documentation, which are listed in Table 5-6.

Table 5-6 Default values of hyper parameters for decision tree regression

Hyper parameter	Default value
splitter	best
Minimum sample split	2
Minimum samples leaf	1

Several functions are available to access the quality of the split in scikit learn for decision tree regression. Apart from the traditional performance metrics like mean squared error or mean absolute error, criterion like Friedman mean squared error and poisson are also available in the scikit learn library. Table 5-7 demonstrates the performance of the decision tree model for the stated criteria.

From *Table 5-7*, it is evident that absolute error split criterion has the best performance of all the stated criterion. Therefore, in this study this criterion is adopted to measure the quality of each split of the dataset.

Table 5-7 Performance of Decision tree for different split criterion

Efficiency prediction criteria	Split criterion	MAE	MSE	MRE	R²
Thermal	Squared error	0.00077	1.21454	0.73574	0.99733
	Friedman mse	0.00077	1.21894	0.73595	0.99732
	Absolute error	0.00075	1.12094	0.70565	0.99754
Exergy	Squared error	0.00198	8.19373	0.76514	0.99627
	Friedman mse	0.00200	8.89063	0.77380	0.99596
	Absolute error	0.00193	7.97914	0.75284	0.99637

Apart from the split criteria, maximum length of the decision tree plays a significant role in improving the performance of the model. *Figure 5.3* demonstrate the effect of increasing the depth of the decision tree on the performance of the decision tree model

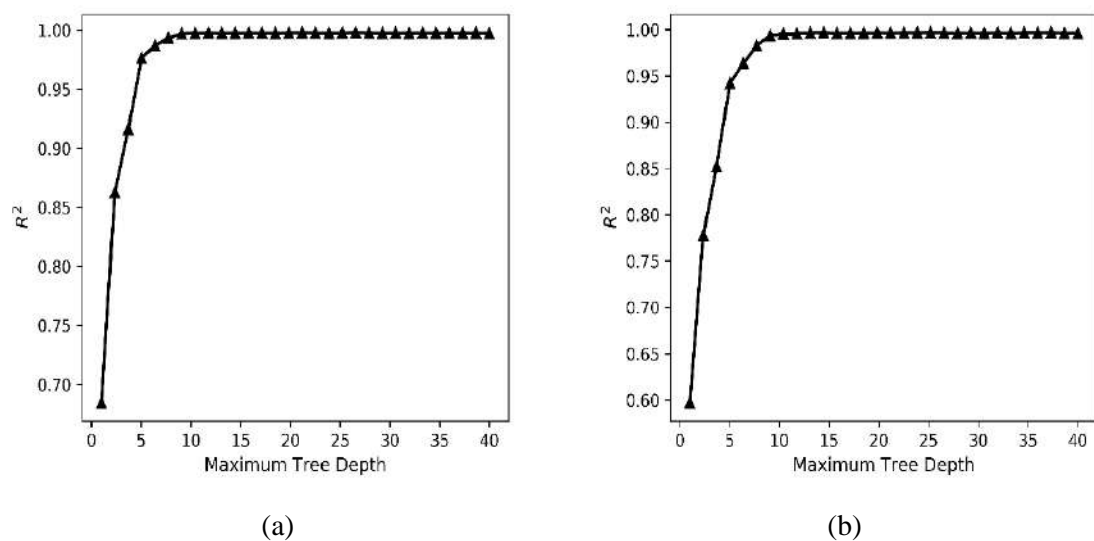


Figure 5.3 Effect of maximum tree depth on the performance of decision tree for (a) thermal efficiency (b) exergy efficiency

From the above figures it is evident that with the increase of the maximum depth of the decision tree, the performance of the decision tree model improves for both the exergy efficiency and the thermal efficiency. However, it is also observed that after a certain value of it (around 10), the performance of both the models become almost steady.

The optimal value of the maximum tree depth generated from the randomized search cv method are demonstrated in *Table 5-8*.

Table 5-8 Optimal value of maximum tree depth for decision tree along with performance indicator

Efficiency prediction criteria	Maximum tree depth	MAE	MSE	MRE	R^2
Thermal	18	0.0008	1.3222	0.7650	0.9978
Exergy	40	0.0019	8.2472	0.7527	0.9963

5.3.4 Random forest regression

Random forest regression is an ensemble machine learning method incorporating the same procedure as the decision tree regressor. Therefore, the hyper parameters described in the previous section like splitting criteria, maximum tree depth, splitter, etc. are applicable in case of this regression method.

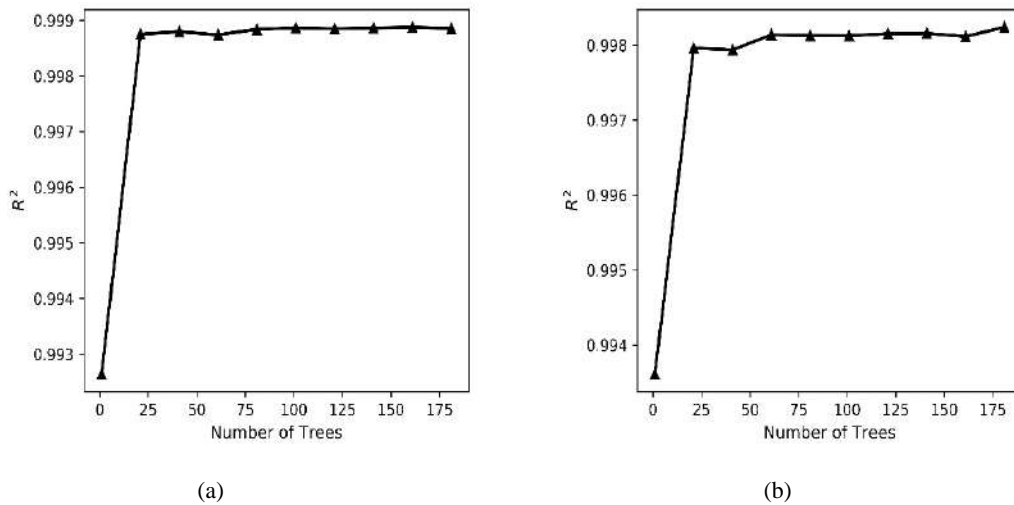


Figure 5.4 Effect of the number of trees on the performance of Random forest regressor for (a) thermal efficiency (b) exergy efficiency

Table 5-9 Optimal value of number of trees for decision tree along with performance indicator

Efficiency prediction criteria	Number of trees	MAE	MSE	MRE	R^2
Thermal	101	0.00052	5.32635	0.49842	0.99883
Exergy	151	0.00142	3.96128	0.55325	0.99820

Table 5-10 Selected hyper parameters for the studied algorithms

Algorithm	Selected hyper parameters for tuning	Optimal value/type by Randomized search CV	Applicable efficiency
Linear regression (lasso)	Regularization parameter	0.01364	Thermal
		0.02273	Exergy
Support vector regression	Kernel function epsilon	RBF	Thermal and Exergy
		0.00001	Thermal
		0.00006	Exergy
Decision tree regression	Split criteria Maximum depth	Absolute error	Thermal and Exergy
		18	Thermal
		40	Exergy
Random forest regression	Number of trees	101	Thermal
		151	Exergy

Moreover, the default values of the hyper parameters stated in *Table 5-6* are also kept here as the defaults for modelling purpose. Again, as derived in the previous section, maximum absolute error is considered as the splitting criteria. Further, the value of the maximum tree depth is considered from the analysis of *Table 5-8*

Apart from the previously stated hyper parameters, the performance of the random forest regressor significantly depends on the number of trees in the defined forest. *Figure 5.4* demonstrates the effect of these values on the overall performance of the model.

From these figures it is observed that increasing the number of trees increases the performance of the random forest regressor model. However, after a certain number of trees (around 50), there is negligible change in the performance of the model.

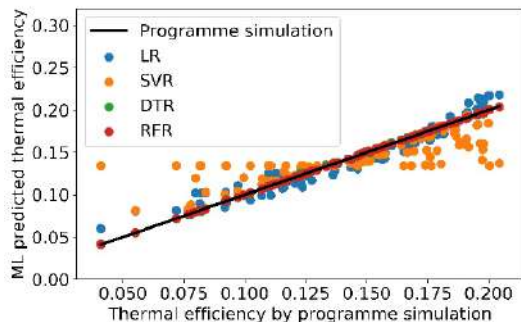
All the tuned hyper parameters for all the models are summarized in *Table 5-10*. *Table 5-9* exhibits the optimal values of the number of trees of the studied model along with the performance parameters. As it is observed, the optimal number of trees are around or slightly more than 100, though it can be lower in practical cases.

5.4 Selection of ML algorithm & determination of model performance metrics for individual working fluid

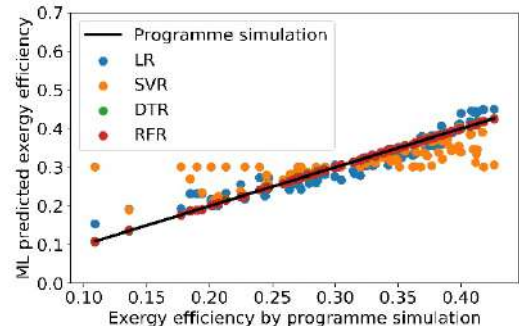
One of the objectives of this study is to select a proper machine learning scheme for thermodynamic modelling purpose. Owing to that reason, a comprehensive analysis and comparative study between the performances of the mentioned machine learning schemes is crucial. In this section the selection procedure of the best machine learning algorithm will be discussed.

To access the viability of the studied models, a database containing the ORC parameters along with the corresponding exergy and energy efficiencies is constructed first for the mentioned four ORC configurations. After that, the performance of each of the algorithms are assessed. *Figure 5.5 - Figure 5.8* demonstrate the prediction performance of the studied ML algorithms for four of the ORC configurations for Cyclohexane as the working fluid

From these figure, it is evident that the prediction results of SVR are the most scattered of all of the ML scheme. Among all the mentioned ML, the RF regressor produces the most accurate prediction result. The DC regressor follows the trend of RF regressor with slightly less prediction accuracy.

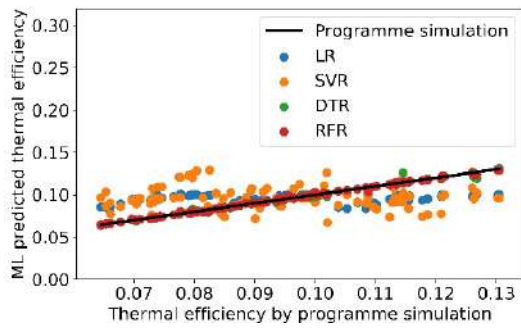


(a)

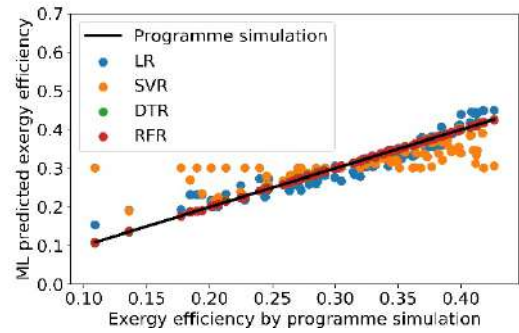


(b)

Figure 5.5 Comparison of predicted efficiency by ML with simulated result of BORC, (a) thermal efficiency, (b) exergy efficiency.

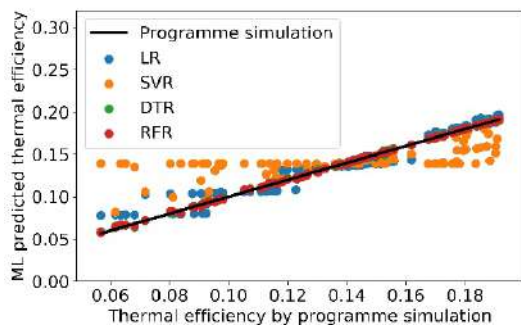


(a)

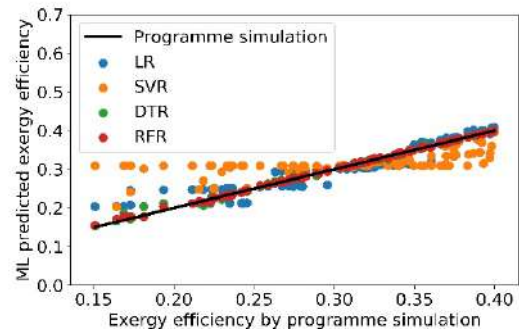


(b)

Figure 5.6 Comparison of predicted efficiency by ML with simulated result of RORC, (a) thermal efficiency, (b) exergy efficiency.



(a)



(b)

Figure 5.7 Comparison of predicted efficiency by ML with simulated result of IORC, (a) thermal efficiency, (b) exergy efficiency.

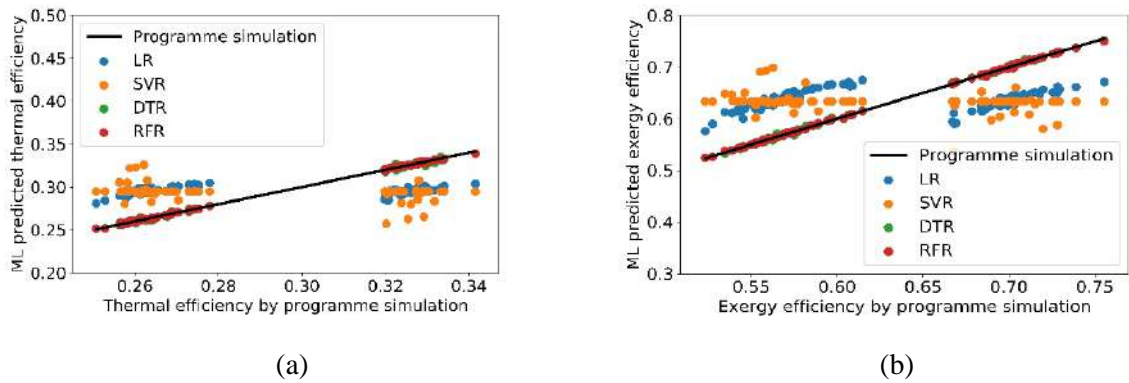


Figure 5.8 Comparison of predicted efficiency by ML with simulated result of CRIORC, (a) thermal efficiency, (b) exergy efficiency.

On the other hand, LR produces a moderate prediction trend for BORC and IORC. However, its performance is significantly dropped in case of RORC and CRIORC as the data are more scattered compared to that of BORC and IORC.

To fully access the performance of each of the ML scheme, four performance metrics namely MSE, MAE, MRE, and R^2 are considered. The performance of the schemes based on the mentioned metrics are compared which are illustrated from *Figure 5.9* to *Figure 5.17* for nine of the working fluids.

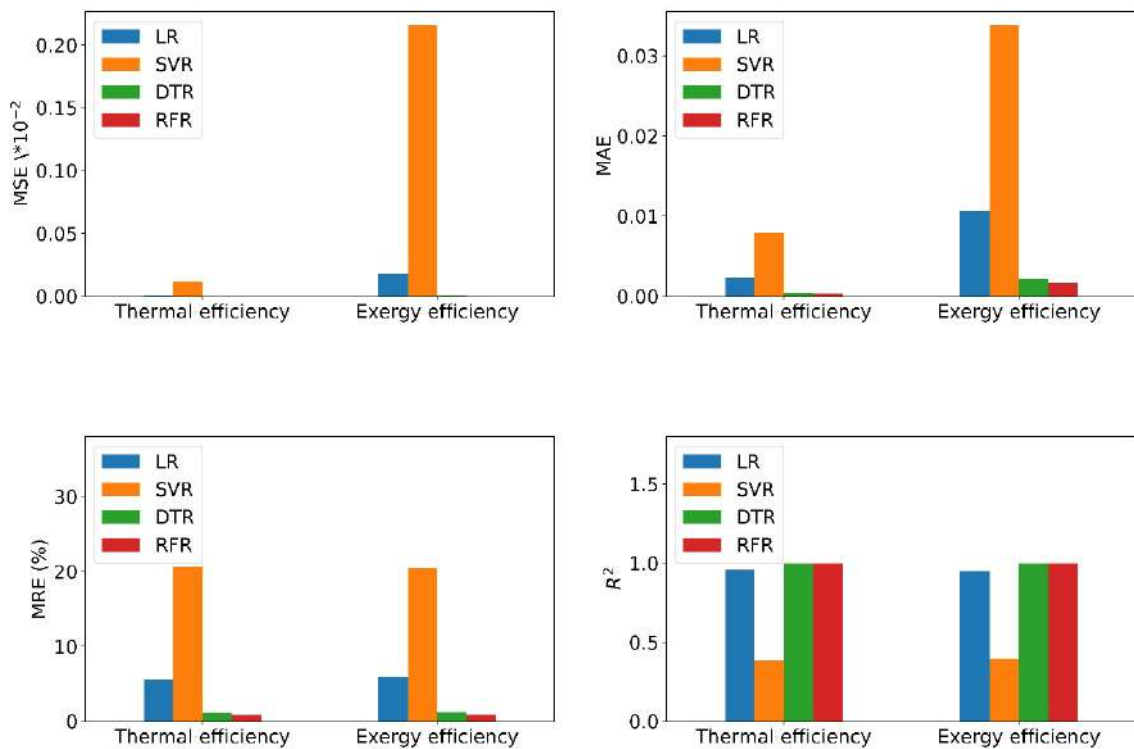


Figure 5.9 Performance metrics of ML algorithms for BORC with R227ea as working fluid

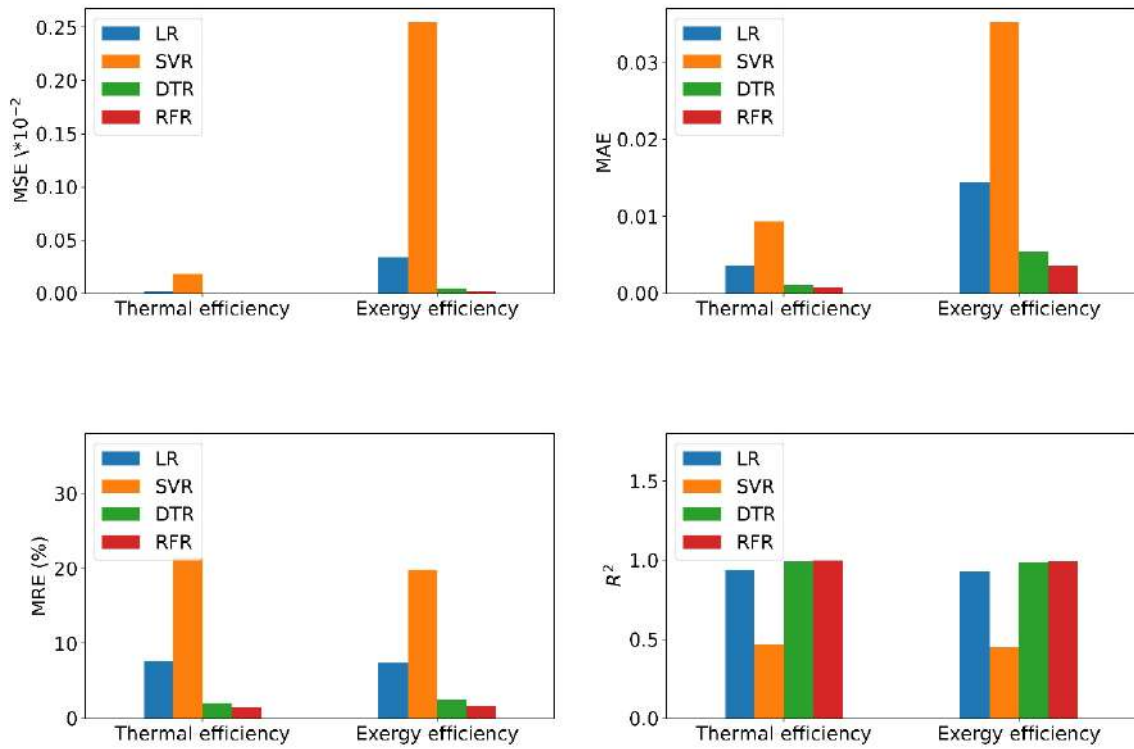


Figure 5.10 Performance metrics of ML algorithms for BORG with RC318as working fluid

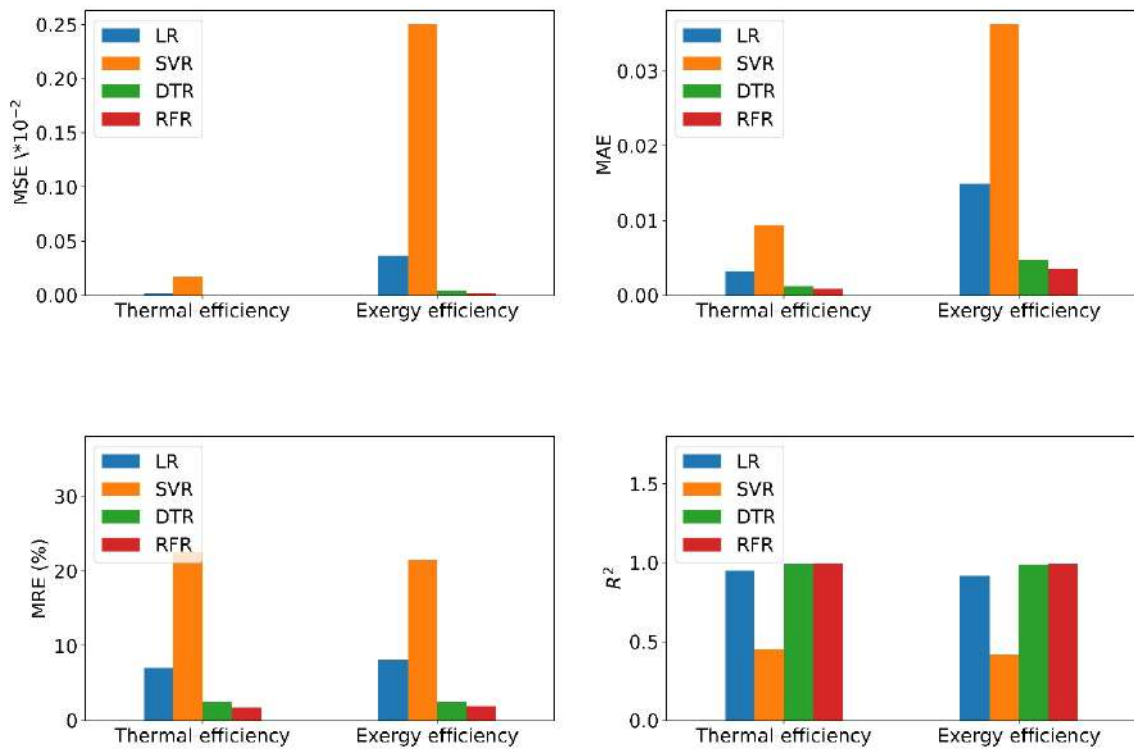


Figure 5.11 Performance metrics of ML algorithms for BORG with R236faas working fluid

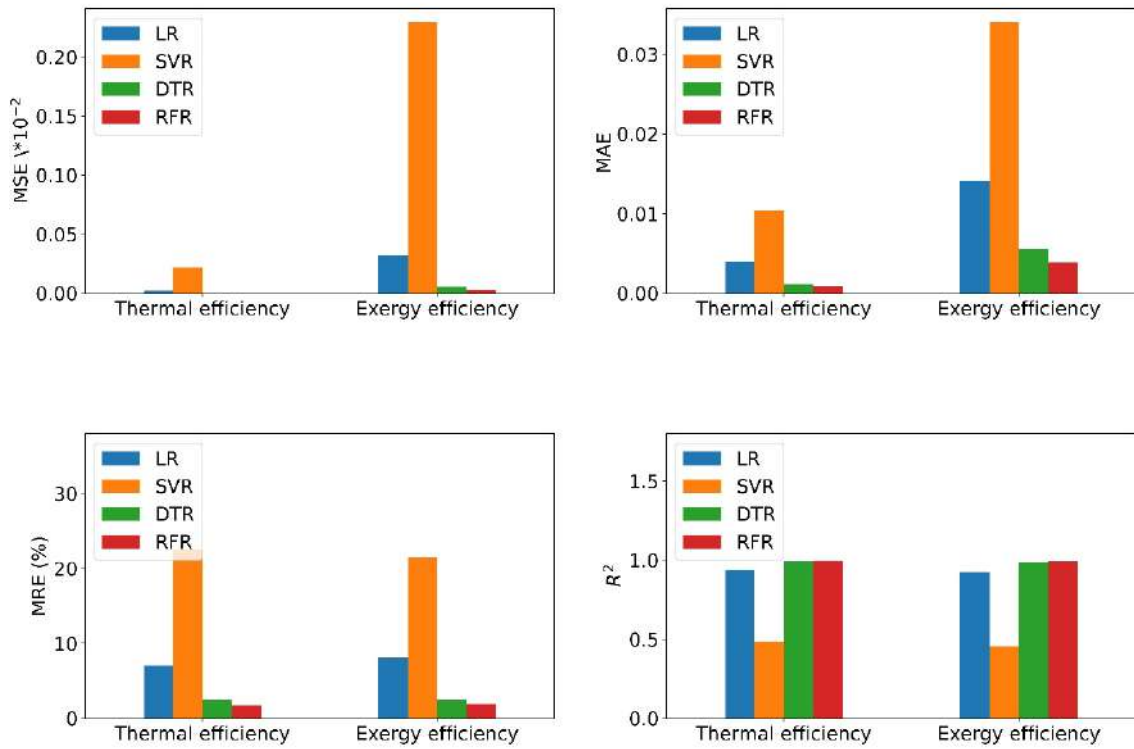


Figure 5.12 Performance metrics of ML algorithms for BORG with R236eaas working fluid

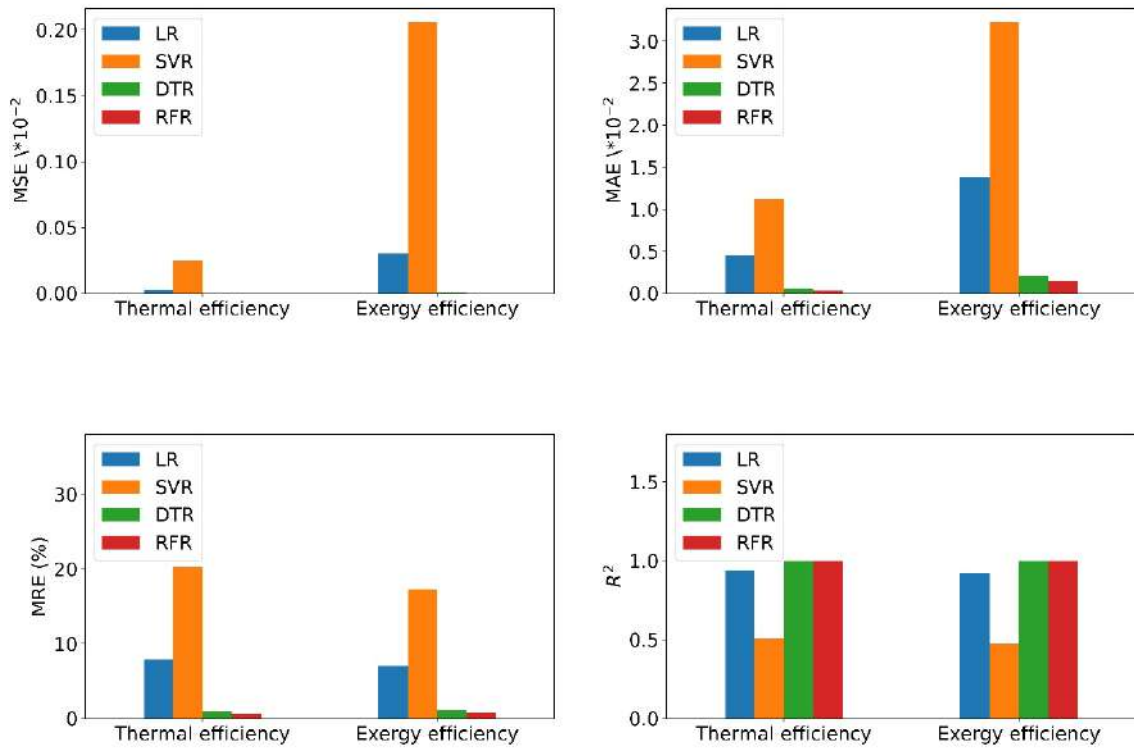


Figure 5.13 Performance metrics of ML algorithms for BORG with R245faas working fluid

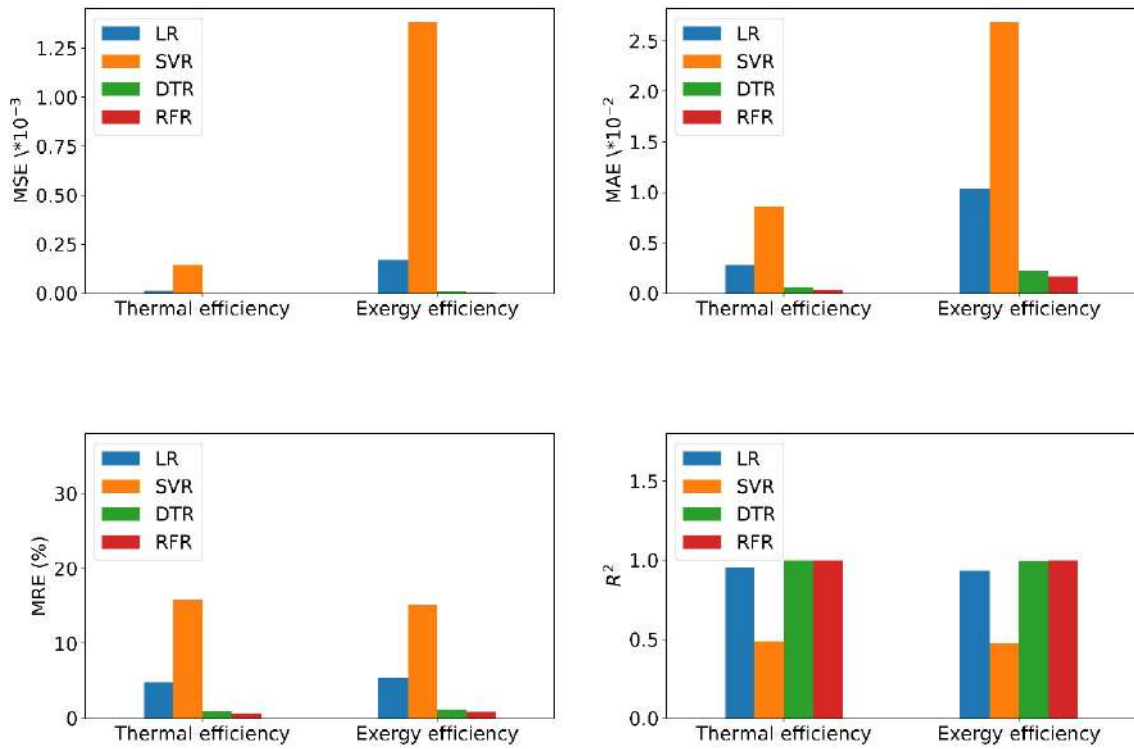


Figure 5.14 Performance metrics of ML algorithms for BORG with R123as working fluid

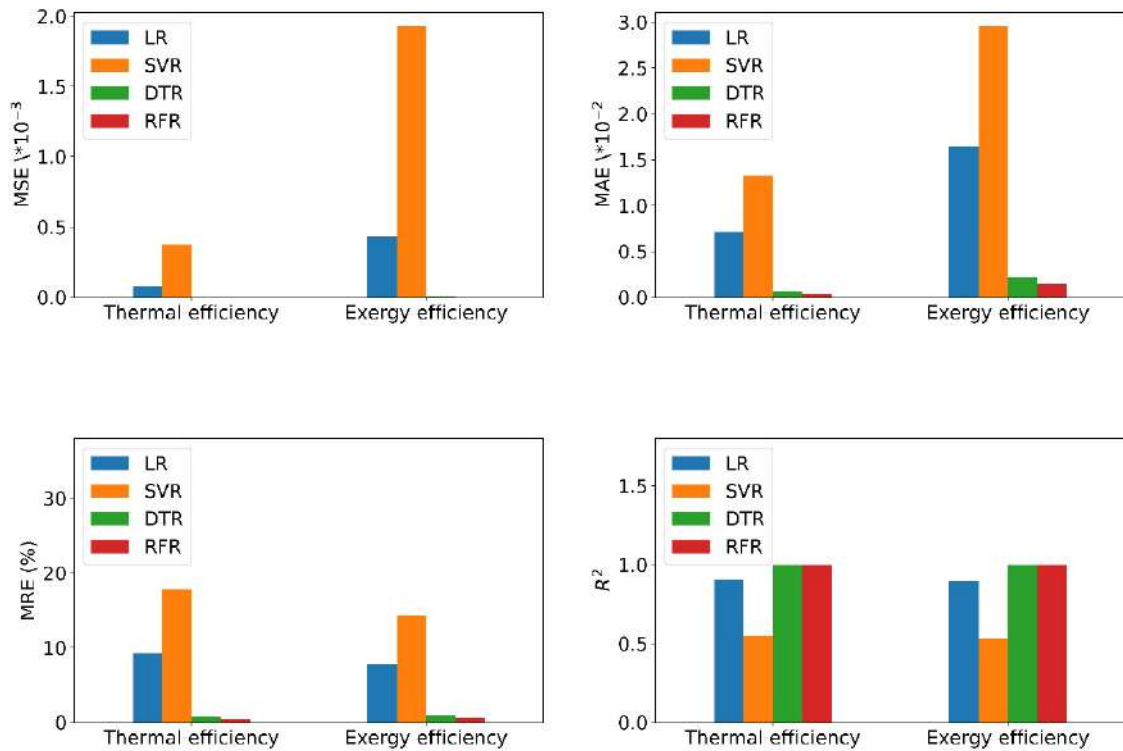


Figure 5.15 Performance metrics of ML algorithms for BORG with R113as working fluid

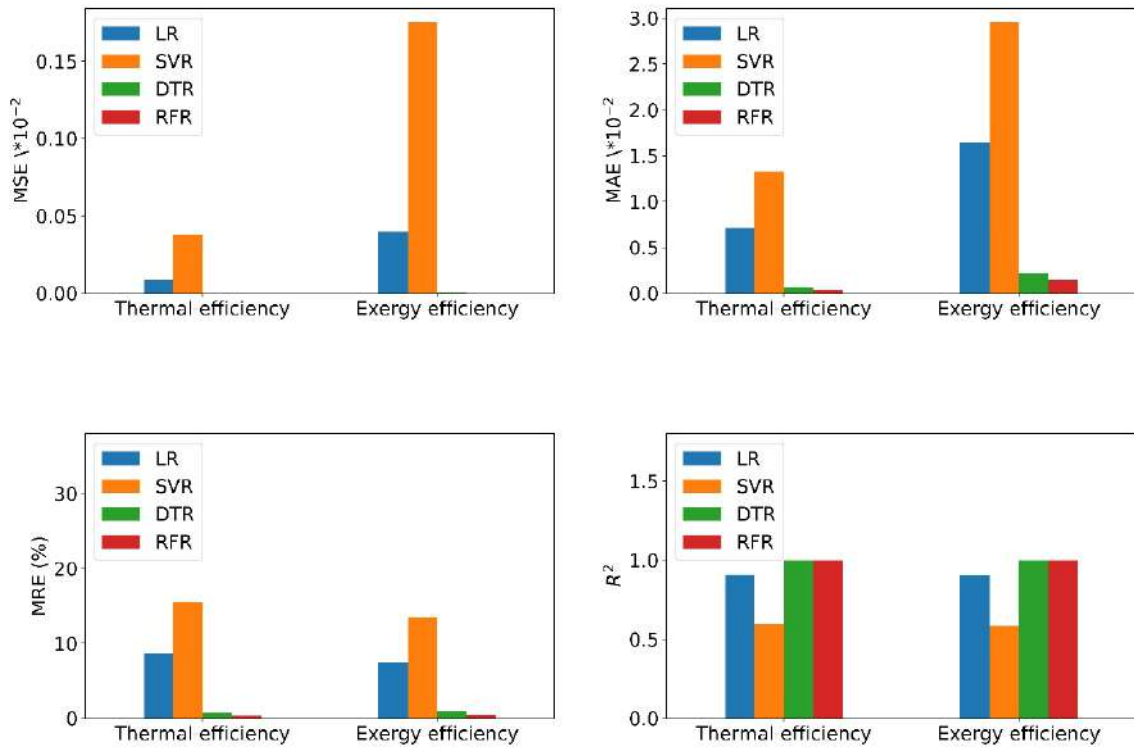


Figure 5.16 Performance metrics of ML algorithms for BORG with Cyclopentane working fluid

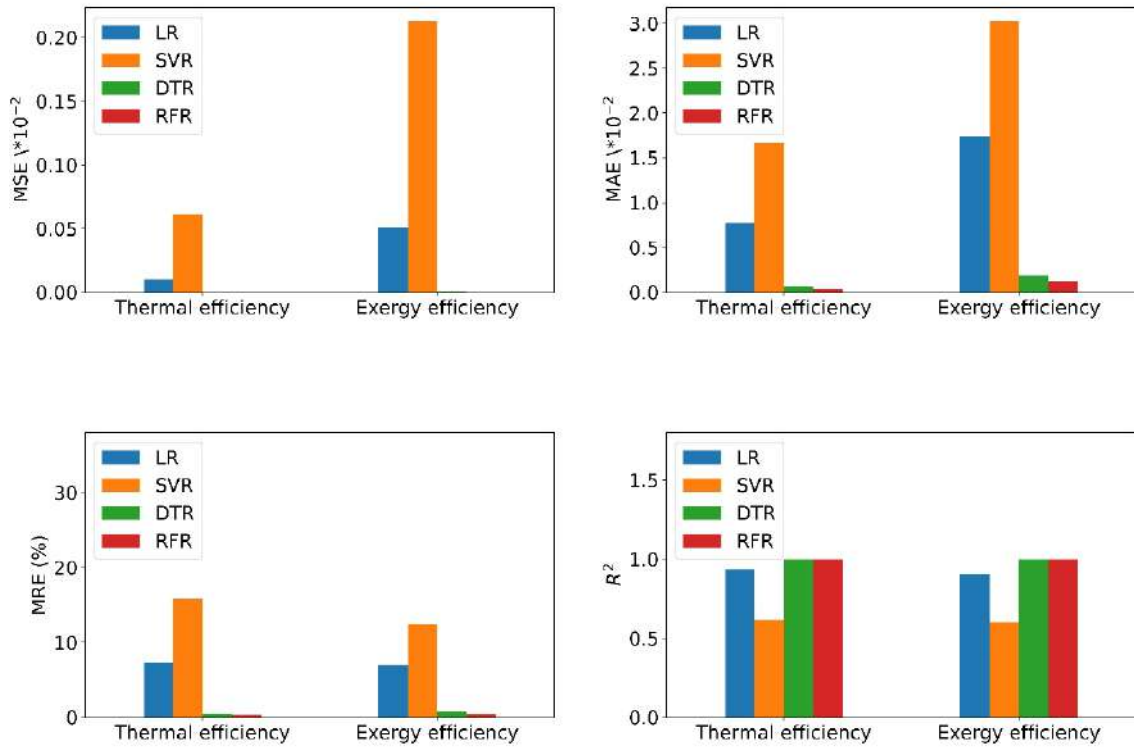


Figure 5.17 Performance metrics of ML algorithms for BORG with Cyclohexane working fluid

From the figures, it is observed that the RFR method produces the best ML performance metrics for all the mentioned nine working fluids. The R^2 scores of RFR are slightly higher than that of DCR for every working fluids. Furthermore, RFR produces the lowest MSE, MRE, and MAE of all the four ML algorithms discussed. LR can be placed below the RFR and DCR in respect of the performance metrics. Among all, SVR demonstrates the poorest prediction performance as illustrated by the figures. With the increase of heat source temperature range for particular fluids like cyclopentane and cyclohexane, the performance of the SVR model improves. The performance indicators, however, still remains lower compared to that of RFR, DCR, and LR.

RFR also demonstrates a comparatively consistent performance irrespective of the working fluid. This special characteristics makes it the suitable algorithm for ORC modelling covering a wide range of fluids. Therefore, RFR is selected as the primary ML algorithm for prediction and optimization purpose of the ORC.

In Table 5-11, Table 5-12, and Table 5-13, the performance metrics of RFR for the other three ORC configurations are illustrated.

Table 5-11 Performance metrics of RFR for RORC configuration

Working fluid	η_{th}				η_{ex}			
	MSE	MAE	MRE	R^2	MSE	MAE	MRE	R^2
R227ea	6.3698	0.0059	3.2724	0.9479	0.0014	0.0276	3.2769	0.9476
RC318	2.3873	0.0035	2.3344	0.9684	0.0005	0.0160	2.3214	0.9700
R236fa	3.1775	0.0042	2.9026	0.9644	0.0006	0.0186	2.9182	0.9650
R236ea	2.8173	0.0040	2.9355	0.9618	0.0005	0.0172	3.0527	0.9649
R245fa	2.5664	0.0039	3.0539	0.9586	0.0005	0.0165	3.1827	0.9635
R123	1.9553	0.0034	2.6806	0.9662	0.0002	0.0116	2.7490	0.9679
R113	6.6401	0.0017	1.4773	0.9855	5.9672	0.0049	1.5122	0.9878
Cyclopentane	4.6522	0.0014	1.2210	0.9883	3.0428	0.0036	1.2077	0.9900
Cyclohexane	2.1946	0.0009	1.2813	0.9935	1.2813	0.0021	0.8944	0.9947

Table 5-12 Performance metrics of RFR for IORC configuration

Working fluid	η_{th}				η_{ex}			
	MSE	MAE	MRE	R ²	MSE	MAE	MRE	R ²
R227ea	1.2269	0.0002	0.6349	0.9992	2.7737	0.0010	0.6157	0.9992
RC318	2.9793	0.0004	0.8149	0.9950	3.7583	0.0014	0.6950	0.9963
R236fa	9.8849	0.0007	1.5833	0.9906	4.5989	0.0015	0.7989	0.9965
R236ea	1.4702	0.0009	1.9576	0.9868	1.0820	0.0020	1.1635	0.9915
R245fa	1.5970	0.0009	2.0613	0.9855	1.0015	0.0021	1.2725	0.9914
R123	1.6333	0.0009	1.5073	0.9899	1.3247	0.0027	1.7991	0.9886
R113	1.0745	0.0008	0.9257	0.9948	7.5818	0.0019	0.8677	0.9972
Cyclopentane	1.6950	0.0010	1.0025	0.9977	9.4935	0.0022	0.9437	0.9966
Cyclohexane	1.3268	0.0008	0.7121	0.9991	6.6961	0.0016	0.6427	0.9984

From the discussed data, it is evident that the evaluation metrics values are within an acceptable range for standard machine learning operation. However the performance differ from one another for distinctive working fluids. As four of the evaluation metrics indicate four distinctive aspect of the ML algorithm, it is not possible to select the best performing working fluid for ML applications. However, focusing on a particular metrics can indicate a general insight about the performance of the working fluid. As in practical application it is important to address the characteristics of a wide range of fluids, the ML algorithms should be able to address the variance. Therefore, R² value can be a key indicator of how the ML algorithm is working.

From the performance data, it is evident that Cyclohexane produces the best performance in respect of R² value. Cyclopentane demonstrates almost similar trend of Cyclohexane except for the IORC configurations. The R² value for all the working fluid lies between the 0.98-0.99 range, indicating RFR a standard algorithm for addressing the variance of the working fluids performance.

Table 5-13 Performance metrics of RFR for CRIORC configuration

Working fluid	η_{th}				η_{ex}			
	MSE /*10 ⁻¹	MAE	MRE	R ²	MSE	MAE	MRE	R ²
R227ea	0.0005	0.0052	3.0984	0.9789	3.1031	0.0235	3.1031	0.9783
RC318	0.0002	0.0028	1.1990	0.9892	2.1168	0.0125	2.1168	0.9886
R236fa	0.0003	0.0039	2.8061	0.9790	2.7413	0.0159	2.7413	0.9797
R236ea	0.0002	0.0034	2.6773	0.9811	2.9327	0.0154	2.9327	0.9783
R245fa	0.0002	0.0035	2.9850	0.9768	3.2390	0.0154	3.2390	0.9732
R123	0.0002	0.0031	2.7402	0.9793	3.0234	0.0114	3.0234	0.9770
R113	0.0001	0.0022	2.1939	0.9863	2.0185	0.0059	2.0185	0.9875
Cyclopentane	0.0001	0.0021	2.0265	0.9865	1.9917	0.0054	1.9917	0.9864
Cyclohexane	0.0000	0.0012	1.4208	0.9929	1.2795	0.0027	1.2795	0.9936

Table 5-14 Model parameters for the studied BPNN

Model parameter	Characteristics/name/number
Package used	Keras under tensorflow
Model type	Sequential
Total number of layers	4 (1 input, 2 hidden, and 1 output)
Number of nodes	8-10 (input layer), 32 and 8 (hidden layer), 1 (output layer)
Activation function	Relu (for input and hidden layer), linear (for output layer)
loss	MSE
Optimizer	Adam
Learning rate	0.02

5.5 Hyper parameters & performance metrics for individual working fluids for BPNN

The performance of BPNN significantly depends on three hyper parameters: learning rate, number of hidden layers, and number of neurons in each layers. Learning rate is the rate which can limit or increase the BPNN adaptability of any given data set. A high learning rate can introduce the over fitting problem while a lower rate can formulate under fitting criteria. Therefore, this study keeps a learning rate of 0.02 which is standard for BPNN approach. The success of BPNN critically depends on the selection of hidden layers. With the increase of the hidden layers the performance of the BPNN tends to increase. However, the success of BPNN with excess amount of hidden layers also depends on computing architecture. Therefore, two hidden layers are used in this study which is an optimal choice for both computing time and prediction performance. Moreover, the number of neurons is also crucial for a successful BPNN algorithm. The neurons in the input and the output layer are application dependent while the user has control over the number of neurons in the hidden layers.

Table 5-15 Performance metrics of BPNN for BORC configuration

Working fluid	η_{th}				η_{ex}			
	MSE /*10 ⁻¹	MAE	MRE	R ²	MSE	MAE	MRE	R ²
R227ea	0.0002	0.0032	7.6124	0.9127	0.0001	0.0024	1.3547	0.9972
RC318	0.0003	0.0045	9.4005	0.9099	0.0007	0.0066	3.1900	0.9845
R236fa	0.0003	0.0044	9.2882	0.9030	0.0013	0.0085	4.9238	0.9694
R236ea	0.0002	0.0027	4.2828	0.9607	0.0002	0.0038	1.8067	0.9946
R245fa	0.0001	0.0018	2.9866	0.9897	0.0001	0.0029	1.4210	0.9966
R123	0.0000	0.0013	2.3027	0.9895	0.0000	0.0016	0.8376	0.9983
R113	0.0004	0.0056	5.9214	0.9494	0.0000	0.0018	0.7646	0.9988
Cyclopentane	0.0000	0.0018	1.5770	0.9966	0.0000	0.0014	0.6312	0.9993
Cyclohexane	0.0000	0.0015	1.3548	0.9976	0.0001	0.0024	0.9723	0.9980

Table 5-16 Performance metrics of BPNN for RORC configuration

Working fluid	η_{th}				η_{ex}			
	MSE /*10 ⁻¹	MAE	MRE	R ²	MSE /*10 ⁻¹	MAE	MRE	R ²
R227ea	0.0004	0.0054	3.0009	0.9632	0.0044	0.0166	2.0291	0.9834
RC318	0.0002	0.0033	2.1739	0.9744	0.0017	0.0098	1.4467	0.9898
R236fa	0.0005	0.0059	4.1055	0.9408	0.0061	0.0199	3.2089	0.9662
R236ea	0.0004	0.0051	3.7415	0.9448	0.0055	0.0188	3.3439	0.9636
R245fa	0.0004	0.0048	3.7674	0.9431	0.0046	0.0168	3.2521	0.9642
R123	0.0003	0.0041	3.2868	0.9567	0.0022	0.0115	2.7168	0.9709
R113	0.0002	0.0035	3.2056	0.9570	0.0008	0.0065	2.0732	0.9837
Cyclopentane	0.0002	0.0034	2.7567	0.9505	0.0007	0.0062	2.0723	0.9776
Cyclohexane	0.0001	0.0031	3.3060	0.9560	0.0003	0.0041	1.8190	0.9856

As the numbers of nodes in input layer vary from 8 to 10, two roughly proportionate hidden layers with 32 nodes and 8 nodes respectively are used in this study. Apart from the number of nodes, activation function in each layer carries a significant importance for proper tuning of the BPNN algorithm. Activation function is responsible for activating any particular neuron and the weights in the neuron connections are modified based on the activation during the training process. In this study, Relu activation function is applied in the input layers as it is the most common and simple activation function. In the output layer on the other hand, linear activation function is used to address the regression criteria of the study.

In this study, keras library inside tensorflow package is used for constructing the BPNN model. The sequential model from keras is used which is a layer by layer addition model. Under the sequential model, one input layer, two hidden layers and one output layer is used for predicting the thermal efficiency and exergy efficiency respectively. Apart from the last layer which uses the linear activation function, the rest of the layers use relu as the activation function. The model parameters of the mentioned BPNN is mentioned in Table 5.14

Table 5-17 Performance metrics of BPNN for IORC configuration

Working fluid	η_{th}				η_{ex}			
	MSE /*10 ⁻¹	MAE	MRE	R ²	MSE /*10 ⁻¹	MAE	MRE	R ²
R227ea	0.0000	0.0009	2.2438	0.9935	0.0000	0.0015	0.7776	0.9992
RC318	0.0000	0.0008	1.6583	0.9785	0.0000	0.0012	0.5711	0.9980
R236fa	0.0000	0.0009	2.0412	0.9865	0.0000	0.0012	0.6330	0.9979
R236ea	0.0001	0.0018	3.8115	0.9385	0.0001	0.0025	1.3887	0.9911
R245fa	0.0001	0.0019	4.5058	0.9113	0.0001	0.0022	1.2132	0.9937
R123	0.0000	0.0012	2.3349	0.9821	0.0001	0.0021	1.1518	0.9941
R113	0.0000	0.0014	1.8225	0.9940	0.0001	0.0022	0.9664	0.9971
Cyclopentane	0.0000	0.0015	1.6341	0.9935	0.0000	0.0013	0.5412	0.9990
Cyclohexane	0.0000	0.0014	1.2490	0.9976	0.0001	0.0020	0.7849	0.9981

Table 5-15- Table 5-18 illustrate the performance of the constructed BPNN for the four ORC configurations for nine of the working fluids. From the tables, it is observed that for fluids with lower working temperature like R227ea, RC318 etc., the performance of the BPNN fluctuates unlike the previously mentioned ML algorithms. However, the performances tend to improve for fluid with higher temperature like Cyclopentane, Cyclohexane, etc. This is mainly because of the number of data for each of the fluid. For fluids with lower working temperature, the dataset is comparatively smaller with the target temperature line approach. However, with the increase of the working temperature, the target temperature line method becomes more flexible for same operating condition and the dataset gets bigger. As the number of data increases for the bottom members of the described tables, the BPNN models become more accurate. The ML algorithms, on the other hand, produces better result with even smaller dataset. However, the computational time for BPNN is lower than that of the previously described ML algorithms. Therefore, the performance of the BPNN is more data sensitive but produces result in shorter times than the ML techniques.

Table 5-18 Performance metrics of BPNN for CRIORC configuration

Working fluid	η_{th}				η_{ex}			
	MSE /*10 ⁻¹	MAE	MRE	R ²	MSE /*10 ⁻¹	MAE	MRE	R ²
R227ea	0.0005	0.0059	3.9115	0.9772	0.0006	0.0064	0.9197	0.9986
RC318	0.0001	0.0022	1.7569	0.9944	0.0006	0.0058	1.0288	0.9979
R236fa	0.0006	0.0045	3.4567	0.9565	0.0011	0.0067	1.1245	0.9957
R236ea	0.0002	0.0030	2.3409	0.9856	0.0015	0.0086	1.5934	0.9927
R245fa	0.0007	0.0055	4.9053	0.9247	0.0017	0.0086	1.7380	0.9898
R123	0.0003	0.0044	3.9037	0.9655	0.0007	0.0060	1.6847	0.9934
R113	0.0001	0.0023	2.2170	0.9854	0.0002	0.0033	1.1625	0.9963
Cyclopentane	0.0001	0.0024	2.5283	0.9827	0.0003	0.0040	1.6662	0.9938
Cyclohexane	0.0000	0.0014	1.7970	0.9940	0.0001	0.0023	1.1785	0.9970

5.6 Combined model performance prediction

In 5.4 and 5.5, the performance of the ML and the BPNN are discussed for nine of the working fluids individually. In order to accept the mentioned two algorithms as an alternative model for traditional analytical method, the performance of the models for wide range of working fluids should be assessed. This section describes the combined prediction scheme for the selected ANN algorithms for nine of the working fluids.

In order to perform the combined prediction, a dataset containing all the data described in 5.3 are combined together to form a unified dataset. Based on this dataset, the RF model and the BPNN model are trained with the established hyper parameters described in 5.3, 5.4 and 5.5. The training result along with the performance metrics are described in *Table 5-11* and *Table 5-12*.

It is to be mentioned that, molecular mass, critical temperature, and critical pressure of the working fluids are the unique features by which a fluid can be differentiated in the established dataset.

From the tables, it is observed that the MSE, MRE, and MAE values are increased slightly while combined dataset is considered. However, the R^2 value is still very high for all of the configurations. The RORC has the lowest value for combined ANN approach, but the value is increased while combined cycle configuration is considered. The higher value of R^2 indicates that the ANN approach can be used for wide variety of working fluids if proper dataset is used for the training purpose.

Table 5-19 Performance metrics of ANN models for thermal efficiency prediction

Configuration	MSE		MAE		MRE		R^2	
	RF	BPNN	RF	BPNN	RF	BPNN	RF	BPNN
BORC	1.7426	1.0297	0.0010	0.0026	1.5304	3.9864	0.9987	0.9923
RORC	3.4030	5.5933	0.0043	0.0058	3.0981	4.1547	0.9719	0.9539
IORC	1.5304	3.2707	0.0008	0.0015	1.2437	2.5578	0.9992	0.9982
CRIORC	0.00063	2.4238	0.0092	0.0039	3.0988	3.3446	0.9814	0.9855

Table 5-20 Performance metrics of ANN models for thermal efficiency prediction

Configuration	MSE		MAE		MRE		R^2	
	RF	BPNN	RF	BPNN	RF	BPNN	RF	BPNN
BORC	1.9294	4.6975	0.0033	0.0052	1.5797	2.2142	0.9960	0.9903
RORC	0.0006	0.0014	0.0168	0.0270	3.1294	7.9068	0.9874	0.9714
IORC	1.2918	1.0859	0.0024	0.0026	1.1888	1.2507	0.9970	0.9974
CRIORC	2.1479	0.0004	0.0032	0.0147	2.5630	3.7210	0.9872	0.9916

5.7 Sensitivity analysis and multi parameter optimization

The prime objective of this study is to find a suitable less time consuming alternative to the traditional analytical thermodynamic modelling in order to perform multi parameter optimization of the discussed four ORC configurations. In order to perform the optimization of

the cycles, the key thermodynamic parameters which have significant effect on the overall performance of the cycles need to be identified first. Therefore, a sensitivity analysis on the ORC configurations is performed first. After that, a multi-objective function containing both the energy and exergy efficiency is constructed and genetic algorithm is used to find the optimized cycle parameters.

5.7.1 Sensitivity analysis for cycle parameters

In order to perform the sensitivity analysis, the parameters discussed in 5.1 are considered. This includes heat source temperature, condensing temperature, pinch point temperature in the evaporator, reheating pressure ratio and internal regenerator efficiency.

As total number of six variables are considered here, effect of any single variable on the cycle efficiencies should be considered within the range of other variables. However, traditional 2D or 3D graph plot can be inconvenient for data visualization purpose in this regard as cycle efficiencies can be nearly identical for different values of same variables for the effect of other variables. Therefore, box plots are considered for data visualization purpose as it can show the range of the effect of a particular variable considering the values within the specified range of other variables.

In box plot data visualization, a box is constructed considering the first and the third quartile of data as the lower and upper limit along with the median in the middle. The minimum and maximum value of data are also shown with a whisker (therefore it is also known as whisker plot). So, a box is capable of addressing the range of data for a particular problem.

For sensibility analysis purpose, Cyclohexane is chosen as the ideal working fluid as it can work in both lower and higher values of the heat source temperature and thus can demonstrate similar trend of the rest of the working fluids.

Figure 5.18 and *Figure 5.19* demonstrate the range of thermal and exergy efficiency for different heat source temperature for four of the cycle configurations. From the figures it is observed that the average value of both thermal efficiency and exergy efficiency increase with the increase of the heat source temperature for BORC and IORC configuration. However, the efficiency slightly drops in case of IORC configuration. This is due to the low grade exit heat source temperature in the evaporator. Owing to its fixed value during simulation, the exit temperature of working fluid can't increase past it though the inlet temperature increases with regeneration process. Therefore, the recovered heat as well as the mass flow rate is reduced which in turns reduces the cycle efficiencies. It is also evident from subplot (a) and (c) that the

range of the thermal efficiency and exergy efficiency are almost non-overlapping, suggesting a nearly unique range of the performance metrics for respective heat source temperature value.

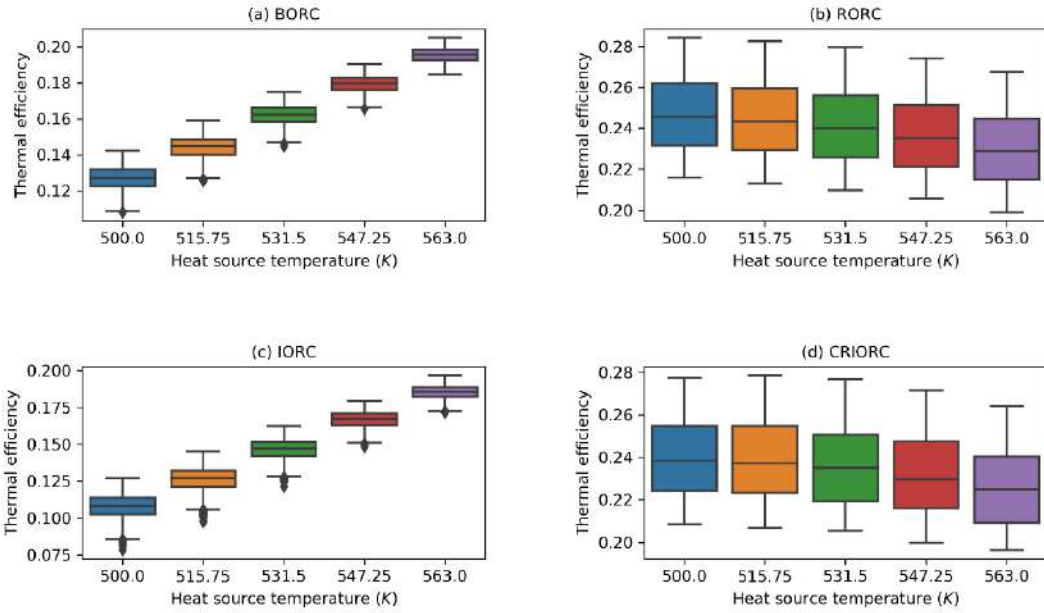


Figure 5.18 Box plot of thermal efficiency and heat source temperature for four cycle configurations

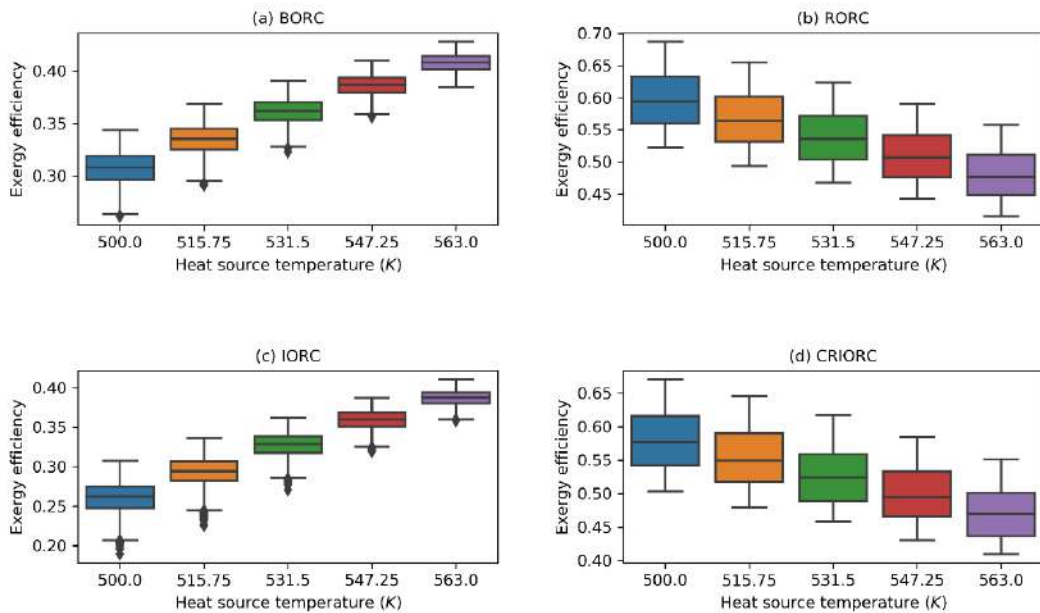


Figure 5.19 Box plot of exergy efficiency and heat source temperature for four cycle configuration

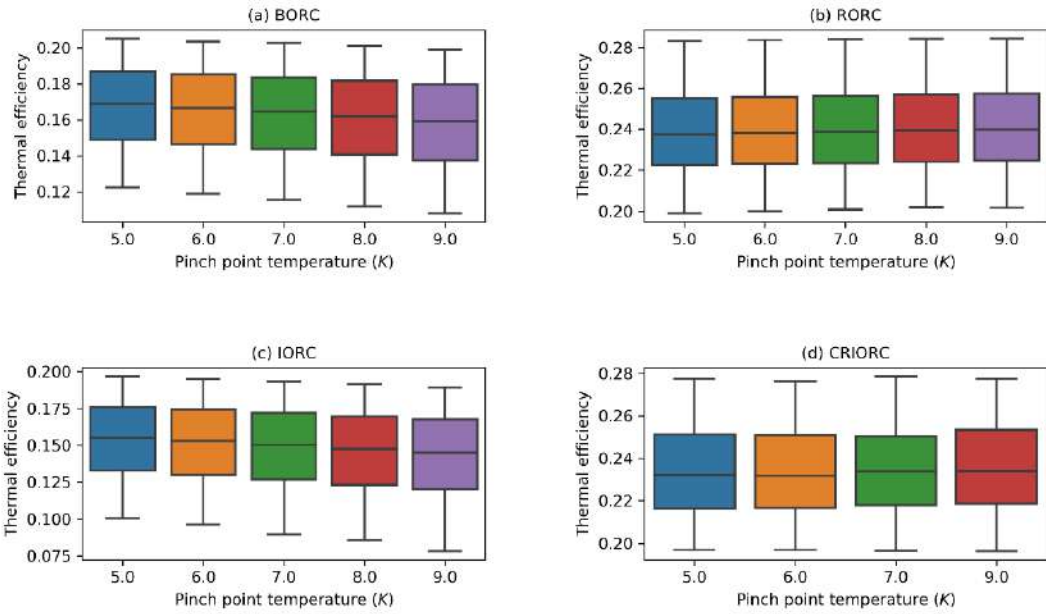


Figure 5.20 Effect of pinch point temperature difference on thermal efficiency for four cycle configuration

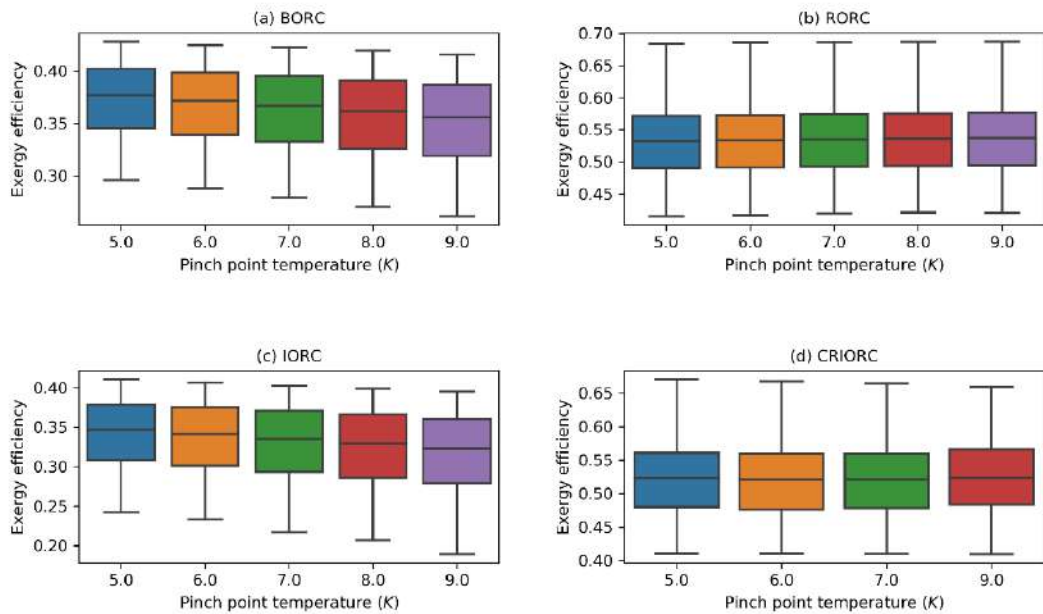


Figure 5.21 Effect of pinch point temperature difference on exergy efficiency for four cycle configuration

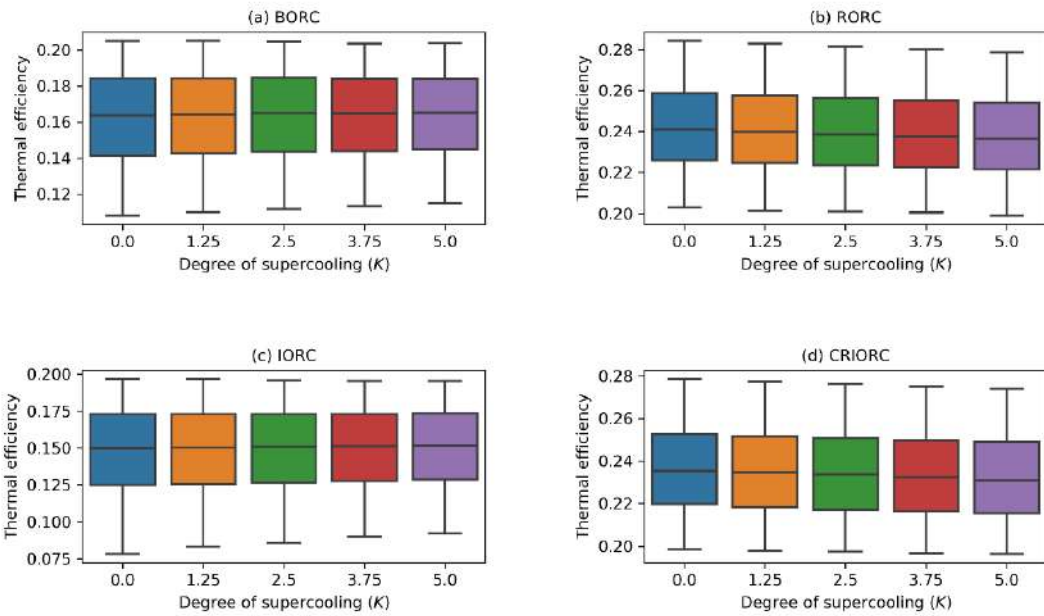


Figure 5.22 Effect of degree of supercooling on thermal efficiency for four cycle configuration

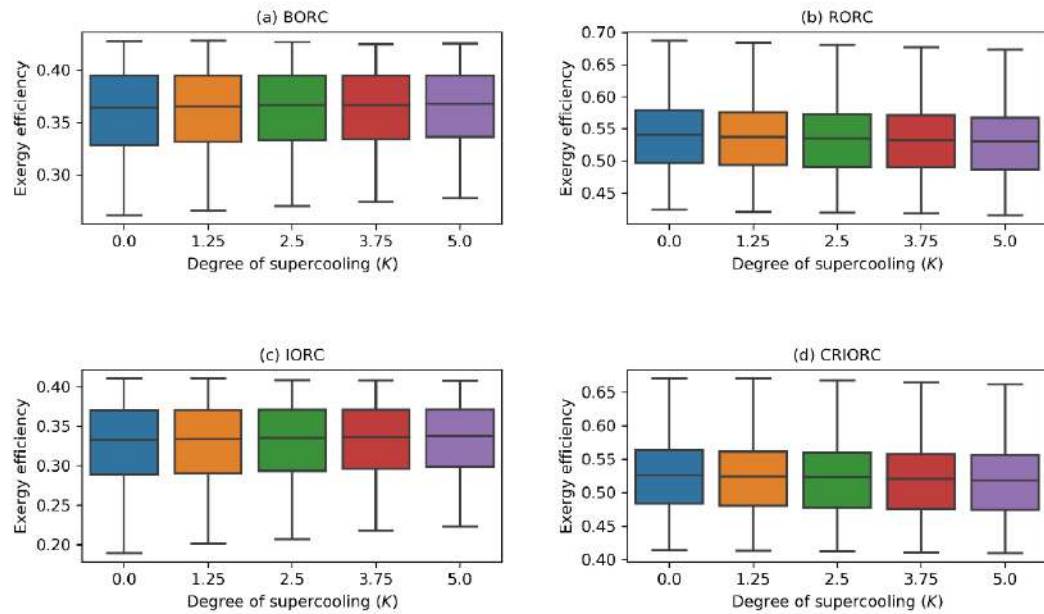


Figure 5.23 Effect of degree of supercooling on exergy efficiency for four cycle configuration

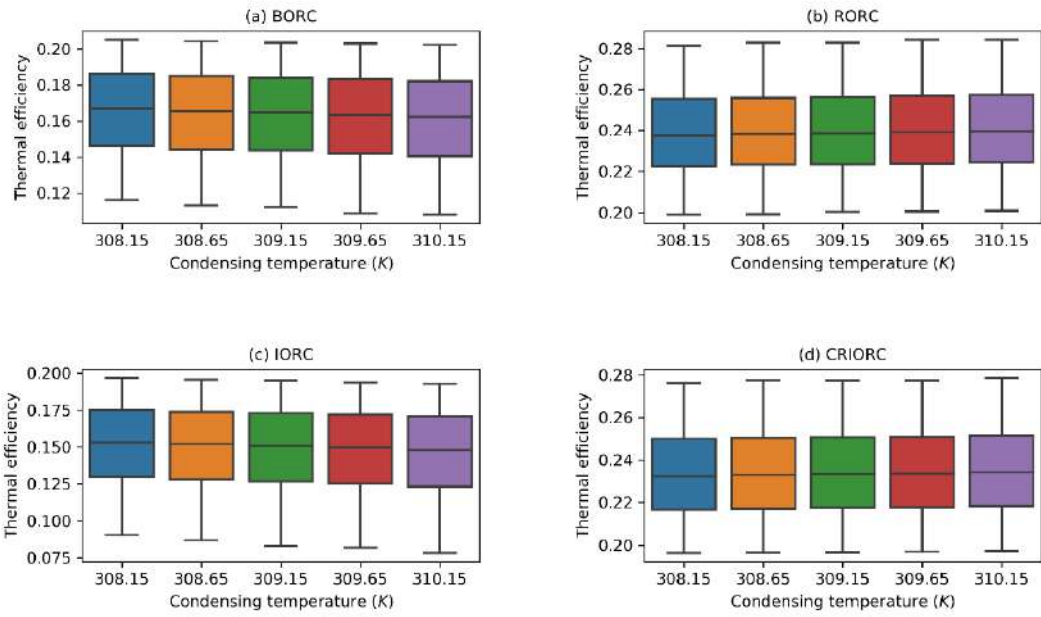


Figure 5.24 Effect of condensing temperature on thermal efficiency for four cycle configurations

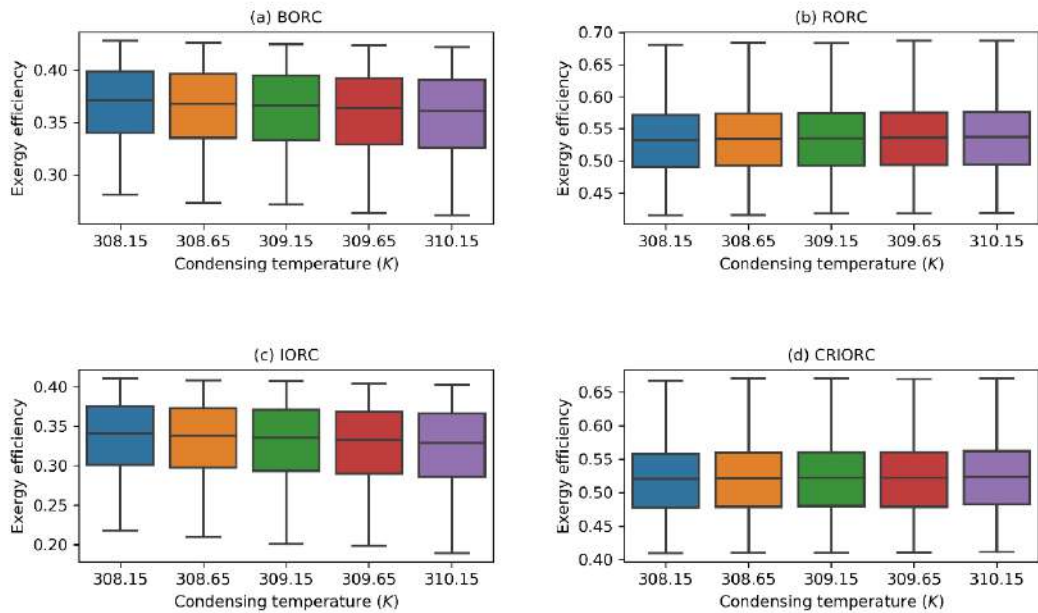


Figure 5.25 Effect of condensing temperature on exergy efficiency for four cycle configurations

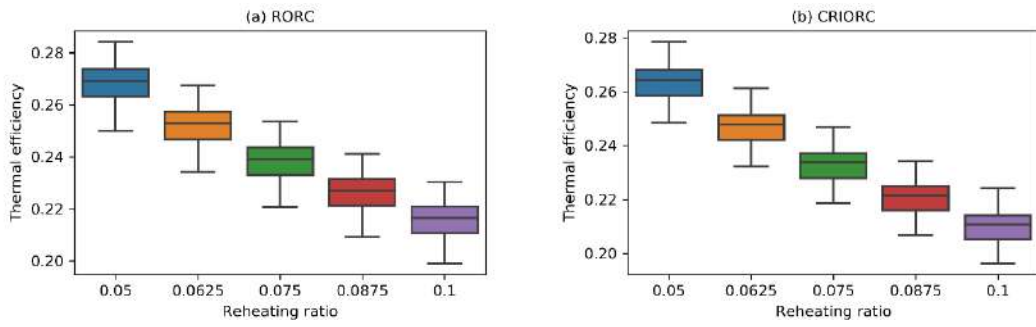


Figure 5.26 Effect of reheating ratio on thermal efficiency for two cycle configuration

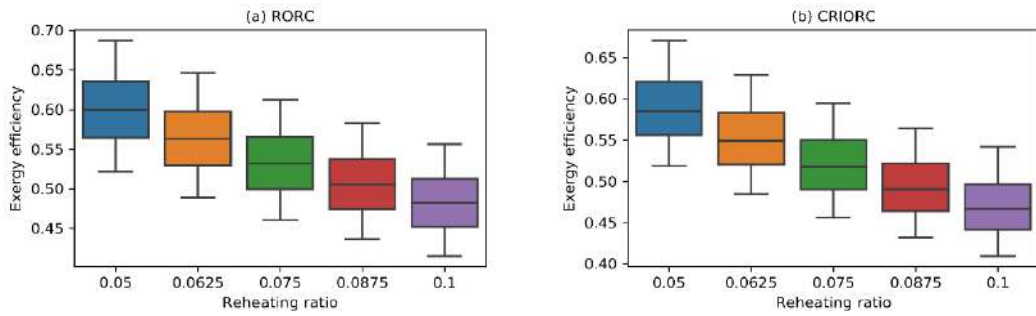


Figure 5.27 Effect of reheating ratio on exergy efficiency for two cycle configuration

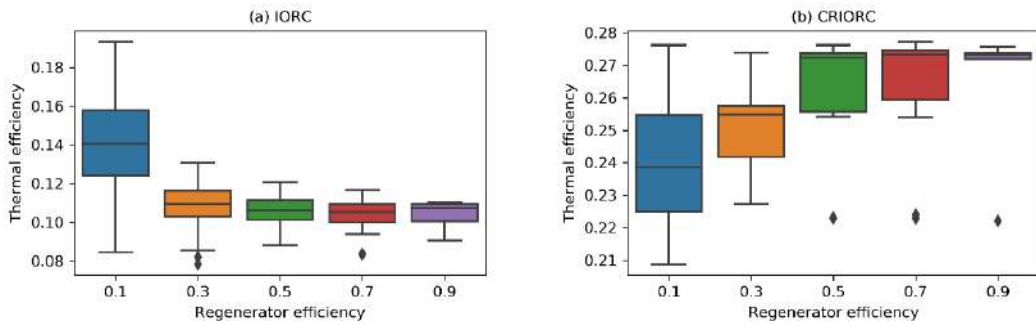


Figure 5.28 Effect of regenerator efficiency on thermal efficiency for two cycle configuration

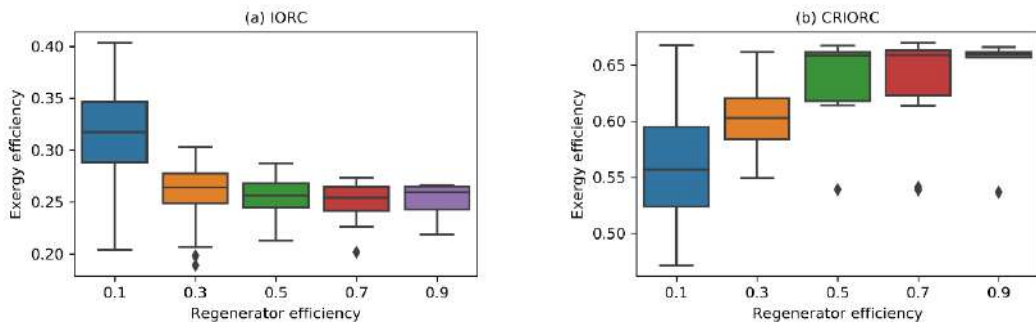


Figure 5.29 Effect of regenerator efficiency on exergy efficiency for two cycle configuration

For the RORC configuration demonstrated in subplot (b), it is observed that the inclusion of reheating essentially increases the performance of the cycle at an initial lower temperature. However, the average values of the performance metrics tend to decrease with the increase of the heat source temperature suggesting that with proper selection of reheating ratio the RORC cycle can operate effectively with a lower heat source temperature. In addition, the range of the efficiency values show a more overlapping condition than that described in (a) and (c) implying that same efficiency values are achievable for different heat source temperatures given that other parameters are adjusted properly.

Including all these, the CRIORC configuration demonstrates the combined performances of all the ORC configurations. The efficiency values in this configuration demonstrate a downward changing trend and similar overlapping trend like the RORC characteristics. However, it demonstrates slightly lower performance than the RORC because of the inclusion of regenerator and the reasons discussed previously.

Figure 5.20 and *Figure 5.21* demonstrate the effect of pinch point temperature difference on the cycle efficiencies. From (a) and (c) it is observed that the average performance of both BORC and IORC drops when the pinch point temperature increases. This phenomena can be attributed to the increased irreversibility for the increase of the pinch point temperature within the evaporator. However, reheating can significantly increase the performance of the cycle irrespective of the pinch point temperature demonstrated in (b). Combining all, the CRIORC exhibits a similar trend like the RORC. Therefore, the parameters of RORC and CRIORC can be adjusted properly in order to bypass the effect of increasing pinch point temperature.

The effect of the degree of supercooling are demonstrated in *Figure 5.22* and *Figure 5.23*. In these figures, the maximum, minimum, and quartile values are within the range demonstrated in the previous figures. However, with the increase of the supercooling effect, nearly no noticeable change of efficiency values are observed within the distinct supercooling temperature groups. Therefore, supercooling has negligible effect on the overall exergy and thermal efficiency of the described four cycle configuration. This statement is further validated by the increased size of the box in the stated plot, indicating that with proper adjustment of other parameters, the effects of supercooling can be bypassed.

Similar trend is noticeable in respect of the condensing temperature in *Figure 5.24* and *Figure 5.25*. Here in both of the figures, it is observed that for all distinct condensing temperature group, similar efficiency can be achievable with the proper adjustment of other parameters.

Therefore, both the degree of supercooling and condensing temperature have negligible effect to improve the cycle efficiencies in four of the stated configurations. In short, parameters on the low Pressure side of the cycle have less deciding effect on the overall cycle efficiencies.

However, they are still important in ML application for increasing the data points of the constructed dataset and increasing the performance of the individual machine learning scheme.

The above mentioned parameters are common to each of the four described configurations. However, two additional parameters are considered in this study which are cycle specific namely the reheating pressure and the regenerator efficiency. Among them, the former is applicable for RORC and the later is applicable for IORC. In addition, their effects are also observed in CRIORC as it combines both of their impact.

Figure 5.26 and *Figure 5.27* demonstrate the effect of reheating ratio on the thermal and exergy efficiency for RORC and IORC. It is evident from the figures that with the increase of reheating pressure ratio both of the efficiencies drop. The overlapping conditions are nearly similar to that of heat source temperature effect. From *Figure 5.18(a)* and *Figure 5.19(a)*, the BORC has a natural tendency to improve its performance with the increase of heat source temperature. However, *Figure 5.18(b),(d)* and *Figure 5.19(b),(d)* demonstrate a similar range as *Figure 5.26* and *Figure 5.27*. Therefore, reheating pressure ratio has the most crucial effect on the overall cycle efficiencies and can surplus the effect of the increasing heat source temperature.

The effect of regenerator efficiency are observed in *Figure 5.28* and *Figure 5.29*. From both of the figures it is observed that in its normal condition without the reheating effect, the efficiency of the cycle drops with the increase of the regenerator efficiency in case of IORC. After a certain value of IORC, however, the efficiency tends to become steady for IORC. For CRIORC, on the other hand, with the increase of the regenerator efficiency, the overall efficiency increases for both of the cases. This phenomena can largely be attributed to the inclusion of reheating in the cycle.

From the above mentioned analysis, it is evident that the discussed six parameters have different effect on the overall cycle efficiencies. For BORC and IORC, the cycle efficiency increases with the heat source temperature and RORC and CRIORC exhibit the opposite trend. The effect of pinch point temperature is more intense in case of BORC and IORC, exhibiting a downward trend of efficiency with increasing pinch temperature. On the other hand, these effects can be bypassed with proper parameter selection I case of RORC and CRIORC. The degree of supercooling and condensing temperature have negligible effect on the cycle efficiencies for four of the configurations given that other parameters are adjusted. Reheating pressure ratio plays a vital role in controlling cycle efficiencies, introducing a downward trend in efficiency with the increase of its value. Regenerator efficiency has a contrasting value for IORC and CRIORC mainly due to the inclusion of reheating in the cycle. While in IORC the efficiency tend to decrease with the increase of regenerator efficiency, the CRIORC faces the opposite condition.

Because of the complex behavior of all the discussed parameters in cycle efficiency, optimization of the parameters in respect of the cycle efficiency is crucial to operate the cycles properly. The next section will discuss the optimization process for both the traditional thermodynamic modeling and the proposed ML based modelling discussed previously.

5.7.2 Multiparameter optimization of the ORC configurations

In traditional thermodynamic approach, mathematical models discussed in chapter 4 are implemented inside the objective function of any optimization algorithm. This process is extremely time consuming as for any optimization scheme the algorithm needs to calculate the complex calculation of the objective function multiple times. In this study, an improved less time consuming approach is adopted where ANN is used as an alternative model to calculate the objective function. Based on the formulated models discussed in 5.4 and 5.5, the RF and the BPNN algorithms are used inside the objective function to provide a simple calculation approach.

Table 5-21 Optimization limit for heat source temperature and reheating ratio

Fluid name	Heat source temperature (T_h) range (K)	Reheating pressure ratio(λ) range
R227ea	373-380	0.60-0.80
RC318	385-395	0.50-0.55
R236fa	395-410	0.37-0.40
R236ea	410-420	0.30-0.33
R245fa	420-440	0.23-0.25
R123	450-470	0.17-0.20
R113	480-493	0.09-0.11
Cyclopentane	510-521	0.05-0.07
Cyclohexane	535-563	0.02-0.05

In this study, genetic algorithm is used as the optimization algorithm which is a widely accepted optimization scheme. The geneticalgorithm package, version 1.0.2 is implemented inside the python programming language to formulate the optimization scheme. The success of a genetic algorithm mainly depends on the crossover process which is dependent on the crossover probability. Therefore, a higher rate of 0.80 is chosen as the crossover rate. Further, mutation rate can limit the incident of premature convergence of solution. Therefore, a minimum mutation rate of 0.1 is selected. Total 300 iterations are allowed for giving enough generation to reach a standard optimum solution. The optimization begins with population having 100 subsets of probable solution. All the parameters of the genetic algorithm applied are listed in Table 5-22.

Table 5-22 Genetic algorithm parameters

Parameter name	Value
Maximum number of iteration	300
Population size	100
Mutation probability	0.1
Elit ratio	0.01
Crossover probability	0.8
Parents portion	0.3
Crossover type	uniform

This study aims to consider all the pivotal ORC parameters for optimization purpose. Therefore, the database incorporating CRIORC configuration is considered for both the analytical optimization and ANN based optimization purpose as it contains all the possible variables of BORC, RORC, and CRIORC. Total six variables are included for the optimization purpose namely the heat source temperature, pinch point temperature difference in the evaporator, degree of supercooling, condensing temperature, reheating ratio, and regenerator efficiency.

It is to be mentioned that the discussed nine working fluids work efficiently for a certain temperature range and beyond that the Coolprop package is unable to produce any state point data as mentioned in *Table 5-2*. This similar trend is noticeable in respect of reheating pressure ratio and therefore proper selection of reheating pressure ratio range is also crucial. As both of

the mentioned variables play the most crucial role in cycle efficiencies, a suitable limit of these values are required for optimization purpose. So, a feasible range of these values are determined first for optimization purpose which are listed in *Table 5-21* . The values of both the heat source temperature and the reheating pressure ratio are varied within maximum possible range and the values which yield realistic values are considered for the optimization working range of both the variables.

Unlike the above-mentioned two parameters, the performance of ORC is less sensitive to the rest of the four parameters. Therefore, a common set of range values of them are considered for nine of the working fluids during the optimization process as stated below,

$$0 \leq T_{sc} \leq 5 \quad (5.1)$$

$$308.15 \text{ K} \leq T_{con} \leq 311.15 \text{ K} \quad (5.2)$$

$$5 \leq \Delta T_{ppe} \leq 11 \quad (5.3)$$

$$0.14 \leq \eta_{ir} \leq 0.99 \quad (5.4)$$

In genetic algorithm like any other optimization scheme, an objective function tests the viability of an intermediate solution to either keep it or reject it during each iteration. Therefore, a suitable objective function needs to be constructed first considering all the objectives of a certain study. As both the exergy and the thermal efficiency indicate the performance of an ORC, in this study an objective function f is constructed giving equal weight to each of the efficiency parameters as stated below,

$$f(T_h, T_{sc}, T_{con}, \Delta T_{ppe}, \lambda, \eta_r) = 0.5\eta_{th} + 0.5\eta_{ex} \quad (5.5)$$

In addition, the success of genetic algorithm depends on the parameters of the algorithms. The parameter values used in this study for genetic algorithm are listed in *Table 5-22*. Based on the established ORC parametric value range, objective function and parametric values of the genetic algorithm, a multi-parameter optimization is conducted on the CRIORC configuration for nine of the working fluids with two approaches. In traditional thermodynamic approach, the modelling discussed in chapter 4 is utilized to construct the objective function (to get thermal efficiency and exergy efficiency values). On the other hand, in ANN approach, the previously established RF algorithm and BPNN are utilized to formulate the objective function. The optimization results for two of the approaches are listed from *Table 5-23* to *Table 5-31*.

Table 5-23 Optimized parameters for R227ea CRIORC

	Thermodynamic model	RF	BPNN
Heat source temperature / K	373.00	373.85	373.02
Pinch point temperature in the evaporator / K	9.5000	7.6336	7.4258
Degree of supercooling	0.0000	0.9853	0.9940
Condensing temperature / K	311.15	310.44	311.22
Reheating ratio	0.6000	0.6931	0.6941
Regeneration efficiency	0.7145	0.9203	0.9498
Energy efficiency	0.0793	0.0787	0.0790
Exergy efficiency	0.3780	0.3612	0.3593

Table 5-24 Optimized parameters for RC318CRIORC

	Thermodynamic model	RF	BPNN
Heat source temperature / K	385.00	385.38	385.85
Pinch point temperature in the evaporator / K	11.000	10.732	11.473
Degree of supercooling	0.0000	4.6472	4.8628
Condensing temperature / K	311.15	310.62	311.49
Reheating ratio	0.5000	0.5028	0.5005
Regeneration efficiency	0.7709	0.7823	0.7571
Energy efficiency	0.1029	0.1024	0.1014
Exergy efficiency	0.4313	0.4276	0.4259

Table 5-25 Optimized parameters for R236faCRIORC

	Thermodynamic model	RF	BPNN
Heat source temperature / K	395.00	396.61	396.39
Pinch point temperature in the evaporator / K	8.0000	7.2501	7.0713
Degree of supercooling	0.0000	2.2816	2.9885
Condensing temperature / K	311.15	311.02	311.33
Reheating ratio	0.3700	0.3792	0.3992
Regeneration efficiency	0.9875	0.9516	0.9844
Energy efficiency	0.1410	0.1403	0.1465
Exergy efficiency	0.5467	0.5430	0.5692

Table 5-26 Optimized parameters for R236eaCRIORC

	Thermodynamic model	RF	BPNN
Heat source temperature / K	410.00	410.00	411.69
Pinch point temperature in the evaporator / K	8.0000	5.1077	5.0183
Degree of supercooling	0.0000	1.2231	2.8132
Condensing temperature / K	311.15	310.74	309.49
Reheating ratio	0.3000	0.3090	0.3005
Regeneration efficiency	0.8321	0.7471	0.7513
Energy efficiency	0.1617	0.1593	0.1458
Exergy efficiency	0.56724	0.5580	0.5370

Table 5-27 Optimized parameters for R245faCRIORC

	Thermodynamic model	RF	BPNN
Heat source temperature / K	420.00	420.07	421.41
Pinch point temperature in the evaporator / K	5.0000	5.1272	5.0356
Degree of supercooling	0.0000	1.2800	1.8438
Condensing temperature / K	311.15	309.89	311.29
Reheating ratio	0.2300	0.2315	0.2309
Regeneration efficiency	0.8381	0.8102	0.9357
Energy efficiency	0.1837	0.1821	0.1846
Exergy efficiency	0.6082	0.6030	0.6112

Table 5-28 Optimized parameters for R123CRIORC

	Thermodynamic model	RF	BPNN
Heat source temperature / K	450.00	450.38	451.40
Pinch point temperature in the evaporator / K	11.000	5.6750	5.1684
Degree of supercooling	0.0000	2.0670	2.9365
Condensing temperature / K	311.15	309.79	308.15
Reheating ratio	0.1700	0.1712	0.1722
Regeneration efficiency	0.1756	0.8613	0.7264
Energy efficiency	0.2126	0.2114	0.2170
Exergy efficiency	0.6100	0.6048	0.6254

Table 5-29 Optimized parameters for R113CRIORC

	Thermodynamic model	RF	BPNN
Heat source temperature / K	480.00	480.04	480.22
Pinch point temperature in the evaporator / K	8.0000	7.9170	7.2515
Degree of supercooling	0.0000	3.1099	3.9283
Condensing temperature / K	311.15	310.67	311.22
Reheating ratio	0.0900	0.0909	0.0902
Regeneration efficiency	0.5633	0.5505	0.5892
Energy efficiency	0.2606	0.2597	0.2733
Exergy efficiency	0.6694	0.66674	0.6734

Table 5-30 Optimized parameters for CyclopentaneCRIORC

	Thermodynamic model	RF	BPNN
Heat source temperature / K	510.00	511.09	511.08
Pinch point temperature in the evaporator / K	11.000	7.1895	7.3023
Degree of supercooling	0.0000	2.3101	4.9737
Condensing temperature / K	311.15	310.27	308.27
Reheating ratio	0.0500	0.0513	0.0508
Regeneration efficiency	0.8200	0.3282	0.3510
Energy efficiency	0.3091	0.3071	0.3292
Exergy efficiency	0.7271	0.7228	0.7272

Table 5-31 Optimized parameters for CyclohexaneCRIORC

	Thermodynamic model	RF	BPNN
Heat source temperature / K	535.00	537.82	535.47
Pinch point temperature in the evaporator / K	11.000	7.3942	7.0115
Degree of supercooling	5.000	5.4599	4.9212
Condensing temperature / K	311.15	309.89	308.38
Reheating ratio	0.0200	0.0264	0.0211
Regeneration efficiency	0.9829	0.3250	0.9682
Energy efficiency	0.3412	0.3407	0.3436
Exergy efficiency	0.7554	0.7534	0.7559

From the optimization result, it is observed that the thermal efficiency and the exergy efficiency values are almost similar for three of the cases. In addition, the optimal heat source temperature values and the reheating pressure ratio values are also close to one another. However, the optimal pinch point temperature difference, degree of supercooling, condensing temperature, and internal regenerator efficiency values differ for three of the cases. This can be explained with the results of sensitivity analysis discussed in 5.7.1. From the mentioned analysis it was observed that heat source temperature and reheating ratio play the most crucial role in ORC efficiency and efficiency values differ from one another for each of the distinct heat source temperature and reheating ratio subgroup. So, their optimized results are essentially similar for three of the cases. On the other hand, the rest of the parameters subgroup can produce similar efficiency results given that other conditions are adjusted. So, in optimization process, any local value of these parameters which are adjusted with other parameters to produce a maxima, is more likely to remain unchanged during the rest of the optimization process. Therefore, the parametric value of them differ in three of the optimization cases though the maximization criteria of the objective function is meet.

It is also evident from the optimization result that the ANN scheme can significantly reduce calculation time. The average calculation time needed for traditional, RF, and BPNN approach are around 90 minutes, 12.16 minutes, and 4.45 minutes respectively, indicating that RF and BPNN are 7.4 times and 20.18 times faster than the traditional method respectively

6 CONCLUSION

In this study, an effective method of multi-parameter optimization for waste heat recovery purpose is discussed for four ORC configurations and nine working fluids incorporating ANN scheme. In the thermodynamic simulation process, a newly developed target temperature line method is adopted to determine evaporator exit pressure, exit temperature as well as working fluid mass flow rate. For the ANN scheme, two approaches incorporating an ML scheme and a BPNN scheme are considered. Further, in ML scheme, the performance of four of the common algorithms namely linear regression, support vector regression, decision tree regression, and random forest regression are compared in respect of their effectiveness in ORC thermal and exergy efficiency prediction. Besides, genetic algorithm is chosen as the optimization algorithm. The key findings of this study are,

- 1) Of the four ML algorithm, Random forest regression is the most accurate regressor for ORC performance prediction for all the four configurations. Decision tree regressor follows similar trend like random forest regression with slightly lower prediction accuracy. Linear regressor produces a moderate prediction performance for ORC without reheating like BORC and IORC but fails to maintain it in case of ORC incorporating reheating like RORC and CRIORC. Therefore, random forest regressor is selected as the effective ML scheme in this study. Additionally, the number of trees which is a hyper parameter of RF regressor is found to be 101 and 150 for reaching optimal prediction accuracy.
- 2) Among BPNN and RF regressor, BPNN is more data sensitive indicating that to establish efficient BPNN scheme, sufficient of data is required. On the contrary, RF can produce fairly accurate prediction result with less amount of data than BPNN. However, BPNN is faster than RF method.
- 3) BPNN and RF are quite efficient in predicting efficiency values of ORC for individual working fluids. They are also efficient for combined prediction for nine of the working fluid when their identity (molecular weight, critical pressure, and critical temperature) are given as the input values along with other parameters. Therefore, they can be reliably used for ORC related calculation purpose.
- 4) The studied four types of ORC performance are mostly affected by heat source temperature and reheating ratio. In BORC and IORC, efficiency values increase with the increase of heat source temperature while for RORC and CRIORC the opposite trend is observed. Again for RORC and CRIORC, increase of reheat pressure ratio has a downward trend in efficiency performance improvement. Moreover, for BORC and

IORC, pinch point temperature has a decreasing effect on the cycle performance though for RORC and CRIORC these effects are negligible. The rest of the parameters has negligible effect on cycle performance improvement.

- 5) The optimized thermal and exergy efficiency are close to one another for traditional thermodynamic modelling, RF, and BPNN, indicating that the proposed ANN scheme can effectively be used as a proxy model for thermodynamic analysis during the optimization process. Again, the RF and BPNN are nearly 7 times and 20 times faster than the traditional approach, indicating that they can successfully be used as a less complex and less time consuming method for ORC modelling.

Recommendation for future work:

1. This study is based on the dataset of nine working fluids. More suitable fluids can be added to the dataset to form a generalized framework for ORC prediction
2. An analysis of the characteristics of the proposed AI for high grade waste heat can be performed and compared with that of the results of this study.
3. More ML algorithms can be introduced and compared with the studied ML algorithms.

REFERENCE

- [1] Tian, H., and Shu, G. Q., 2017, “Organic Rankine Cycle Systems for Large-Scale Waste Heat Recovery to Produce Electricity,” *Org. Rank. Cycle Power Syst. Technol. Appl.*, pp. 613–636.
- [2] Astolfi, M., Romano, M. C., Bombarda, P., and Macchi, E., 2014, “Binary ORC (Organic Rankine Cycles) Power Plants for the Exploitation of Medium–Low Temperature Geothermal Sources – Part B: Techno-Economic Optimization,” *Energy (Oxford)*, **66**(Complete), pp. 435–446.
- [3] Brückner, S., Liu, S., Miró, L., Radspieler, M., Cabeza, L. F., and Lävemann, E., 2015, “Industrial Waste Heat Recovery Technologies: An Economic Analysis of Heat Transformation Technologies,” *Appl. Energy*, **151**, pp. 157–167.
- [4] Galuppo, F., Reiche, T., Lemort, V., Dufour, P., and Nadri, M., 2021, “Organic Rankine Cycle Based Waste Heat Recovery Modeling and Control of the Low Pressure Side Using Direct Condensation and Dedicated Fans,” *Energy*, **216**, p. 119074.
- [5] Matsui, K., Thu, K., and Miyazaki, T., 2020, “A Hybrid Power Cycle Using an Inverted Brayton Cycle with an Indirect Evaporative Device for Waste-Heat Recovery,” *Appl. Therm. Eng.*, **170**, p. 115029.
- [6] Khan, Y., and Shyam Mishra, R., 2021, “Thermo-Economic Analysis of the Combined Solar Based Pre-Compression Supercritical CO₂ Cycle and Organic Rankine Cycle Using Ultra Low GWP Fluids,” *Therm. Sci. Eng. Prog.*, **23**, p. 100925.
- [7] Liu, Z., Xie, N., and Yang, S., 2020, “Thermodynamic and Parametric Analysis of a Coupled LiBr/H₂O Absorption Chiller/Kalina Cycle for Cascade Utilization of Low-Grade Waste Heat,” *Energy Convers. Manag.*, **205**, p. 112370.
- [8] Cao, Y., Mihardjo, L. W. W., Dahari, M., and Tlili, I., 2021, “Waste Heat from a Biomass Fueled Gas Turbine for Power Generation via an ORC or Compressor Inlet Cooling via an Absorption Refrigeration Cycle: A Thermo-economic Comparison,” *Appl. Therm. Eng.*, **182**, p. 116117.
- [9] Laazaar, K., and Boutammachte, N., 2020, “Modelling and Optimization of Stirling Engine for Waste Heat Recovery from Cement Plant Based on Adiabatic Model and Genetics Algorithms,” *Lect. Notes Networks Syst.*, **144**, pp. 287–296.
- [10] Dong, S., Habib, B., Li, B., Yu, W., and Young, B., 2019, “Organic Rankine Cycle Systems Design Using a Case-Based Reasoning Approach,” *Ind. Eng. Chem. Res.*,

58(29), pp. 13198–13209.

- [11] Bufi, E. A., Camporeale, S., Fornarelli, F., Fortunato, B., Pantaleo, A. M., Sorrentino, A., and Torresi, M., 2017, “Parametric Multi-Objective Optimization of an Organic Rankine Cycle with Thermal Energy Storage for Distributed Generation,” *Energy Procedia*, **126**, pp. 429–436.
- [12] Chatzopoulou, M. A., and Markides, C. N., 2018, “Thermodynamic Optimisation of a High-Electrical Efficiency Integrated Internal Combustion Engine – Organic Rankine Cycle Combined Heat and Power System,” *Appl. Energy*, **226**, pp. 1229–1251.
- [13] Zhang, Y., Deng, S., Zhao, L., Lin, S., Ni, J., Ma, M., and Xu, W., 2018, “Optimization and Multi-Time Scale Modeling of Pilot Solar Driven Polygeneration System Based on Organic Rankine Cycle,” *Appl. Energy*, **222**, pp. 396–409.
- [14] Zhai, L., Xu, G., Wen, J., Quan, Y., Fu, J., Wu, H., and Li, T., 2017, “An Improved Modeling for Low-Grade Organic Rankine Cycle Coupled with Optimization Design of Radial-Inflow Turbine,” *Energy Convers. Manag.*, **153**, pp. 60–70.
- [15] Dumont, O., Parthoens, A., Dickes, R., and Lemort, V., 2018, “Experimental Investigation and Optimal Performance Assessment of Four Volumetric Expanders (Scroll, Screw, Piston and Roots) Tested in a Small-Scale Organic Rankine Cycle System,” *Energy*, **165**, pp. 1119–1127.
- [16] Xu, W., Zhang, J., Zhao, L., Deng, S., and Zhang, Y., 2017, “Novel Experimental Research on the Compression Process in Organic Rankine Cycle (ORC),” *Energy Convers. Manag.*, **137**, pp. 1–11.
- [17] Yang, J., Sun, Z., Yu, B., and Chen, J., 2018, “Experimental Comparison and Optimization Guidance of R1233zd(E) as a Drop-in Replacement to R245fa for Organic Rankine Cycle Application,” *Appl. Therm. Eng.*, **141**, pp. 10–19.
- [18] Ziviani, D., Gusev, S., Lecompte, S., Groll, E. A., Braun, J. E., Horton, W. T., van den Broek, M., and De Paepe, M., 2017, “Optimizing the Performance of Small-Scale Organic Rankine Cycle That Utilizes a Single-Screw Expander,” *Appl. Energy*, **189**, pp. 416–432.
- [19] Li, X., Xu, B., Tian, H., and Shu, G., 2021, “Towards a Novel Holistic Design of Organic Rankine Cycle (ORC) Systems Operating under Heat Source Fluctuations and Intermittency,” *Renew. Sustain. Energy Rev.*, **147**, p. 111207.
- [20] Zahedi, R., Ahmadi, A., and Dashti, R., 2021, “Energy, Exergy, Exergoeconomic and Exergoenvironmental Analysis and Optimization of Quadruple Combined Solar, Biogas, SRC and ORC Cycles with Methane System,” *Renew. Sustain. Energy Rev.*, **150**, p.

111420.

- [21] Nondy, J., and Gogoi, T. K., 2021, “Exergoeconomic Investigation and Multi-Objective Optimization of Different ORC Configurations for Waste Heat Recovery: A Comparative Study,” *Energy Convers. Manag.*, **245**, p. 114593.
- [22] Mieloszyk, M., Majewska, K., Zywicka, G., Kaczmarczyk, T. Z., Jurek, M., and Ostachowicz, W., 2020, “Fibre Bragg Grating Sensors as a Measurement Tool for an Organic Rankine Cycle Micro-Turbogenerator,” *Measurement*, **157**, p. 107666.
- [23] Gomaa, M. R., Mustafa, R. J., Al-Dhaifallah, M., and Rezk, H., 2020, “A Low-Grade Heat Organic Rankine Cycle Driven by Hybrid Solar Collectors and a Waste Heat Recovery System,” *Energy Reports*, **6**, pp. 3425–3445.
- [24] Bellos, E., and Tzivanidis, C., 2018, “Investigation of a Hybrid ORC Driven by Waste Heat and Solar Energy,” *Energy Convers. Manag.*, **156**, pp. 427–439.
- [25] Marchionni, M., Bianchi, G., Karvountzis-Kontakiotis, A., Pesyridis, A., and Tassou, S. A., 2018, “An Appraisal of Proportional Integral Control Strategies for Small Scale Waste Heat to Power Conversion Units Based on Organic Rankine Cycles,” *Energy*, **163**, pp. 1062–1076.
- [26] White, M. T., Oyewunmi, O. A., Chatzopoulou, M. A., Pantaleo, A. M., Haslam, A. J., and Markides, C. N., 2018, “Computer-Aided Working-Fluid Design, Thermodynamic Optimisation and Thermoeconomic Assessment of ORC Systems for Waste-Heat Recovery,” *Energy*, **161**, pp. 1181–1198.
- [27] Lazzaretto, A., Manente, G., and Toffolo, A., 2018, “SYNTHSEP: A General Methodology for the Synthesis of Energy System Configurations beyond Superstructures,” *Energy*, **147**, pp. 924–949.
- [28] Toffolo, A., 2014, “A Synthesis/Design Optimization Algorithm for Rankine Cycle Based Energy Systems,” *Energy*, **66**, pp. 115–127.
- [29] Bekiloğlu, H. E., Bedir, H., and Anlaş, G., 2019, “Multi-Objective Optimization of ORC Parameters and Selection of Working Fluid Using Preliminary Radial Inflow Turbine Design,” *Energy Convers. Manag.*, **183**, pp. 833–847.
- [30] Fang, Y., Yang, F., and Zhang, H., 2019, “Comparative Analysis and Multi-Objective Optimization of Organic Rankine Cycle (ORC) Using Pure Working Fluids and Their Zeotropic Mixtures for Diesel Engine Waste Heat Recovery,” *Appl. Therm. Eng.*, **157**, p. 113704.
- [31] Bao, J., and Zhao, L., 2013, “A Review of Working Fluid and Expander Selections for

- Organic Rankine Cycle,” *Renew. Sustain. Energy Rev.*, **24**, pp. 325–342.
- [32] Zhang, X., Zhang, C., He, M., and Wang, J., 2019, “Selection and Evaluation of Dry and Isentropic Organic Working Fluids Used in Organic Rankine Cycle Based on the Turning Point on Their Saturated Vapor Curves,” *J. Therm. Sci.* 2019 284, **28**(4), pp. 643–658.
- [33] He, C., Liu, C., Zhou, M., Xie, H., Xu, X., Wu, S., and Li, Y., 2014, “A New Selection Principle of Working Fluids for Subcritical Organic Rankine Cycle Coupling with Different Heat Sources,” *Energy*, **68**, pp. 283–291.
- [34] Huster, W. R., Schweidtmann, A. M., and Mitsos, A., 2020, “Working Fluid Selection for Organic Rankine Cycles via Deterministic Global Optimization of Design and Operation,” *Optim. Eng.*, **21**(2), pp. 517–536.
- [35] Huster, W. R., Schweidtmann, A. M., and Mitsos, A., 2020, “Hybrid Mechanistic Data-Driven Modeling for the Deterministic Global Optimization of a Transcritical Organic Rankine Cycle,” *Computer Aided Chemical Engineering*, Elsevier, pp. 1765–1770.
- [36] Peng, Y., Lin, X., Liu, J., Su, W., and Zhou, N., 2021, “Machine Learning Prediction of ORC Performance Based on Properties of Working Fluid,” *Appl. Therm. Eng.*, **195**, p. 117184.
- [37] Joback, K. G., and Reid, R. C., 1987, “Estimation of Pure-Component Properties from Group-Contributions,” *Chem. Eng. Commun.*, **57**(1–6), pp. 233–243.
- [38] Lampe, M., Stavrou, M., Bucker, H., ... J. G.-I. &, and 2014, undefined, 2014, “Simultaneous Optimization of Working Fluid and Process for Organic Rankine Cycles Using PC-SAFT,” *ACS Publ.*, **53**(21), pp. 8821–8830.
- [39] Papadopoulos, A. I., Stijepovic, M., and Linke, P., 2010, “On the Systematic Design and Selection of Optimal Working Fluids for Organic Rankine Cycles,” *Appl. Therm. Eng.*, **30**(6–7), pp. 760–769.
- [40] Su, W., Zhao, L., Energy, S. D.-A., and 2017, undefined, 2017, “Simultaneous Working Fluids Design and Cycle Optimization for Organic Rankine Cycle Using Group Contribution Model,” *Elsevier*, **202**, pp. 618–627.
- [41] Su, W., Zhao, L., Management, S. D.-E. C. and, and 2017, undefined, 2017, “Developing a Performance Evaluation Model of Organic Rankine Cycle for Working Fluids Based on the Group Contribution Method,” *Elsevier*, **132**, pp. 307–315.
- [42] Luo, X., Wang, Y., Liang, J., Qi, J., Su, W., Yang, Z., Chen, J., Wang, C., and Chen, Y., 2019, “Improved Correlations for Working Fluid Properties Prediction and Their

- Application in Performance Evaluation of Sub-Critical Organic Rankine Cycle,” *Energy*, **174**, pp. 122–137.
- [43] Peng, Y., Su, W., Zhou, N., and Zhao, L., 2020, “How to Evaluate the Performance of Sub-Critical Organic Rankine Cycle from Key Properties of Working Fluids by Group Contribution Methods?,” *Energy Convers. Manag.*, **221**(April), p. 113204.
- [44] Mahmoudi, S. M. S., and Ghavimi, A. R., 2016, “Thermoeconomic Analysis and Multi Objective Optimization of a Molten Carbonate Fuel Cell – Supercritical Carbon Dioxide – Organic Rankin Cycle Integrated Power System Using Liquefied Natural Gas as Heat Sink,” *Appl. Therm. Eng.*, **107**, pp. 1219–1232.
- [45] Imran, M., Park, B., Kim, H., Lee, D., ... M. U.-E. C. and, and 2014, undefined, 2014, “Thermo-Economic Optimization of Regenerative Organic Rankine Cycle for Waste Heat Recovery Applications,” *Elsevier*, **87**, pp. 107–118.
- [46] Hajabdollahi, Z., Hajabdollahi, F., Tehrani, M., and Hajabdollahi, H., 2013, “Thermo-Economic Environmental Optimization of Organic Rankine Cycle for Diesel Waste Heat Recovery,” *Energy*, **63**, pp. 142–151.
- [47] Agromayor, R., and Nord, L. O., 2017, “Fluid Selection and Thermodynamic Optimization of Organic Rankine Cycles for Waste Heat Recovery Applications,” *Energy Procedia*, **129**, pp. 527–534.
- [48] Zhang, H., Wang, E., ... M. O.-A. M., and 2011, undefined, “Study of Parameters Optimization of Organic Rankine Cycle (ORC) for Engine Waste Heat Recovery,” *Trans Tech Publ.*
- [49] Zhang, X., Bai, H., Zhao, X., Diabat, A., Zhang, J., Yuan, H., and Zhang, Z., 2018, “Multi-Objective Optimisation and Fast Decision-Making Method for Working Fluid Selection in Organic Rankine Cycle with Low-Temperature Waste Heat Source in Industry,” *Energy Convers. Manag.*, **172**, pp. 200–211.
- [50] Galindo, J., Climent, H., Dolz, V., and Royo-Pascual, L., 2016, “Multi-Objective Optimization of a Bottoming Organic Rankine Cycle (ORC) of Gasoline Engine Using Swash-Plate Expander,” *Energy Convers. Manag.*, **126**, pp. 1054–1065.
- [51] Bian, S., Wu, T., and Yang, J. F., 2014, “Parametric Optimization of Organic Rankine Cycle by Genetic Algorithm,” *Appl. Mech. Mater.*, **672–674**, pp. 741–745.
- [52] Kai, Z., Mi, Z., Yabo, W., Zhili, S., Shengchun, L., and Jinghong, N., 2015, “Parametric Optimization of Low Temperature ORC System,” *Energy Procedia*, **75**, pp. 1596–1602.
- [53] Nasir, M. T., and Kim, K. C., 2016, “Working Fluids Selection and Parametric

- Optimization of an Organic Rankine Cycle Coupled Vapor Compression Cycle (ORC-VCC) for Air Conditioning Using Low Grade Heat,” *Energy Build.*, **129**, pp. 378–395.
- [54] Gutiérrez-Arriaga, C. G., Abdelhady, F., Bamufleh, H. S., Serna-González, M., El-Halwagi, M. M., and Ponce-Ortega, J. M., 2014, “Industrial Waste Heat Recovery and Cogeneration Involving Organic Rankine Cycles,” *Clean Technol. Environ. Policy* 2014 173, **17**(3), pp. 767–779.
- [55] Zhang, X., Bai, H., Zhao, X., Diabat, A., Zhang, J., Yuan, H., and Zhang, Z., 2018, “Multi-Objective Optimisation and Fast Decision-Making Method for Working Fluid Selection in Organic Rankine Cycle with Low-Temperature Waste Heat Source in Industry,” *Energy Convers. Manag.*, **172**, pp. 200–211.
- [56] Larsen, U., Pierobon, L., Baldi, F., Haglind, F., and Ivarsson, A., 2015, “Development of a Model for the Prediction of the Fuel Consumption and Nitrogen Oxides Emission Trade-off for Large Ships,” *Energy*, **80**, pp. 545–555.
- [57] Ebrahimi-Moghadam, A., Moghadam, A. J., and Farzaneh-Gord, M., 2020, “Comprehensive Techno-Economic and Environmental Sensitivity Analysis and Multi-Objective Optimization of a Novel Heat and Power System for Natural Gas City Gate Stations,” *J. Clean. Prod.*, **262**, p. 121261.
- [58] Chen, Y., Xu, J., Zhao, D., Wang, J., and Lund, P. D., 2021, “Exergo-Economic Assessment and Sensitivity Analysis of a Solar-Driven Combined Cooling, Heating and Power System with Organic Rankine Cycle and Absorption Heat Pump,” *Energy*, **230**, p. 120717.
- [59] Ashwni, Sherwani, A. F., Tiwari, D., and Kumar, A., 2021, “Sensitivity Analysis and Multi-Objective Optimization of Organic Rankine Cycle Integrated with Vapor Compression Refrigeration System,” <https://doi.org/10.1080/15567036.2021.1916132>.
- [60] Liu, C., Wang, S., and Ren, J., 2021, “Organic Rankine Cycle Driven by Geothermal Heat Source: Life Cycle Techno-Economic–Environmental Analysis,” *Renewable-Energy-Driven Futur.*, pp. 67–124.
- [61] Wang, J., Dai, Y., and Gao, L., 2009, “Exergy Analyses and Parametric Optimizations for Different Cogeneration Power Plants in Cement Industry,” *Appl. Energy*, **86**(6), pp. 941–948.
- [62] Andreasen, J., Larsen, U., Knudsen, T., Energy, F. H.-, and 2015, undefined, 2015, “Design and Optimization of a Novel Organic Rankine Cycle with Improved Boiling Process,” *Elsevier*, **91**, pp. 48–59.
- [63] Larsen, U., Sigthorsson, O., Energy, F. H.-, and 2014, undefined, 2017, “A Comparison

- of Advanced Heat Recovery Power Cycles in a Combined Cycle for Large Ships,” Elsevier, **74**(C), pp. 260–268.
- [64] Hajabdollahi, H., 2015, “Investigating the Effects of Load Demands on Selection of Optimum CCHP-ORC Plant,” *Appl. Therm. Eng.*, **87**, pp. 547–558.
- [65] Gutiérrez-Arriaga, C. G., Abdelhady, F., Bamufleh, H. S., Serna-González, M., El-Halwagi, M. M., and Ponce-Ortega, J. M., 2015, “Industrial Waste Heat Recovery and Cogeneration Involving Organic Rankine Cycles,” *Clean Technol. Environ. Policy*, **17**(3), pp. 767–779.
- [66] Kalikatzarakis, M., and Frangopoulos, C. A., 2015, “Multi-Criteria Selection and Thermo-Economic Optimization of an Organic Rankine Cycle System for a Marine Application,” *Int. J. Thermodyn.*, **18**(2), pp. 133–141.
- [67] Aliahmadi, M., Moosavi, A., and Sadrhosseini, H., 2021, “Multi-Objective Optimization of Regenerative ORC System Integrated with Thermoelectric Generators for Low-Temperature Waste Heat Recovery,” *Energy Reports*, **7**, pp. 300–313.
- [68] Yang, A., Su, Y., Shen, W., Chien, I. L., and Ren, J., 2019, “Multi-Objective Optimization of Organic Rankine Cycle System for the Waste Heat Recovery in the Heat Pump Assisted Reactive Dividing Wall Column,” *Energy Convers. Manag.*, **199**, p. 112041.
- [69] Jankowski, M., and Borsukiewicz, A., 2019, “Multi-Objective Approach for Determination of Optimal Operating Parameters in Low-Temperature ORC Power Plant,” *Energy Convers. Manag.*, **200**, p. 112075.
- [70] Wang, Z., Hu, Y., Xia, X., Zuo, Q., Zhao, B., and Li, Z., 2020, “Thermo-Economic Selection Criteria of Working Fluid Used in Dual-Loop ORC for Engine Waste Heat Recovery by Multi-Objective Optimization,” *Energy*, **197**, p. 117053.
- [71] Wang, L., Bu, X., and Li, H., 2020, “Multi-Objective Optimization and off-Design Evaluation of Organic Rankine Cycle (ORC) for Low-Grade Waste Heat Recovery,” *Energy*, **203**, p. 117809.
- [72] Sadeghi, M., Chitsaz, A., Marivani, P., Yari, M., and Mahmoudi, S. M. S., 2020, “Effects of Thermophysical and Thermochemical Recuperation on the Performance of Combined Gas Turbine and Organic Rankine Cycle Power Generation System: Thermoeconomic Comparison and Multi-Objective Optimization,” *Energy*, **210**, p. 118551.
- [73] Ochoa, G. V., Peñaloza, C. A., and Forero, J. D., 2019, “Thermoeconomic Optimization with PSO Algorithm of Waste Heat Recovery Systems Based on Organic Rankine Cycle

- System for a Natural Gas Engine,” *Energies* 2019, Vol. 12, Page 4165, **12**(21), p. 4165.
- [74] Zhou, Y., Li, S., Sun, L., Zhao, S., and Ashraf Talesh, S. S., 2020, “Optimization and Thermodynamic Performance Analysis of a Power Generation System Based on Geothermal Flash and Dual-Pressure Evaporation Organic Rankine Cycles Using Zeotropic Mixtures,” *Energy*, **194**, p. 116785.
- [75] Park, K., Oh, S.-R., and Won, W., 2019, “Techno-Economic Optimization of the Integration of an Organic Rankine Cycle into a Molten Carbonate Fuel Cell Power Plant,” *Korean J. Chem. Eng.* 2019 363, **36**(3), pp. 345–355.
- [76] Sadeghi, S., Maghsoudi, P., Shabani, B., Gorgani, H. H., and Shabani, N., 2018, “Performance Analysis and Multi-Objective Optimization of an Organic Rankine Cycle with Binary Zeotropic Working Fluid Employing Modified Artificial Bee Colony Algorithm,” *J. Therm. Anal. Calorim.* 2018 1364, **136**(4), pp. 1645–1665.
- [77] Arslan, O., and Yetik, O., 2011, “ANN Based Optimization of Supercritical ORC-Binary Geothermal Power Plant: Simav Case Study,” *Appl. Therm. Eng.*, **31**(17–18), pp. 3922–3928.
- [78] Rashidi, M., Galanis, N., Nazari, F., Energy, A. P.-, and 2011, undefined, 2011, “Parametric Analysis and Optimization of Regenerative Clausius and Organic Rankine Cycles with Two Feedwater Heaters Using Artificial Bees Colony and Artificial Neural,” *Elsevier*, **36**(9), pp. 5728–5740.
- [79] Massimiani, A., Palagi, L., Sciubba, E., and Tocci, L., 2017, “Neural Networks for Small Scale ORC Optimization,” *Energy Procedia*, Elsevier Ltd, pp. 34–41.
- [80] Zhi, L. H., Hu, P., Chen, L. X., and Zhao, G., 2019, “Multiple Parametric Analysis, Optimization and Efficiency Prediction of Transcritical Organic Rankine Cycle Using Trans-1,3,3,3-Tetrafluoropropene (R1234ze(E)) for Low Grade Waste Heat Recovery,” *Energy Convers. Manag.*, **180**(October 2018), pp. 44–59.
- [81] Yang, F., Cho, H., and Zhang, H., 2019, “Performance Prediction and Optimization of an Organic Rankine Cycle Using Back Propagation Neural Network for Diesel Engine Waste Heat Recovery,” *J. Energy Resour. Technol. Trans. ASME*, **141**(6).
- [82] Feng, Y., Liu, Y., Wang, X., He, Z., Hung, T., and Wang, Q., 2020, “Performance Prediction and Optimization of an Organic Rankine Cycle (ORC) for Waste Heat Recovery Using Back Propagation Neural Network,” *Energy Convers. Manag.*, **226**(August), p. 113552.
- [83] Ali, A., Kamal, K., Ratlamwala, T. A. H., Sheikh, M. F., and Arsalan, M., 2021, “Power Prediction of Waste Heat Recovery System for a Cement Plant Using Back Propagation

- Neural Network and Its Thermodynamic Modeling,” *Int. J. Energy Res.*, **45**(6), pp. 9162–9178.
- [84] Mert, İ., Bilgic, H. H., Yağlı, H., and Koç, Y., 2020, “Deep Neural Network Approach to Estimation of Power Production for an Organic Rankine Cycle System,” *J. Brazilian Soc. Mech. Sci. Eng.*, **42**(12).
- [85] Kılıç, B., and Arabacı, E., 2019, “Alternative Approach in Performance Analysis of Organic Rankine Cycle (ORC),” *Environ. Prog. Sustain. Energy*, **38**(1), pp. 254–259.
- [86] Zhang, J., Lin, M., Shi, F., Meng, J., and Xu, J., 2014, “Set Point Optimization of Controlled Organic Rankine Cycle Systems,” *Chinese Sci. Bull.*, **59**(33), pp. 4397–4404.
- [87] Zhang, J., Song, S., Wang, P., Ning, M., and Yin, X., 2017, “Operating Conditions Monitoring of Vehicle Internal Combustion Engine Waste Heat Utilization Systems Based on Support Vector Machines,” *Proc. - 2017 Chinese Autom. Congr. CAC 2017, 2017-January*, pp. 6124–6128.
- [88] Dong, S., Zhang, Y., He, Z., Deng, N., Yu, X., and Yao, S., 2018, “Investigation of Support Vector Machine and Back Propagation Artificial Neural Network for Performance Prediction of the Organic Rankine Cycle System,” *Energy*, **144**, pp. 851–864.
- [89] Wang, W., Deng, S., Zhao, D., Zhao, L., ... S. L.-E. C. and, and 2020, undefined, “Application of Machine Learning into Organic Rankine Cycle for Prediction and Optimization of Thermal and Exergy Efficiency,” Elsevier.
- [90] Yan, D., Yang, F., Yang, F., Zhang, H., Guo, Z., Li, J., and Wu, Y., 2021, “Identifying the Key System Parameters of the Organic Rankine Cycle Using the Principal Component Analysis Based on an Experimental Database,” *Energy Convers. Manag.*, **240**, p. 114252.
- [91] Brieman, Friedman, Olshen, S., 2012, “Classification A Nd R Egression Trees,” Chapman & Hall/Crc, **66**, pp. 37–39.
- [92] Rodriguez-Galiano, V., Sanchez-Castillo, M., Chica-Olmo, M., and Chica-Rivas, M., 2015, “Machine Learning Predictive Models for Mineral Prospectivity: An Evaluation of Neural Networks, Random Forest, Regression Trees and Support Vector Machines,” *Ore Geol. Rev.*, **71**, pp. 804–818.
- [93] Liaw, A., news, M. W.-R., and 2002, undefined, 2002, “Classification and Regression by RandomForest,” *cogns.northwestern.edu*, **2**(3).
- [94] Holland, J. H., 1975, “Adaptation in Natural and Artificial Systems | The MIT Press,”

Univ. Michigan Press [Online]. Available: <https://mitpress.mit.edu/books/adaptation-natural-and-artificial-systems>. [Accessed: 07-Apr-2021].

- [95] Haq, M. Z., 2021, "Optimization of an Organic Rankine Cycle-Based Waste Heat Recovery System Using a Novel Target-Temperature-Line Approach," *J. Energy Resour. Technol. Trans. ASME*, **143**(9).
- [96] Hærvig, J., Sørensen, K., and Condra, T. J., 2016, "Guidelines for Optimal Selection of Working Fluid for an Organic Rankine Cycle in Relation to Waste Heat Recovery," *Energy*, **96**, pp. 592–602.
- [97] Amiri Rad, E., Mohammadi, S., and Tayyeban, E., 2020, "Simultaneous Optimization of Working Fluid and Boiler Pressure in an Organic Rankine Cycle for Different Heat Source Temperatures," *Energy*, **194**, p. 116856.